
MASTER THESIS

*Dynamic analysis of the stinger hang-off system cable forces
using ship motion data of Audacia.*

S.L. de Rijke, BSc., 4008588

*A thesis submitted to the specialisation
Bottom founded structures*

*For the degree of
Master of Science Offshore and Dredging Engineering*

This thesis is CONFIDENTIAL and cannot be made public

Graduate Professor: *Prof. Dr. A.V. Metrikine*
University supervisor Hydraulic engineering: *Ir. T.J. Zitman*
University daily supervisor Structural Mechanics: *Dr. Ir. A. Tsouvalas*
Company representative: *Ir. P. Demeersseman*

Delft, 2015

The author holds no responsibility for information in this report that is incomplete or inaccurate. A printing restriction applies to this document due to confidentiality of the report.

©Copyright Allseas

Copyright of all published material including technical descriptions, photographs, drawings and images in this document remains vested in Allseas' contributors as appropriate. Accordingly, neither the whole nor any part of this document shall be reproduced in any form nor used in any manner without express prior written permission and applicable acknowledgements. No trademark, copyright or other notice shall be altered or removed from any reproduction.

TABLE OF CONTENTS

TABLE OF CONTENTS	5
LIST OF SYMBOLS	9
PREFACE	13
SUMMARY	15
1. INTRODUCTION	17
1.1 BACKGROUND.....	17
1.1.1 <i>Technical University of Delft</i>	17
1.1.2 <i>Allseas</i>	17
1.2 INTRODUCTION OF THE VESSEL	17
1.3 INTRODUCTION OF THE EQUIPMENT	18
1.3.1 <i>The stinger</i>	18
1.3.2 <i>The stinger handling frame</i>	19
1.3.3 <i>The lower block structure & lower sheave block</i>	19
1.4 AXIS SYSTEMS	20
1.5 CONVENTIONS.....	20
1.6 THESIS STRUCTURE	21
2. PROBLEM DEFINITION	23
2.1 UPLIFT DEFINITION.....	23
2.2 GOAL	23
2.3 PROBLEM DEFINITION & RESEARCH QUESTIONS	23
3. RESEARCH STRATEGY	25
3.1 INITIAL COMPARISON	25
3.2 MODEL QUALITIES	25
3.3 MODEL PERFORMANCE	25
4. GENERAL ANALYSIS	27
4.1 FACTOR ANALYSIS	27
4.1.1 <i>Ship motions</i>	27
4.1.2 <i>Environmental loads</i>	27
4.1.3 <i>On-board equipment</i>	27
4.1.4 <i>Operational settings</i>	28
4.1.5 <i>Deformations</i>	28
4.2 EVALUATION OF THE GENERAL ANALYSIS.....	28
5. DATA ANALYSIS	31
5.1 DATA LOGGER	31
5.2 RESAMPLING DATA.....	32
5.3 FILTERING DATA	33
5.3.1 <i>Filter</i>	33
5.3.2 <i>Filter range and Nyquist frequency</i>	34
5.3.3 <i>Frequency plots</i>	35
5.3.4 <i>Inverse Fourier Transformation</i>	36
5.4 DIFFERENTIATION OF DATA.....	37
5.5 COMPARISON OF FREQUENCY-DOMAIN PLOTS.....	38
5.6 COMPARISON OF TIME-DOMAIN DATA PLOTS.....	39
5.7 EVALUATION OF THE DATA ANALYSIS	40
6. RIGID LINKS MODEL	43
6.1 MODEL OF A RIGID BODY WITH RIGID LINKS	43
6.2 FREQUENCY -AND TIME TRACE ANALYSIS.....	44
6.2.1 <i>Reviewing methods</i>	44
Normalised cross covariance plots	44
Standard deviation	45
Correlation of peak amplitudes.....	45
Mean peak amplitude difference & time difference	46

Minimum distance method	46
Frequency plot and spectrogram	46
6.2.2 <i>The target values</i>	47
6.2.3 <i>RL model analysis</i>	48
Time-domain analysis.....	48
Frequency-domain analysis	50
Time- & frequency-domain analysis	51
6.3 EVALUATION OF THE RL MODEL ANALYSIS.....	52
7. FLEXIBLE LINKS MODEL	55
7.1 MODEL OF A RIGID BODY WITH FLEXIBLE LINKS	55
7.2 MODEL SCHEMATISATION AND DESCRIPTION.....	55
7.3 THE DERIVATION OF EQUATIONS OF MOTION	58
7.3.1 <i>Lagrangian formalism</i>	58
7.3.2 <i>The kinetic and potential energy</i>	59
Kinetic energy	59
Potential energy	61
7.3.3 <i>Differentiation and linearization</i>	62
7.3.4 <i>Equations of motion</i>	63
Stiffness matrix.....	64
Note on the centre of gravity	64
Addition of damping	64
Addition of sheave friction	65
7.3.5 <i>Static buoyancy</i>	66
7.4 SOLVING METHODS FOR THE EQUATIONS OF MOTION	66
7.5 PREPARATORY CALCULATIONS.....	68
7.5.1 <i>Defining system parameters</i>	68
Stiffness values.....	68
Equipment weights, static buoyancy and rotational inertia	69
The initial conditions	70
Complications concerning Matlab.....	70
7.5.2 <i>Using the ordinary differential equations results</i>	70
7.6 VALIDATION OF ASSUMPTIONS	71
7.6.1 <i>Small angle approximation</i>	71
7.6.2 <i>2-D-analysis approximation</i>	71
7.6.3 <i>Contribution of lower block structure mass</i>	71
7.7 VALIDATION FL MODEL USING DIRECT TIME-INTEGRATION	72
7.7.1 <i>The base case</i>	72
7.7.2 <i>Static and free vibration test</i>	73
7.7.3 <i>Harmonic excitation tests</i>	74
7.8 BASE CASE ANALYSIS.....	76
7.8.1 <i>Reviewing methods recapitulation</i>	77
7.8.2 <i>The target values recapitulation</i>	77
7.8.3 <i>RL model recapitulation</i>	78
7.8.4 <i>FL model using direct time-integration</i>	80
7.8.5 <i>FL model using modal method</i>	84
7.8.6 <i>Parameter improvement for base case models</i>	86
7.9 FL MODEL WITH PARAMETER IMPROVEMENT	87
7.9.1 <i>Adjusted FL model using direct time-integration</i>	87
7.9.2 <i>Adjusted FL model using modal method</i>	89
7.9.3 <i>Sub result of RL and FL model comparison</i>	92
7.10 UNCERTAINTY ANALYSIS BY INPUT ERRORS.....	92
7.10.1 <i>RL model</i>	93
7.10.2 <i>FL model using direct time-integration</i>	93
7.10.3 <i>Error in the measured cable force</i>	93
7.10.4 <i>Uncertainty in mass and centre of gravity</i>	94
7.10.5 <i>Concluding for the FL model uncertainty</i>	94
7.11 SENSITIVITY ANALYSIS BY PARAMETER VARIATION.....	94
7.11.1 <i>Model parameters</i>	94
7.11.2 <i>Significant motion analysis</i>	96
7.11.3 <i>Conclusion of sensitivity analysis</i>	96
7.12 HIGH FREQUENCY DISTURBANCES	96
7.12.1 <i>Possible sources</i>	96

Spectral leakage	97
Time step in the data traces	97
Resampling type	99
Reaction with the first mode	99
7.12.2 Conclusion	99
7.13 EVALUATION OF THE FL MODEL ANALYSIS	99
8. COMPARISON OF FL AND RL MODELS	101
9. CONCLUSION AND RECCOMENDATIONS	103
9.1 CONCLUSIONS	103
9.2 RECOMMENDATIONS FOR FURTHER UPLIFT ANALYSIS.....	103
9.3 RECOMMENDATIONS FOR MORE DETAILED ANALYSIS	104
BIBLIOGRAPHY	107
LIST OF TABLES	109
LIST OF FIGURES	111
APPENDIX A. MATLAB FOR DATA ANALYSIS	113
Readout data	113
Finding time ranges	113
Frequency-domain	113
APPENDIX B. FAST FOURIER TRANSFORM	115
Spectral leakage	115
Ringing	116
Round-off error	116
APPENDIX C. ADDITIONAL DATA ANALYSIS RESULTS.....	117
Pitch.....	117
Roll	118
Acceleration plots of heave and surge.....	119
APPENDIX D. EQUATIONS OF MOTION	121
Differentiation of the Lagrangian formalism for φ	121
Differentiation of the Lagrangian formalism for α	121
The resulting equations of motion	122
APPENDIX E. STIFFNESS MATRIX.....	125
APPENDIX F. MODAL ANALYSIS	127
General.....	127
Equations of motion & initial conditions	127
Matlab	128
APPENDIX G. SPECTROGRAM.....	131
Segmenting the signal & overlap.....	131
Windowing function	131
APPENDIX H. MATLAB FOR FL MODEL	133
Model build-up	133
Definition of tolerances	134
The solver.....	134
The solver's 1 st order input	135
Solver results	135
Peak matching for reviewing.....	135
APPENDIX I. CALCULATION OF BLOCK MASS CONTRIBUTION	137

LIST OF SYMBOLS

Symbol	Name	Unit
α	The sheave rotation	rad
$\dot{\alpha}$	Rotational velocity of a sheave	rad/s
β	Hang-off angle	rad
β_1	Hang-off angle of cables	rad
B_2	Hang-off angle of lower block structure	rad
γ	Main hinge angle	rad
δ	Section 2 angle relative to the main hinge angle	rad
ϵ	Total strain	-
ϵ_{Static}	Strain by static force acting on the hang-off cables	-
$\epsilon_{\text{self-weight}}$	Strain by self-weight of the hang-off cables	-
η	Section 3 angle relative to the angle of section 2	rad
ρ	Normalised correlation coefficient of peak values	-
$\sigma_{A/B}$	Standard deviation of data trace A or B	kN
ϕ/φ	The stinger angular motion	rad
$\dot{\phi}$	Rotational velocity of the stinger	rad/s
φ_r	Roll	rad
θ	Pitch angle	rad
$\ddot{\theta}$	Pitch acceleration	rad/s ²
θ_{custom}	Artificial pitch input with chosen parameters	rad
$\ddot{\theta}_{\text{normalised}}$	Normalised pitch acceleration	rad/s ²
$\mu_{-i/A/B}$	Mean value of the data trace. An index indicates the specific data trace of which the mean value was taken.	kN
ψ	Yaw	rad
ω	(Chosen) rotational frequency (for motion input)	rad/s
A	Area	m ²
A_i/B_i	Amplitude of vector value i of data trace A or B	Multiple units
ΔA_{mean}	Mean peak amplitude difference.	kN
$\Delta \text{ang}1$	Angular difference of cables with linear line connection point B and C	rad
$\Delta \text{ang}1$	Angular difference of LBS with linear line connection point B and C	rad
B	Amplitude	-
C^*	Modal damping matrix	$\frac{kg \cdot m^2}{s \cdot rad}$
$C_{1...14}$	Constant numbers with number 1 up to 14	Multiple units
$\text{Corr}_{t\&A}$	Peak correlation based on minimum distance.	-
C_{xy}	Cross covariance of data traces x and y	-
Δd	Distance of linear line between point C and B to the lower sheave block	m
$D_{1/2}$	Damping terms of type 1, corresponding with sheave angular velocity, and of type 2, corresponding with the stinger angular velocity	$\frac{kg \cdot m^2}{s \cdot rad}$
D^*	Modal damping matrix	$\frac{kg \cdot m^2}{s \cdot rad}$
$d\theta$	Contact angle of the wire rope on the sheave	rad
d_{bore}	Bore diameter	m
df	Frequency step	Hz
d_{ii}^*	Modal damping of mode i	$\frac{kg \cdot m^2}{s \cdot rad}$
d_{ii}^{critical}	Critical modal damping of mode i	$\frac{s \cdot rad}{kg \cdot m^2}$
dof	Degree of freedom	Multiple units
D_{physical}	Physical damping matrix derived from the modal damping matrix	$\frac{kg \cdot m^2}{s \cdot rad}$
dt	Time step	s
er_{red}	Reduction of error	-
E	Eigen matrix containing all eigenvectors or normal modes	-
E_d	Spectral energy	J/multiple ² /Hz
E_{Norm}	The normalised eigenvector matrix.	-
E_y	Youngs modulus	N/m ²
f	Frequency	Hz
f^0	Central bin frequency to the zeroth order	Hz

F	Force vector with forces acting on each degree of freedom	Nm
F_{BR}	Force lower block structure	N
$F_{c,total}$	Total predicted cable force	N
F_{ex}	External forces	N
$F_{LC,n}$	Cable force at load cell number n	N
$f_{nyquist}$	The Nyquist frequency	Hz
f_r	Frictional coefficient of the double cylindrical roller bearing	-
F_{RH}	Horizontal component of tension T	N
F_{RV}	Vertical component of tension T	N
F_{sh}	Force by the lower sheave block	N
$F_{stinger}$	Force by the stinger	N
F_z	Force in z-direction	N
g	Gravitational acceleration	m/s^2
$g_f(\dot{\alpha})$	Velocity dependent function to give the friction component the right directional sign depending on the velocity of the sheave.	-
i	Imaginary unit or imaginary number	-
I_{sheave}/I_{sh}	Rotational inertia of a sheave	$kg \cdot m^2$
K	Physical stiffness matrix	$kg \cdot m^2$
k	Frequency	$s^2 \cdot rad$
K^*	Modal stiffness matrix	Hz
K1	Spring stiffness of the wire rope between point D and point C	$kg \cdot m^2$
K2	Spring stiffness of the wire rope between point C and point B, running to load cell	$s^2 \cdot rad$
K3#	Spring stiffness of the wire rope running to winch number #=1, 2, 3 or 4	Hz
k_{ii}^*	Modal stiffness of mode i	$kg \cdot m^2$
K_{part}	Stiffness value of a cable part	$s^2 \cdot rad$
l	Length along a stinger section	N/m
l_2	Cable length projected on the linear line between point C and B.	N/m
L	Lagrangian function	m
L_0	Distance from main hinge to the stinger connection point	m
L1	Length of section 1	J
L2	Length of section 2	m
L3	Length of section 3	m
L_A	Distance along the x-axis of the centre of gravity to point A	m
L_C	Distance along the x-axis of the centre of gravity to point C	m
L_{bsp}	Length lower block structure projected on the linear line between point C and B.	m
$l_{stretched}$	Stretched rope length	m
$l_{unstretched}$	Original unstretched rope length	m
m	Mass	kg
m_{ii}^*	Modal mass of mode i	$kg \cdot m^2$
m_0	Zeroth order moment	$\frac{rad}{kg \cdot m^2}$
M	Physical mass matrix	Multiple units
M^*	Modal mass matrix	$kg \cdot m^2$
M1	Mass of the stinger section 1	$\frac{rad}{kg \cdot m^2}$
M2	Mass of the stinger section 2	rad
M3	Mass of the stinger section 3	kg
M_B	Moment about point B	kg
M_f	Frictional moment term	kg
ml	The time shift or also called the lag	Nm
M_{LBS}	Mass of the lower block structure at the stinger connection point.	Nm
mpm	Mass per meter of steel wire rope	s
m_{sh}	Mass of a sheave	kg
M_{static}	Static external moment working on the system	kg
M_w	Mass of the hang-off wires	Nm
N	Vector length of the data trace	kg
No	Normal force or radial force on a sheave axis	-
		N

NI	Length of a data trace	-
odefun	Function which calculates the right hand side of the inserted 1st order ordinary differential equations to be solved	-
options	Option function for odefun	-
p	Number of sections	-
q	Generalised coordinates	Multiple units
R	Radius of the sheaves	m
S	Standard deviation of the data trace	kN
StatIC	Static initial values of all degrees of freedom	rad
Δt	Sampling time	s
t	Time	s
T	Kinetic energy in the system	J
T_c	Cable tension	N
T_e	Tension in the cable parts running over a sheave	N
Δt_{mean}	Mean peak amplitude difference.	s
Tnum	Solver output vector containing the time steps corresponding to the rows of Ynum	s
tspan	Vector which specifies the integration interval output for odefun.	-
Δu	Differential stretch of the hang-off cables	m
u_0	Modal displacement initial conditions	rad
\dot{u}_0	Modal velocity initial conditions	rad/s
$u_i(t)$	Modal time function	Multiple units
v_t	A random time function	-
V	Potential energy in the system	J
V_t	Random time function's representation in frequency domain	-
x	Surge	m
\underline{x}	Generalized displacements of all degrees of freedom	Multiple units
\dot{x}	Velocity in x-direction	m/s
x_0	Displacement initial conditions	rad
\dot{x}_0	Velocity initial conditions	rad/s
\ddot{x}_A	Acceleration in x-direction in point A	m/s^2
$x_{A/C/D}$	Surge motion in points A, C and D	m
x_b	x-distance from the centre of gravity to the stinger connection point	m
x_i	Data trace value i of data trace x. Note that the *-symbol indicates the use of a complex conjugate.	Multiple units
\hat{x}_i	i^{th} Normal mode of the system	-
X(n)	Value at time step index j.	Multiple units
y	Sway	m
y0	Vector with initial conditions specified by the user for odefun.	-
y_b	y-distance from the centre of gravity to the stinger connection point	m
y_i	Data trace value i of data trace y. Note that the *-symbol indicates the use of a complex conjugate.	Multiple units
Y	Filtered parameter values in frequency domain.	Multiple units
Y*	Complex conjugate of filtered parameter values in frequency domain	Multiple units
Y(k)	Amplitude and phase in a complex number of the frequency k.	Multiple units
Ynum	Solver output matrix containing all motion (mot) and velocity (vel) values of the DOF's.	Multiple units
z	Heave or vertical displacement	m
\dot{z}	Velocity in z-direction	m/s
\ddot{z}_A	Acceleration in z-direction in point A	m/s^2
$z_{A/C/D}$	Heave motion in A, C and D	m
z_b	z-distance from the centre of gravity to the stinger connection point	m

PREFACE

After a successful internship at Allseas I was offered a graduation position in the company. I was asked to perform a dynamic analysis of the stinger hang-off system cable forces using ship motion data of Audacia. The sponsor of this thesis is Allseas. Allseas has provided for the subject, all necessities for writing my thesis and all the necessary background information for the subject. The thesis was performed in the specialisation of Bottom Founded Structures for the degree of Masters of Science in Offshore and Dredging engineering.

The members of the graduation committee are:

Prof. Dr. Andrei Metrikine	Graduate Professor	Delft university of technology
Ir. Tjerk Zitman	University supervisor Hydraulic engineering	Delft university of technology
Dr. Ir. Apostolos Tsouvalas	University daily supervisor Structural Mechanics	Delft university of technology
Ir. Pieter Demeersseman	Company representative	Allseas

Firstly, I would like to thank Prof. Dr. Metrikine for his guidance during my graduation. I would like to thank him for the motivation and the insights he provided me with. Also, I would like to thank him for the opportunities to get a kick start on multiple subjects during my thesis and for the opportunity to perform my thesis for the bottom founded structures specialisation under his supervision.

Additionally I would like to thank Ir. Tjerk Zitman for his help during different phases of my graduation and providing with support for multiple parts of my thesis. I would also like to thank him for all his very clear comments and ideas which helped me tackle multiple problems. Furthermore, his flexibility in planning and supervision throughout the thesis have been a great support.

I very much appreciate all the help and guidance of Apostolos Tsouvalas who was my daily supervisor from the university side and I would like to thank him for that. His flexibility in planning and his detailed reviews of my work have helped me solve multiple issues. Discussion with him gave me more insight of the subject and his critical view helped me improve my models to great extent.

Furthermore I would like to thank Ir. Pieter Demeersseman who was my company supervisor for the guidance, support and help during my graduation. His resourcefulness was a great help during my thesis and his constructive critiques were a good way to keep focus and improve the thesis further and further.

I would also like to thank multiple Allseas employees who provided me with good tips, thus helping me out on multiple issues. Specifically I would then like to thank Niels, Keran, Toni and Ewoud.

Furthermore, I would like to thank my family who has supported me throughout all my years of education and during my thesis. Many thanks go out to Simone Dijkhuis who supported me throughout my graduation and with whom I spent several days and evenings to work when deadlines needed to be met. Last but not least I want to thank Menno, who has been a true tower of strength throughout my graduation. When times were tough and days got long he was always there to support me.

*S.L. de Rijke,
Delft, 17-12-2015*

SUMMARY

Already for some time the desire exists to acquire insight into the phenomenon of stinger uplift. This is the situation where external forces and motions acting on the stinger and the hang-off wires cause the hang-off cable tensions to be lower than a specific threshold value. If uplift occurs there is little or no cable tension, which means that when the stinger “comes down” snap loads occur in the cables. This situation should be avoided. To gain quantitative insight into uplift occurrences, four load cells have been installed on the vessel Audacia to record stinger cable forces. However, the usability of these recordings was unclear. It was therefore decided to develop two dynamic models to predict measured cable forces on the basis of measured ship motions. This is the subject of the present study: A computational model is presented to predict time-varying cable forces for the operational setting that the stinger is lifted out of the water. The more complex case of a partly submerged stinger is recommended for further research. The research questions that need to be addressed are:

1. What is the most accurate model type to predict the cable forces based on ship motions?
2. What is the excitation frequency which amplifies the motion of the system?
3. What is the influence of noise in the measurement system on the model results?
4. What parameter has the most influence on the predicted cable forces?
5. Which ship motion is governing for the predicted cable forces?

Ultimately, when the computational model is finished the model can be used as follows. Before the operation the ship receives weather data of the predicted weather during the operations. From this weather data ship motions can be predicted. These predicted ship motions can be used as input for the model after which the model results will provide time-varying cable forces. These predicted (time varying) cable forces can then be used to find statistical properties of the predicted cable forces, which in turn can be used to calculate the chance of an uplift occurrence.

Before the models were created, a direct comparison was performed between the measured cable forces and the motions at the centre of gravity of the ship. The purpose of this is to find out the usability of specific ship motions for the prediction of cable forces and which ship motions are governing for the cable force prediction. The motion data was compared in the frequency- domain and time-domain with the measured cable forces. It appeared that, that the pitch motion is the most influential motion for the cable forces. However, a type of prediction of the cable forces directly by the time traces of the motions in the centre of gravity is not considered accurate enough. Additionally, it became evident that the roll motion showed no correlation at all. Therefore, maintaining the 2-D analysis in further stages of the thesis is considered justified.

This thesis considers two dynamic models which are performance compared, i.e. the rigid links model (RL model) and the flexible links model (FL model). The rigid links model assumes the complete system of the ship, stinger and hang-off wires to be rigid. The flexible links model assumes the ship and the stinger rigid but it accounts for a hinged stinger connection to the bow of the ship and stretching of the cables. Additionally, the flexible links model is based on multiple approaches. The first approach is a direct time-integration method for solving the equations of motion for the degrees of freedom. The second approach is using the modal analysis to solve the equations of motion. Audacia’s on board measured motion data is used as input for the computational models. For verification of the model results, the measured cable forces are used. The information of the measured displacement data is read-out, resampled, filtered and processed for reviewing. Filtering is performed in the frequency domain and the frequency domain is acquired through the fast Fourier transform.

The Rigid Links model (RL model) is created using linearized rigid body dynamics through which expected inertia forces acting on the hang-off cables can be predicted. The results of the prediction by the RL model show underestimation of the actual measured cable forces and a frequency difference is visible between the predicted and the measured cable force time traces. The limitation of the RL model is that it is not possible, using this model, to see the interaction between the stinger and the sheaves, while the load cell which measures these cable forces could actually be influenced by these sheaves and their interactions with the equipment. Furthermore, the model does not allow for expansion or the adjustment of model parameters. It is not possible using the RL model to create a more accurate prediction of the amplitudes of the cable forces occurring.

For the creation of the flexible links model (hereafter FL model) the Lagrangian formalism is used. The derived non-linear equations are linearized using a small angle approximation. The FL model accounts for: cable flexibility, relative motion of the hang-off system and the stinger, stinger dynamics, sheave

dynamics, some dissipation terms in the form of viscous damping, optionally inclusion of sheave friction and static buoyancy. The FL model is preferable because it accounts for stretching of the cables and with this, it allows for relative motion of the stinger and the top sheaves. Because of that the FL model describes the system response more accurately than the RL model as will be concluded in a later paragraph. The limitation of the FL model is that damping is introduced as a viscous term which is actually not a realistic representation of the dissipation in the actual system. Therefore, the damping introduced in the system is an estimated or fitted parameter which accounts for some dissipation in the system. Improving the damping terms and thus removing this limitation is one of the recommendations of this thesis.

The RL model and the FL model were reviewed for their correlations and/or similarities to the measured cable forces. The similarities were defined using several reviewing methods. These are:

- Analysis of time and frequency domain plots
- Normalised cross-covariance over the complete data trace.
- Standard deviation of the cable force time-traces.
- Correlation of peak amplitudes.
- Mean peak amplitude difference.
- Mean peak time difference.
- Minimum distance method
- Spectrograms, simultaneous time-frequency analysis.

Reviewing these results it can be concluded that the most accurate model to predict the cable forces in the hang-off system based on ship motions is the FL model. This model can predict the standard deviation of the cable forces with an accuracy of 9.9 kN (order of 3,7%), which is essentially the worst case scenario uncertainty due to input errors and the uncertainty due to errors in the measured cable forces. This accuracy of on a total predicted mean cable force of 1.89E4 kN (with an accuracy of order 0.08%) can be regarded satisfactory for the data time trace considered. When studying the FL model sensitivity the stiffness values appeared to play a dominant role. This is logical considering that the fundamental frequency (1.9 Hz as stated later in this paragraph) of the system is well above the excitation frequencies of the wave spectrum (which has its maximum frequency at 0.2 Hz in this thesis) it is exposed to. This means the system response for the FL model is quasi-static and thus the stiffness in the system dominates. The first and closest eigenfrequency, considering the FL model, is 1.9 Hz (or 0.52 seconds period). Logically, the most sensitive excitation frequencies are the frequencies closest to this first eigenfrequency.

Noise in the measured data used as model input may adversely affect the utility of model results. In general, there is always noise present in measured data due to un-avoidable physical effects. However, noise can also be amplified and/or introduced by different calculations, which are performed with the input data. The frequency plots of the RL and FL model both are found to contain high frequency noise. The fact that the noise is present in both the RL model and the FL model confirms that the noise has its roots in the input data, which is logical considering the fact that the RL and FL models are linear models. After research it was apparent that the high frequency noise can be caused by un-avoidable physical effects, spectral leakage and the resampling type. Another apparent cause is the time step used in the motion displacement data in combination with the differentiation of this data to acceleration values. The high frequency noise can be amplified by the first mode of the FL model. If the noise is present in frequencies close to the eigenfrequencies of the modelled system the model will exhibit resonance in response to a false excitation. Furthermore it is found that high frequency noise can be suppressed by using the modal damping applied in the FL model and increasing the damping on the second and higher modes.

Reviewing the models it is apparent that the performance of the FL model is better than the performance of the RL model in prediction of the cable forces based on the ship motions at the centre of gravity, for the cases considered in this thesis. The primary recommendation considering the FL model itself is to improve the model by getting a physical grasp on the damping in the system. If one wants to continue the uplift analysis using the current model, it is recommended to test the current model on a different time trace before elaborating it by implementing stinger submergence.

1. INTRODUCTION

The goal of this thesis is to create a computational model to predict time-varying cable forces for the operational setting that the stinger is lifted out of the water. The main research question of this thesis is: What is the most accurate model type predict the cable forces based on ship motions?

Ultimately, if the model is expanded for submerged stinger configurations, it can be used to provide one with the expected cable forces based on predicted ship motions (in which case the ship motions are based on weather predictions). The statistical properties of the predicted cable forces can then be used to calculate the chance that the cable forces reach values below a certain threshold value.

This chapter provide background on the company which provided for this assignment and the university for which this graduation thesis is written in order to graduate for the title of engineer. After this first section the vessel is presented about which this thesis is concerned and details are given on the equipment which is present on board of this vessel. Then the axis system is presented, the conventions are defined and the structure of the document is presented for this graduation report.

1.1 BACKGROUND

1.1.1 TECHNICAL UNIVERSITY OF DELFT

This thesis has been written in light of finalising the 2 year Masters of Science track of Offshore and Dredging engineering within the specialisation of Bottom Founded Structures. The Offshore and Dredging engineering MSc programme exists since 2004 and is a multidisciplinary cooperation between Civil Engineering, Mechanical Engineering and Marine Technology. The master track includes design of fixed and floating offshore structures and subsea and dredging equipment.

1.1.2 ALLSEAS

The thesis subject and sponsoring have been provided by Allseas. Allseas is a world-wide operating offshore company specialising in pipeline installation, subsea construction and heavy lifting. It is an innovative company with much in-house knowledge and offering services during design, project management, engineering, procurement, installation and commissioning. To provide these services a wide range of versatile vessels are in Allseas' fleet. The vessel considered during the thesis will be introduced in the next section.

1.2 INTRODUCTION OF THE VESSEL

The vessel concerned in this thesis is the pipe lay vessel Audacia, which can be seen in Figure 1.1. The Audacia is the third largest pipelay vessel of the Allseas fleet. It has the ability to lay pipelines up to 1.5 meter diameter. Some additional vessel characteristics are given in Table 1.1.



Figure 1.1 The Audacia.

Characteristic	Value	Unit
Length (excl. stinger)	225	Meters
Stinger length	110	Meters
Minimum radius	80	Meters
Maximum speed	8.2	Meters per second
Tension capacity	525	Tons

Table 1.1 Specifications of the Audacia.

1.3 INTRODUCTION OF THE EQUIPMENT

The Audacia, shown in Figure 1.2, has a suspended stinger consisting of 3 connected sections. This stinger is suspended with four steel wire ropes which run through a sheave system. These sheaves are connected by cylindrical roller bearings to an axis. The assembly, consisting of the sheaves with, axis is hereafter called sheave block, as shown in Figure 1.3. The sheave block attached to the lower block structure is called the lower sheave block. The sheave block attached to the hang-off structure is called the top sheave block. The figure also shows a part of the cable windings of the hang-off system. The complete system of the sheaves, lower block structure, the wire rope and hang-off frame is called the stinger hang-off system. The separate elements are elaborated on in the next sections.

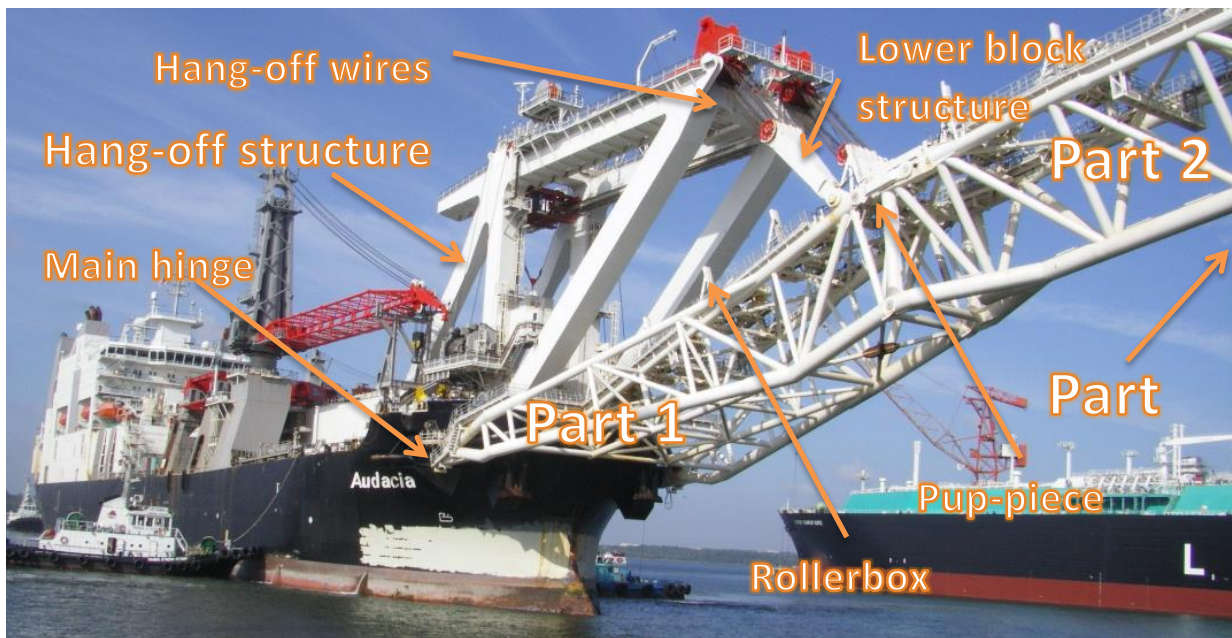


Figure 1.2 Audacia points of interest.

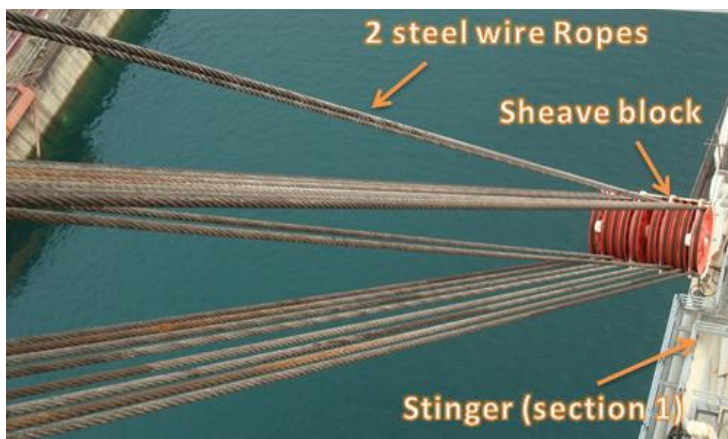


Figure 1.3 Hang-off wires and sheave block.

1.3.1 THE STINGER

The purpose of the stinger is to support a suspended pipeline while the ship is operating. It also induces a bend in the pipeline, which it needs in order to lower it to the sea floor in good condition and in a controlled manner.

The stinger consists of three truss structures. Each structure can separately adjust its angle using the pup-pieces which connect the stinger sections. The stinger adjustment system enables the relative rotation of the separate stinger sections. This adjustment of stinger angles means changing the stinger radius, depending on the operation type required. The approximate stinger section weights of the stinger are respectively 4.4E2, 3.2E2 1.5E2 tons. On top of the stinger rollerboxes are mounted over which the pipeline is lowered into the water. The heights of the roller boxes are adjustable. This is practical when changing the stinger radius in order to keep proper contact with the pipeline present on the stinger. The stinger also contains walkways which are used for maintenance work on both the stinger and the equipment on the stinger.

1.3.2 THE STINGER HANDLING FRAME

The stinger handling frame is the rigid structural part of the hang-off system consisting of two longitudinal and transverse girders supported by two diagonal struts on the bow side and two diagonal tie down members on the aft side of stinger the handling frame, as can be observed in Figure 1.2. It is thus a type of truss structure which supports the winches, 24 sheaves through which the hang-off cables run and the flippers. A complete drawing of the handling frame and the equipment it contains is given in section 7.2.

The flippers are the red elements on top of the stinger handling frame which support the dead ends of the hang-off cables and multiple sheaves of the hang-off system. They can be seen in Figure 1.4. Each flipper has ten sheaves through which the cables are wound. The flippers are rigidly connected to the stinger handling frame. A side view of the flippers is given in Figure 1.5. This figure also indicates the location of the load cells in the hang of cable's dead ends and the top sheave block. The wire ropes which are wound through the top sheave block also wind through the lower block structure, which will be elaborated on in section 1.3.3.



Figure 1.4 Flippers supporting the dead ends of hang-off cable with load cells. © Hans@Fotovlieger.nl.

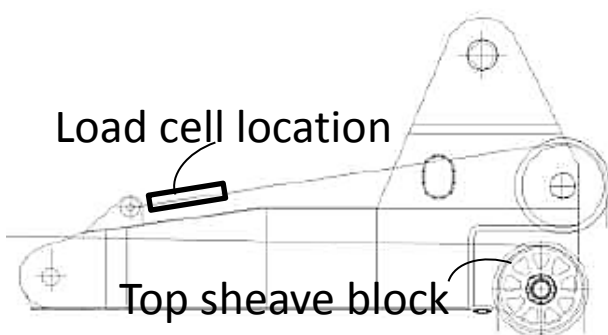


Figure 1.5 Side-view of the flippers on top of the stinger handling frame.

The sheaves used in the flippers and the lower block structures are cast sheaves which contain double row cylindrical roller bearings. Their outer diameter is 1540 mm and their inner diameter is 1330 mm. The hang-off wires are 6 strand, galvanised, steel wire ropes of 72 mm diameter. Four of these wire types are used in the hang-off system. Their mass per meter wire is 20.6 kg.

1.3.3 THE LOWER BLOCK STRUCTURE & LOWER SHEAVE BLOCK

The lower block structure connects the lower sheave block with the stinger in the stinger connection point. It contains sheaves through which the hang-off wires are wound. The lower blocks have ten sheaves each and the structure connects with the stinger connection point on stinger section 1. The

connection with the stinger section is a hinge connection. A side view and a front view of the complete lower block structure are given in Figure 1.6.

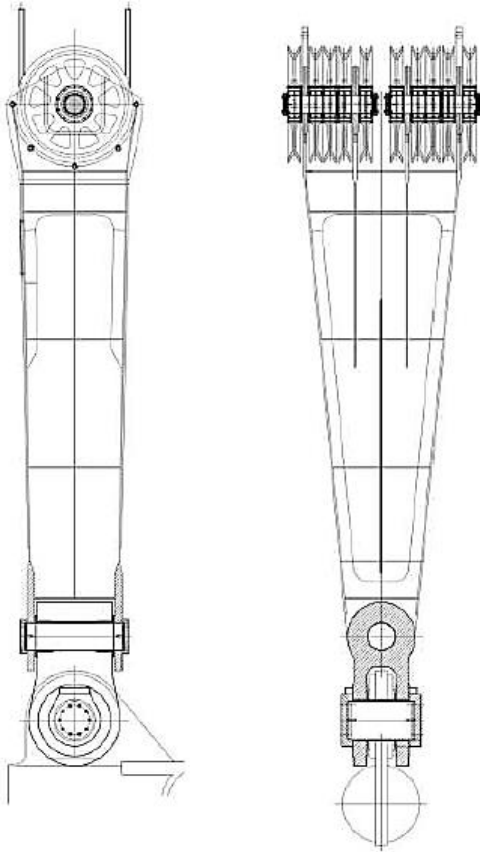


Figure 1.6 Side view (left) and front view (right) of the lower block structure and its connection to the stinger.

1.4 AXIS SYSTEMS

The coordinate system, as used in this thesis, is given in Figure 1.7. Note that the origin of the axis system resides in the centre of gravity of the vessel. However, as will be stated later in the report, only the 2-D system in the x,z -plane of the vessel motions is considered therefore the yaw, roll and sway motion are not considered of interest. Motions of interest are:

1. Pitch motion (angular motion about the y -axis).
2. Heave motion (in z -axis direction).
3. Surge motion (in x -axis direction).

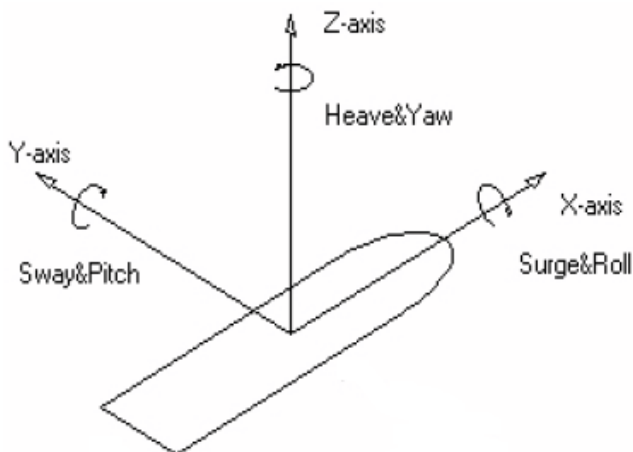


Figure 1.7 Axis conventions used in calculations.

1.5 CONVENTIONS

All calculations performed in this thesis have been performed utilizing SI units. In the event that an calculation does not utilize the SI units, this will be noted along with the concerning calculation.

1.6 THESIS STRUCTURE

In Chapter 2 the problem definition is given on which the thesis is based. Chapter 3 elaborates on the research strategy of this thesis. The general analysis of the problem is performed in Chapter 4 after which the data analysis is performed in Chapter 5. The next chapters explain the rigid links model (RL model) and the flexible links model (FL model) including the methods used to calculate them and their results. The RL model description can be found in Chapter 6 and the FL model can be found in Chapter 7. In Chapter 8 the two models are compared. Lastly, Chapter 9 contains the conclusions of the thesis corresponding with the questions defined in the problem statement chapter, Chapter 2.

2. PROBLEM DEFINITION

The original intention of this thesis was to find all physical factors which could induce the phenomenon uplift and to acquire insight in the extent of their influence on uplift. The idea is that before an operation commences, weather predictions will be received by the ship. These weather predictions can be used to calculate the expected ship motions during the operation. In order to predict uplift the cable forces will need to be predicted, based on these ship motions. It was therefore decided to develop multiple dynamic models to predict measured cable forces on the basis of measured ship motions. Not only will this provide a tool which has the potential to predict uplift after elaboration, it will also provide insight in the characteristics of the system and consequences of the usage of (raw) data.

2.1 UPLIFT DEFINITION

When the ship is at rest and there are no external forces acting on the ship, the stinger or the hang-off system, the hang-off cables will carry the static weight of the stinger. In reality the ship moves and external forces are acting on the stinger. These forces and motions could become thus large and in unfavourable direction, resulting in compensation of the static weight of the stinger by these phenomena and thus the hang-off cables carry little to no load, as shown in Figure 2.1. If the hang-off cable tension reaches these minimum or zero values the stinger will not be carried by the cables and could even, depending on the motions and forces, move upward and thus uplift occurs. Logically, this causes the cables of the hang-off system to become slack after which it is inevitable that snap loads occur in the hang-off system. This is thus a situation which should be prevented in all cases.

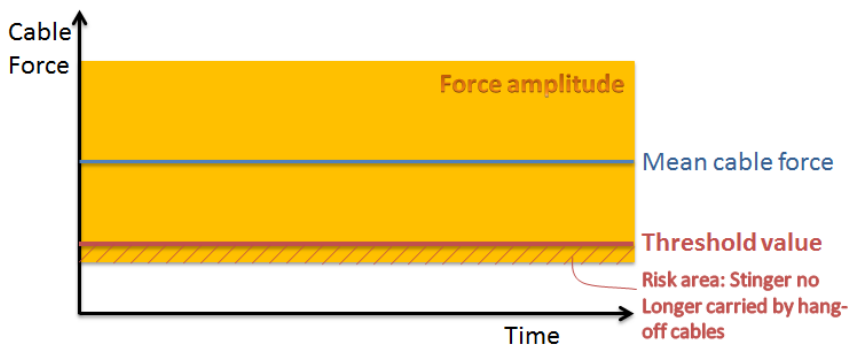


Figure 2.1 Sketch of cable force variation potentially causing uplift.

The physical meaning of uplift is: *The physical situation where external forces and motions acting on the stinger and the hang-off wires cause the hang-off cable tensions to be lower than a specified threshold value.*

2.2 GOAL

The goal of this thesis is to predict the cable forces in the hang-off system based on ship motions in a 2-D plane for the operational setting that the stinger is lifted out of the water. To be able to ultimately predict uplift one must understand the dynamics of the hang-off system of the Audacia and understand how the on-board measurements relate to the physics.

2.3 PROBLEM DEFINITION & RESEARCH QUESTIONS

A computational model must be produced which predicts time-varying cable forces for the operational setting that the stinger is lifted out of the water. This dynamic model must predict the mean cable forces and cable force amplitudes by using ship motions as data input. It must have the potential to (after elaboration for a submerged state), predict whether the force amplitude in the hang-off cables can, over a certain time period, reach values under a defined threshold value based on these ship motions. The research questions which go hand in hand with this problem statement are:

1. What is the most accurate model type predict the cable forces based on ship motions? The rigid links model, the flexible links model or a direct relation between the measured motions in the centre of gravity of the ship?
2. What is the excitation frequency which amplifies the motion of the system?
3. What is the influence of noise in the measurement system on the model results?
4. What parameter has the most influence on the predicted cable forces?
5. Which ship motion is governing for the predicted cable forces?

3. RESEARCH STRATEGY

Before an operation commences, weather data will be received by the ship which states what the expected weather conditions are at the time of the operation. These weather predictions can be used to calculate the expected ship motions during the operation. Based on these ship motions one wants to be able to predict whether there is a risk of uplift occurring during the operations. The goal of this thesis is to present a computational model to predict time-varying cable forces for the operational setting that the stinger is lifted out of the water. These time varying cable forces can ultimately be used to find statistical properties of the predicted cable forces, which in turn can be used to calculate the chance of an uplift occurrence.

3.1 INITIAL COMPARISON

Previous to the creation of the dynamic models a direct comparison was performed between the measured cable forces and the motions at the centre of gravity of the ship. Simultaneously measured data is available of both the cable forces and the ship motions sim, which will be used as input (motions) for the model and verification (cable forces). The purpose of this is to find out the usability of specific ship motions for the prediction of cable forces, which ship motions are governing for the cable force prediction and which are not. It appeared that, that the pitch motion is the most influential motion for the cable forces. However, a type of prediction of the cable forces directly by the time traces of the motions in the centre of gravity is not considered accurate enough. For the complete data analysis please refer to Chapter 5.

3.2 MODEL QUALITIES

Two linear models were created to predict cable forces based on ship motions: the rigid links model (RL model) and the flexible links model (FL model). Each model describes the forces using different assumptions and methods.

The RL model assumes the complete system of the ship, stinger and hang-off wires to be rigid. It is created using linearized rigid body dynamics through which expected inertia forces acting on the hang-off cables can be predicted. The limitation of the RL model is that it is not possible, using this model, to see the interaction between the stinger and the sheaves, while the load cell which measures these cable forces could actually be influenced by these sheaves and their interactions with the equipment. Furthermore, the model does not allow for expansion or the adjustment of model parameters. It is not possible using the RL model to create a more accurate prediction of the amplitudes of the cable forces occurring. A detailed description of the RL model can be found in Chapter 6.

For the creation of the FL model the Lagrangian formalism is used. The FL model accounts for: cable flexibility, relative motion of the hang-off system and the stinger, stinger dynamics, sheave dynamics, some dissipation terms in the form of viscous damping, coupled motions of the sheaves and the stinger, optionally inclusion of sheave friction and static buoyancy. The limitation of the FL model is that damping, as introduced, is not a realistic representation of the dissipation in the actual system. Furthermore, it does not account for non-linear effects influencing the cable stiffness of the wires. Therefore, the damping introduced in the system is an estimated or fitted parameter which accounts for some dissipation in the system. A detailed description of the FL model can be found in Chapter 7.

3.3 MODEL PERFORMANCE

In order to review model performance an input data trace of measured ship motions was used. A simultaneously measured cable force data trace is used in order to validate the model results. The same input data is used for all models and therefore they can be compared with both the measured cable force data trace and with each other. Comparing model results with the measured data will provide information on the accuracy of the predictions. Consequently, this accuracy information can be used to compare which model is the best model to predict the cable forces based on ship motions for this particular case. The performance of the RL model is reviewed in Chapter 6 and that of the FL model is reviewed in Chapter 7.

From reviewing the models, it is apparent that the performance of the FL model is better than the RL model in prediction of the cable forces based on the ship motions at the centre of gravity, for the cases considered in this thesis. This can be found in Chapter 8. It appears that the FL model is preferable

because it accounts for stretching of the cables it allows for relative motion of the stinger and the top sheaves.

The primary recommendation considering the FL model itself is to improve the model by getting a physical grasp on the damping in the system. If one wants to continue the uplift analysis using the current model, it is recommended to test the current model on a different time trace before elaborating it by implementing stinger submergence. More explanation and additional recommendations can be found in Chapter 9.

4. GENERAL ANALYSIS

Starting of this graduation thesis a general analysis was performed, which serves the purpose of giving insight into the ship's equipment, the ship layout and the physical factors that could influence the uplift phenomenon. Note that the ship equipment and ship layout have already been elaborated on in Chapter 1. Also, in Chapter 2 the definition of the phenomenon is given, providing some insight in the actual phenomenon considered. In this Chapter the identification of potential factors involved in stinger uplift is described.

4.1 FACTOR ANALYSIS

There are many external loads or phenomena which could influence the occurrence of stinger uplift. At first, all possible influences are noted, after which the main factors of influence are chosen. In this section the different factors are listed which were found to be of importance considering the stinger uplift. A total overview of the identified factors is given in the sketch of Figure 4.1.

4.1.1 SHIP MOTIONS

Logically, ship motions can excite the stinger and the hang-off system. Therefore it is logical to consider ship motions to be one of the main factors influencing the cable forces in the hang-off system. The ship motions generate inertia forces of the stinger which causes force excitations on the cables. Thus ship motions contribute to the variation of tensions in the hang-off cables.

Indirectly the ship motions (can) cause:

- Change in buoyancy
- Cable stretching (depending on the stiffness of the cables)
- Sheave motions
- Stinger motion
- Slamming

4.1.2 ENVIRONMENTAL LOADS

Next to the ship motions the forces on the system induced by the environment is one of the factors that could influence the occurrence of a stinger uplift. For various stinger positions different environmental forces should be accounted for. If the stinger is positioned in the water the following environmental forces apply:

- Buoyancy
- Change in buoyancy
- Waves
- Current
- Slamming

The buoyancy reduces the net weight of the stinger acting on the hang-off wires. The waves and the current excite forces on the trusses of the stinger. Furthermore, these environmental forces cause changes in buoyancy and ship motions. If the stinger is positioned in the water with a pipeline or A&R (abandonment and retrieval) cable on the stinger another environmental factor which influences the forces acting on the stinger needs to be added: the water depth. It influences the operational settings chosen, the vertical length of the pipeline in s-lay and thus its tension. When the stinger is lifted out of the water, wind excites forces in the same way as currents do. However, wind force is expected to excite lower forces on the stinger compared to the forces by waves, current and buoyancy.

4.1.3 ON-BOARD EQUIPMENT

A direct influence on the hang-off cable tension is the static weight of the stinger and parts of the hang-off system. The static weight of the stinger includes the weight of rollerboxes, walkways and pup-pieces. The self-weight of the wires should be accounted for as well.

During operation a pipeline or an A&R cable can be present on the stinger. These items are under tension, thus next to the self-weight of the pipeline or A&R cable contributing to the measured cable forces, the applied tension in these items also generates force components. A tensioner is a type of equipment which keeps a pipeline under tension while operating. This prevents the pipeline from buckling. Also, environmental forces acting on the pipeline or A&R cable contribute to the forces these equipment pieces excite on the stinger.

Naturally, changing the cable length of the hang-off system by reeling will change the moments about the main hinge and thus influence the forces measured in the cables.

Another influence could be the bow thruster wake, which works in the same way as currents excite forces on the stinger members. However, this effect is estimated to be very small and is assumed to have little or no influence.

4.1.4 OPERATIONAL SETTINGS

Operational settings have a large impact on the forces measured in the hang-off cables either directly or indirectly. Some direct influences are:

- Stinger hinge angles
- Tensioner force
- Ship velocity
- Draught

Stinger hinge angles influence the cable forces directly, due to change in locations of the centres of gravity of the stinger sections and all the equipment the stinger sections contain. The locations of these centres of gravity are crucial for the static moment acting on the hang-off cables and the cable angles. Furthermore, the stinger hinge angles determine which parts of the sections are submerged and therefore subjected to environmental forces, as explained in section 4.1.2.

In the second paragraph of section 4.1.3 it is indicated that the tensioner forces determine the tension in the pipeline, which excites forces on the stinger and thus results in the cable forces.

An indirect effect influencing the hang-off cable forces is draught. Varying the draught of a ship can cause different ship motions and affects the measure of stinger submergence depending on the stinger angle.

Another phenomenon to take into account is ship velocity, which has an effect on the relative velocities of waves and current and it can enlarge the thruster wakes. However, the ship velocity while operating is very low. Therefore, the influence is insignificant compared to the direct effects of environment and operational settings.

4.1.5 DEFORMATIONS

Other physical effects which, although small, could have an effect on the cable forces, are:

- Deformation of the stinger
- Deformation of the hang-off structure
- Stretching of the hang-off cables

The deformations indicated above have a range of effects. The most important one is the potential to deform to such extent, resulting in a change of the location of the centres of gravity, by for example the stretching of the ropes. Deformation of the hang-off structure and of the stinger could influence the amount of submerged volume. It could also change the exact angle at which the waves and current hit a member of the stinger sections.

4.2 EVALUATION OF THE GENERAL ANALYSIS

In the previous section the factors influencing the occurrence of stinger uplift is described in detail, including their significance to the uplift analysis. The factors which have major influence are considered in the analysis performed in this research study. It is chosen to take the following factors into account:

- Ship motions in the x,z -plane (2-D).
- Equipment weights
- Stinger hinge angles
- Draught
- Stretching of the hang-off system's steel wire ropes.
- Sheave motion
- Stinger motion

First a rigid links model (hereafter: RL model) will be set-up which uses the first four points. Then the last three points are added in the flexible links model (hereafter: FL model) described in Chapter 7.

Furthermore, it should be noted that the situation considered for this thesis is the operational setting where the stinger is lifted out of the water, as has been announced in the research strategy in Chapter 3.

This is done to prevent too many factors from influencing the cable forces when doing the initial predictions on ship motions causing cable force variation.

As indicated at the start of this chapter a summarizing overview of all mentioned factors is given in Figure 4.1.

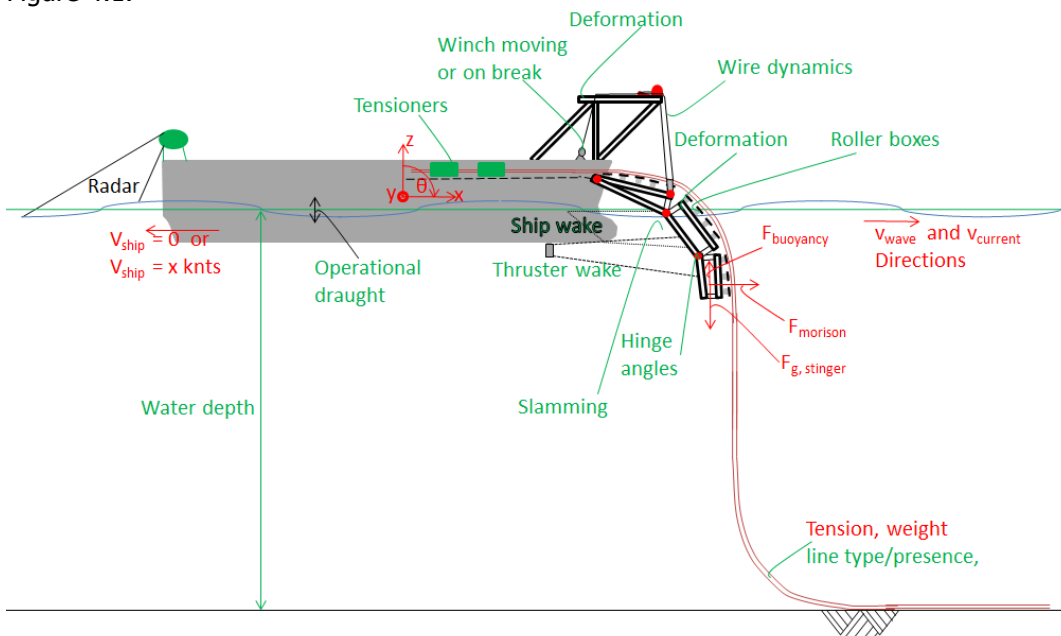


Figure 4.1 Result of the general analysis.

5. DATA ANALYSIS

The goal of the data analysis is to make on board measured data usable for several purposes. Either for performing calculations to obtain predictions of the cable forces or for validation of these predictions. Another purpose of the data analysis is to find out if prediction of cable forces through ship motions is indeed possible and which ship motions are most important for the cable force prediction.

On board of the Audacia there are many physical effects which are being measured. This includes motions, forces, speeds, angles and many more. To be able to predict an uplift occurrence one must be able to calculate cable forces as function of time. To predict these cable forces, information is needed on multiple factors described in Chapter 4, such as the ship motions. Furthermore, the flexible links and rigid links models, which will be elaborated on in Chapters 6 and 7, predicting the cable forces should be compared with measured data of the cable forces to validate the calculations. Following from the general analysis conclusion in section 4.2 and the in Chapter 2 described model requirements; the following data traces are obtained:

1. The ship motions as input, to predict the cable forces based on these motions.
2. The cable forces as validation, to validate if the cable forces are calculated correctly.

These time traces are raw data traces and their data must undergo some processing before this data is usable. Only if the data has been resampled and has been filtered, it can be used to compare against predicted values, with other data traces.

When working with offshore data traces one must take into account that within certain amounts of time the sea state can change significantly. Therefore a 3-hour data range will be used for the spectral data analysis.

5.1 DATA LOGGER

Before elaborating on the data processing necessary, first the type of system where the data comes from is described. The data used in this thesis is obtained from the Audacia's data logger. The data logger uses a single system with one single master clock which time stamps all data. Therefore, all parameters work with a single master clock system and thus are logged at approximately the same time instance.

One data processing action within the logging system is the transformation of amperes into the required units, as for example tons (which is used by the logger for the stinger hang-off cable loads). The documentation on the measurement and transforming equipment does not mention a type of filtering for the measured cable forces. The documentation does however mention that some motion directions are measured using accelerations which are then interpolated to obtain the displacements. Bias caused by this operation is nullified by an internal filter of the equipment itself.

The cable forces are measured by multiple tensile load cells. The ship motions are measured by the Octans (a measuring unit measuring both angular and linear motions) which measures the motions of the sensor and converts this data to the motions occurring at the centre of gravity of the ship. This conversion is necessary since the measuring unit is not located at the centre of gravity of the ship.

Because data is electrically transported through the system, the latency between measurement and time stamping can be of a duration up to a few milliseconds. This means there can exist a delay between the measured data trace's time stamping and the actual physical effect occurring. When working with multiple equipment pieces this can cause a slight delay between two different data traces of two different measurement devices. If this is the case, one would observe a constant time delay and if that is the case the delay can easily be filtered out.

The documentation on the measurement equipment states the measurement errors inherent to the system's resolution. These errors are given in Table 5.1. The data of this table is used to check the possible influence of input errors on the prediction of cable forces. This check is described in section 7.10.

Measured parameter	Error
Heave	0.025 meters or 2.5%, whichever is larger
Surge	0.025 meters or 2.5%, whichever is larger
Pitch	0.01 degrees
Hang-off cable forces	0.1% plus 0.01% per degree Celsius of the reading

Table 5.1 Errors of the measurement equipment.

5.2 RESAMPLING DATA

As mentioned at the beginning of this chapter, the raw data needs to be processed before it can be used. There are multiple difficulties when using the raw data which need to be solved. It should be pointed out that operations such as for example reading out the data logger files into Matlab are described in Appendix A.

The first complication of the use of raw data is that the measurement equipment measures its physical parameters with a frequency of approximately, but not exactly, one Hertz. Therefore, the measurement time steps are not constant. The second encountered difficulty is that if the parameter being measured remains constant for a period of time the data logger does not create new time stamps each second with the same parameter value [1]. Instead it will not record any new value until the measured parameter changes magnitude. This means there are time gaps in the measured time traces where the traces contain no time or parameter value information. Though knowing that the jumps should have the value of the previous unchanged parameters it is possible to fill the gaps.

Firstly the solution to the second complication is given: the time gaps present in the measured data. As stated in an earlier paragraph, the time gaps are caused because the parameter which is being measured remains constant for a period of time. The data logger will in response not record any new measurement as long as the parameter remains constant. This means that each value to be interpolated needs to be the value of the last logged parameter before the time gap. An example sketch of this interpolation is given in Figure 5.1.

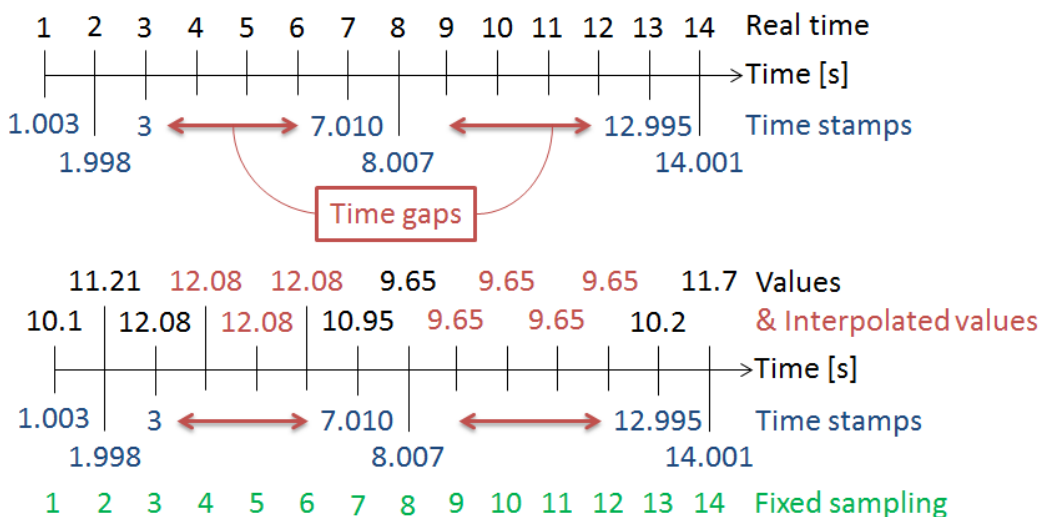


Figure 5.1 Example sketch of the "previous" and "nearest" interpolation type.

Interpolating the gaps (indicated with the red arrows and numbers) with this "previous" interpolation method gives the interpolated values at exact time steps of one second. However, there are still time steps within the usable time ranges (the black numbers) which contain time stampings of not exactly one second but which are a few milliseconds off of the one Hertz sampling. For the resampling of these data ranges a sample rate has been chosen of one second, the same as for the interpolation of the time gaps. This particular time step was chosen to keep the resampled data as close as possible to the real measured data. The resampling of the usable time ranges (the black numbers) to exactly one second is performed by finding the inexact time steps corresponding to the rounded time steps of a predetermined time vector (which contains time steps of one second). The values of the inexact time steps are then linked to the rounded time values. This method is essentially a "nearest" interpolation method and was chosen because the original stamping is just a few milliseconds off of the target value.

5.3 FILTERING DATA

It is not yet possible use raw data after resampling for the calculation of cable forces and for validation. The raw data can still contain disturbances which distort the data in comparison with what physically occurs. In this thesis distortion is frequency information in the data which lies outside of the frequency range of natural ocean waves and thus ship motions. This noise will need to be filtered from the data to gain time traces which contain information of the physical effects of interest only.

There are multiple causes of noise. For example, it could be introduced by the measurement equipment itself, radio frequency interference, electromechanical interference, moisture and temperature. All these phenomena can interfere with the electrical signal moving from the load cell to the controller.

To be able to filter the data, the data should first be transformed into the frequency-domain by using a fast Fourier transform (an optimised form of the discrete Fourier transform in computation time), after which the filter can be applied. Then the results are reviewed in both the frequency-domain as in the time-domain. A flow chart of this is shown in Figure 5.2. A more comprehensive description of these steps is given in the following sections and more information on the fast Fourier transform can be found in Appendix B.

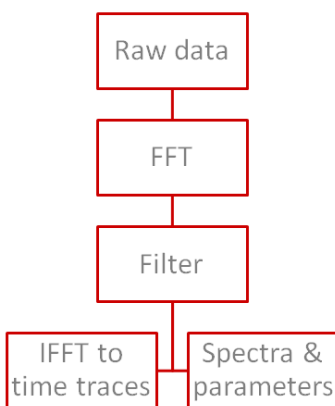


Figure 5.2 Flow chart of the filtering process and the data analysis.

5.3.1 FILTER

A basic filter is applied to remove unwanted frequencies from the frequency-domain traces. The frequency domain traces contain information for frequencies from zero up to infinity. Filtering the data is performed by finding the wanted frequency range (see section 5.3.2) and removing the unwanted frequency information. Because the calculations in this thesis consider external forcing by ship motions one is interested in the frequency range in which ship motions can occur. Since ship motions are induced by waves, the frequency range of interest is thus the frequency range in which natural waves can occur.

The filtering is performed by selecting the wanted frequencies within the total frequency domain. This means a rectangular cut-off window is used, also called a band filter. No edge-smoothing functions are applied in this case which could in theory cause spectral leakage [2] and ringing [3]. These effects have been elaborated on in Appendix B. As an example the unfiltered energy density spectrum of the cable forces in the stinger hang-off cables is shown in Figure 5.3. In Figure 5.4 the filtered energy density spectrum of the cable forces in the stinger hang-off cables is shown.

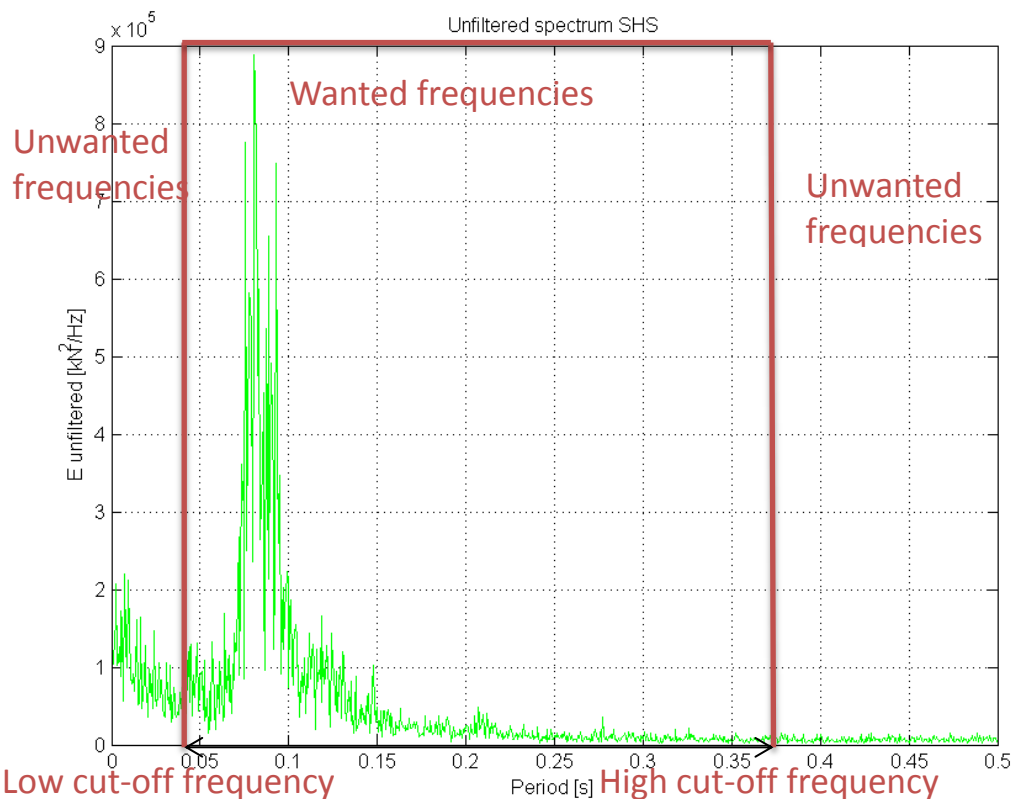


Figure 5.3 Unfiltered density spectrum of stinger hang-off system measured cable forces.

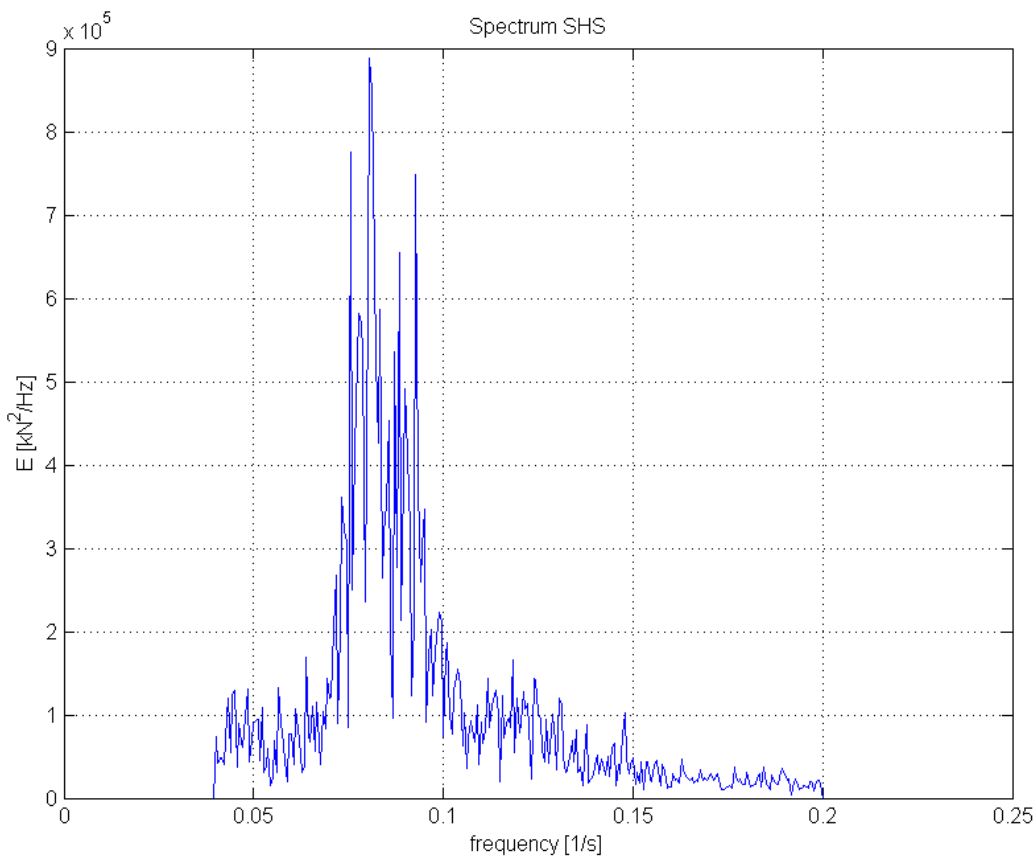


Figure 5.4 Filtered density spectrum of stinger hang-off system measured cable forces. Note that the x-axis has been reduced in size in comparison with the previous figure.

5.3.2 FILTER RANGE AND NYQUIST FREQUENCY

Since, as stated in the enumeration at the beginning of this chapter, ship motions will be used as an input variable to predict the cable forces. The frequency range of interest is the frequency range of natural waves which cause these ship motions. The periods of natural waves usually lie between 5 seconds and 25 seconds. Therefore, the cut-off frequencies of the filter to be applied lie at 0.2 Hz and

0.04 Hz. However, these values are applied only if the Nyquist frequency falls outside of this frequency range.

Since the sampling time is one second and the Nyquist frequency is calculated using equation 5.1 [4], the cut-off frequency to prevent aliasing is 0.5 Hz. This means any frequency higher than 0.5 Hz should be removed from the data.

$$f_{Nyquist} = \frac{1}{2 \cdot \Delta t} \quad 5.1$$

In which:

$f_{Nyquist}$: The Nyquist frequency [Hz]
 Δt : Sampling time [s]

As can be seen the Nyquist frequency, for a sampling time of one second, would be a higher upper limit than the cut off frequencies defined earlier in this section. Since the upper limit from the natural waves' frequencies is lower than the maximum Nyquist frequency, the upper limit of natural wave frequencies is chosen as the upper limit for the frequency band. This limit is the 0.2 Hz corresponding to the minimum wave period of 5 seconds.

5.3.3 FREQUENCY PLOTS

Using the data in the frequency-domain several spectral plots were constructed. These spectral plots are useful to find the frequencies at which a specific parameter contains most of the energy. The energy spectrum is calculated with equation 5.2 [4].

$$E_d = \frac{0.5 \cdot YY^*}{df} = 0.5 \cdot YY^* \cdot dt \quad 5.2$$

In which:

E_d : Spectral energy [J/x²/Hz], in which x is the unit of the parameter considered (Y).
 Y : Filtered parameter values in the frequency-domain. Note: the *-symbol indicates the use of the complex conjugate.
 df : Frequency step [Hz]
 dt : Time step [s]

The data trace used in this thesis is only one wave record from which the energy spectrum is estimated as indicated above. However, these traces only give a single measurement per time step from which the energy density must be estimated. With only one data trace to work with this estimate is a raw estimate and can have a large error. To reduce the error with a factor 2.45 [4] the data trace was separated in six segments. The equation with which the factor was calculated is given in equation 5.4.

$$er_{red} = \frac{1}{\sqrt{p}} \quad 5.3$$

In which:

er_{red} : Reduction of error
 p : Number of sections

These segments are separately Fourier analysed after which their energy densities is estimated with the average of these values for each frequency separately [4]. This is called ensemble averaging. The downside of segmenting the data traces when making spectral plots is that segmentation can cause spectral leakage. While creating the spectral plots, no windowing function was used to mitigate spectral leakage [2]. It is expected to have little influence on the models and their results so no steps of mitigation were taken concerning spectral leakage at this point. Nonetheless, the influence of this effect is tested in section 7.12. Furthermore, additional information on spectral leakage can be found in Appendix B.

When filtering has been applied the energy spectrum obtained still looks "grassy", as in Figure 5.4. To create a more "readable" spectrum in order to find the actual peak frequencies the energy spectrum will be plotted in bins. Bins are a collection of frequency steps containing a certain amount of energy. The energy spectrum in this analysis has been plotted using an equal energy method, which means that all bins should contain an equal amount energy. Therefore, if there is more energy in a certain range of frequencies, the bin width will become smaller and if there is less energy at a certain range of frequencies, the bin width will increase. This target value of equal energy is defined in such a way that

the maximum spectral peaks have a bin width of no more than five times the frequency step. Using this method one can easily identify the peak frequencies but the method does results in an overall less detailed spectrum. The resolution at less relevant frequencies is greatly reduced. The less relevant frequencies, in this thesis, are the frequencies containing low energy. This effect is observed because more frequency steps are required to fill a bin with the energy required to equal the energy in the other bins. Figure 5.5 shows the binned energy density spectrum of the cable forces in the stinger hang-off cables, including the bin boarders.

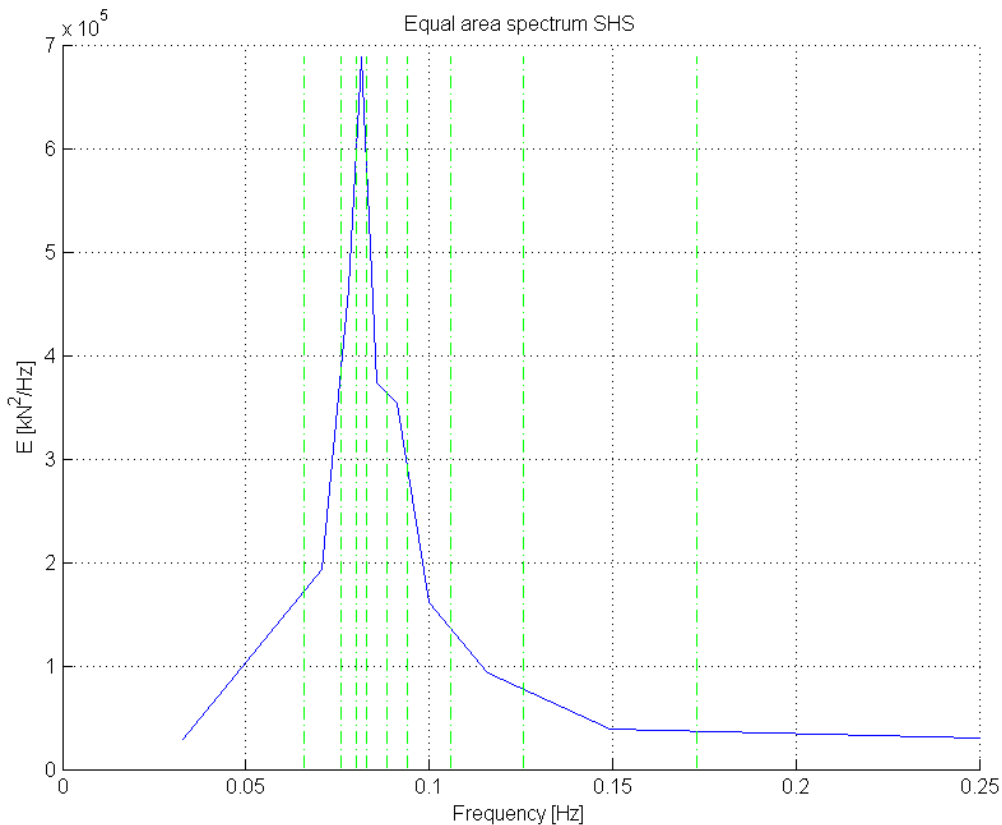


Figure 5.5 The energy density spectrum of the measured cable forces. Bin boarders are shown with green dotted lines.

5.3.4 INVERSE FOURIER TRANSFORMATION

Filtering the data traces in the frequency domain removes noise present in the data. The effect of this is that the measured data trace gives a more real and accurate representation of the real situation when transformed back into the time-domain. An example of the improvement of a time trace is given in Table 5.2. As can be seen, the standard deviation of the unfiltered time trace exceeds that of the filtered time trace. The standard deviation calculated through the 0th-order moment of the frequency-domain spectra should give about the same results as the standard deviation calculation of the filtered time trace. As can be seen this is not the case. This is due to the raw data which contains round-off errors inherent to the measuring equipment. Adding to this, when recalculating these data points through resampling and filtering, numerical errors are introduced. These two types of errors prevent the time-domain values transformed by the Fourier function of having an exact complex conjugate. Therefore, when transforming the data back from the frequency domain to the time-domain, the time-domain values are no longer real values. To avoid this problem one can force the system into symmetry, avoiding these small errors, and then transform the data from frequency-domain back to time domain. This has been explained in Appendix B. When not using this symmetric function the spectral standard deviation is approximately equalled by the filtered standard deviation of the time trace.

The equation for the calculation of the zeroth order moment is given in equation 5.4 [4]. To obtain the standard deviation one must take the square root of the 0th-order moment.

$$m_0 = \int_0^{\infty} f^0 E_d(f) df \quad 5.4$$

In which:

m_0 : 0th-Order moment [x], in which x is the unit of which the density spectrum has been plotted. In this example of the cable forces x would be in [kN].

- f^0 : Central bin frequency in [Hz]. The zero power is used because the 0th-order moment is being calculated.
- E : Variance density spectrum in [x^2 /Hz], in which x is the unit of which the density spectrum has been plotted. In this example, x would be in [kN].

Standard deviation calculation type	Spectral ($\sqrt{m_0}$)	Filtered	Unfiltered
Standard deviation cable forces [kN]	170.7	267.7	311.3

Table 5.2 Example of data results after data filtering in the frequency-domain for the measured cable forces.

5.4 DIFFERENTIATION OF DATA

The input data consists of displacements or displacement angles. Considering that the input data is used to review the ship motion effects on the cable forces and that the cable forces are subjected to the inertia forces of the stinger, it is interesting to review the accelerations in all motion directions. To obtain the accelerations in the current motion direction the data vectors must be differentiated. This can be done either by performing numerical differentiation [5] or by differentiation in the frequency domain. The preferred option for differentiation in this thesis is the differentiation in the frequency domain. This option was chosen because the use of numerical differentiation generates noise in the high frequency region of the data [6].

Differentiation in the frequency domain means that the data traces will be differentiated with respect to time in the frequency-domain. It is applied after the data time trace has been transformed to frequency domain using the fast Fourier transform and after the noise is filtered. The idea behind the frequency-domain differentiation is that the signal is represented as a summation of sinusoids and these sinusoids are apparent after applying the fast Fourier transform. In frequency-domain one consequently has information on both magnitude and frequency of the sinusoids. When differentiating a sinusoidal function in the time domain it has the form of equation 5.5. In frequency domain this is no different, so equation 5.6 can be applied. The data of the Fourier transform is multiplied with the imaginary frequency of the signal.

$$\frac{dv}{dt} = \frac{d}{dt}(B e^{i\omega t}) = i2\pi f B e^{i2\pi f t} \quad 5.5$$

$$\frac{d}{dt}v(t) \leftrightarrow i2\pi f V(f) \quad 5.6$$

In which:

- v_t : A random time function
 V_t : Random time function's representation in frequency domain
 B : Amplitude
 ω : Rotational frequency in [rad/s]
 f : Frequency in [Hz]
 t : Time [s]

In order to obtain acceleration the same principle can be applied once more. The frequency-domain differentiation prevents the introduction of noise in the higher frequencies of the data in contrary to the numerical differentiation. Derivation in general does, however, emphasize the higher frequencies when differentiating because of the multiplication of the frequency term becomes larger with each frequency step. That means that high frequency noise, which is always present in measured data, will also be emphasised. This phenomenon is illustrated in Figure 5.6. More on this subject can be found in section 7.12.

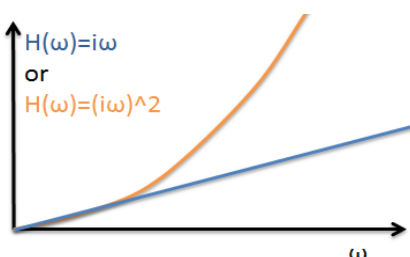


Figure 5.6 The effect of differentiation: Emphasizing the higher frequencies.

5.5 COMPARISON OF FREQUENCY-DOMAIN PLOTS

Of the motion data available both the displacements and the accelerations are motions of interest. The displacements are of interest when reviewing relative displacements when assuming the cables of the system as springs. However, if inertia forces are the core interest, it is better to review the accelerations by differentiating the input data. Since the first model, the rigid links model (Section 6), is based on accelerations it was chosen (for the sake of brevity) to elaborate on the accelerations only in this section. The accelerations will be reviewed both using frequency plots in this section and time traces in section 5.6.

The frequency plots of the ship accelerations of the ship's centre of gravity in the 2-D (vertical x,z-plane) are compared against the frequency plot of the measured cable forces. The peak frequencies and some additional frequencies of interest are given in Table 5.3. The frequency plots of the measured cable forces and the pitch acceleration have been included as per example. They can be found in Figure 5.7 and Figure 5.8. The numbers in the figure correspond to the numbers in the table to clarify which values are noted in the table from which part of the plots.

One exception is made for assumption of the 2-D analysis. The exception is made for the roll motion. For this motion, the spectrum is reviewed to see if there was reason to believe that the roll motion has more influence than initially expected. The peak frequencies of roll are included in Table 5.3 and the frequency plots can be found in Appendix C. It is apparent from the frequency plot analysis that the roll motion has no similarities with the cable forces.

Frequency spectrum	f_{peak} [Hz] (1)	$f_{\text{Left hand side, peak}}$ [Hz] (2)	$f_{\text{Right hand side, peak}}$ [Hz] (3)	$f_{\text{others of interest}}$ [Hz] (4)
Measured cable forces	0.08167	0.07084	0.08584	0.0914
Heave acceleration	0.07584	--	--	0.09918 up to 0.2
Pitch acceleration	0.08167	0.07806	0.08584	0.0914
Surge acceleration	0.07528	--	0.09334	--
Roll acceleration	0.07834	--	--	0.1247 up to 0.2

Table 5.3 The frequencies of interest from the frequency plots of the ship accelerations and measured cable forces. The table includes ranges of frequencies of interest. The numbering corresponds to the figures below.

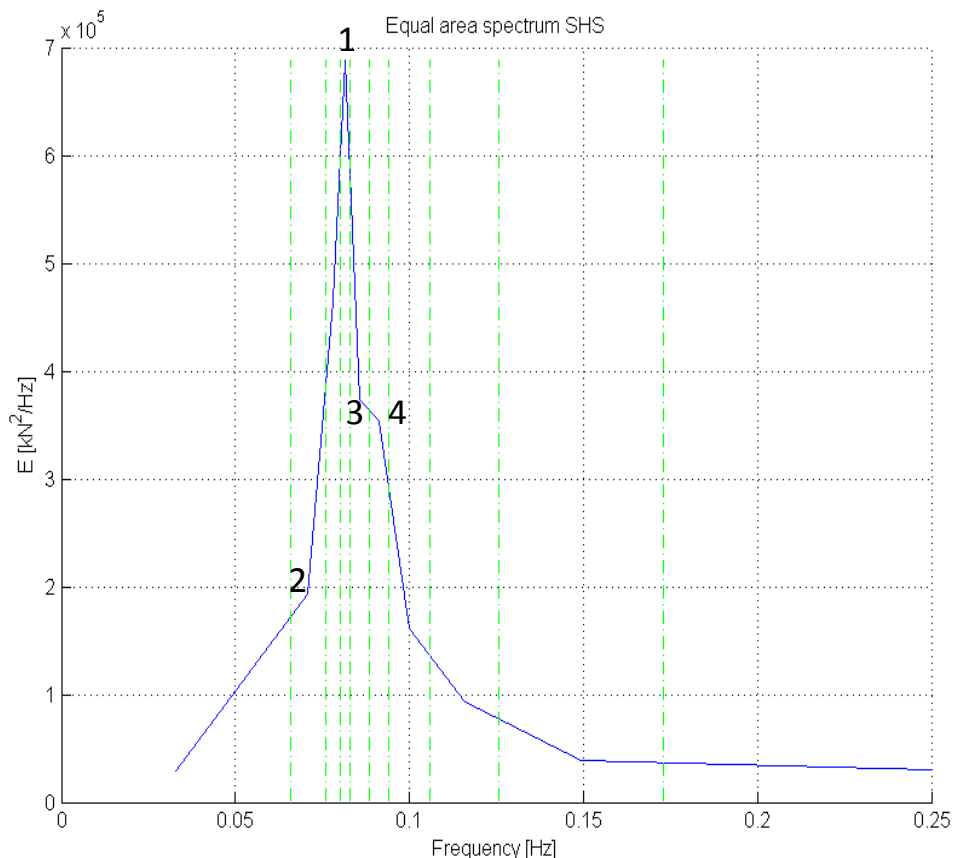


Figure 5.7 Binned frequency spectrum of the measured cable forces. Numbers correspond with Table 5.3.

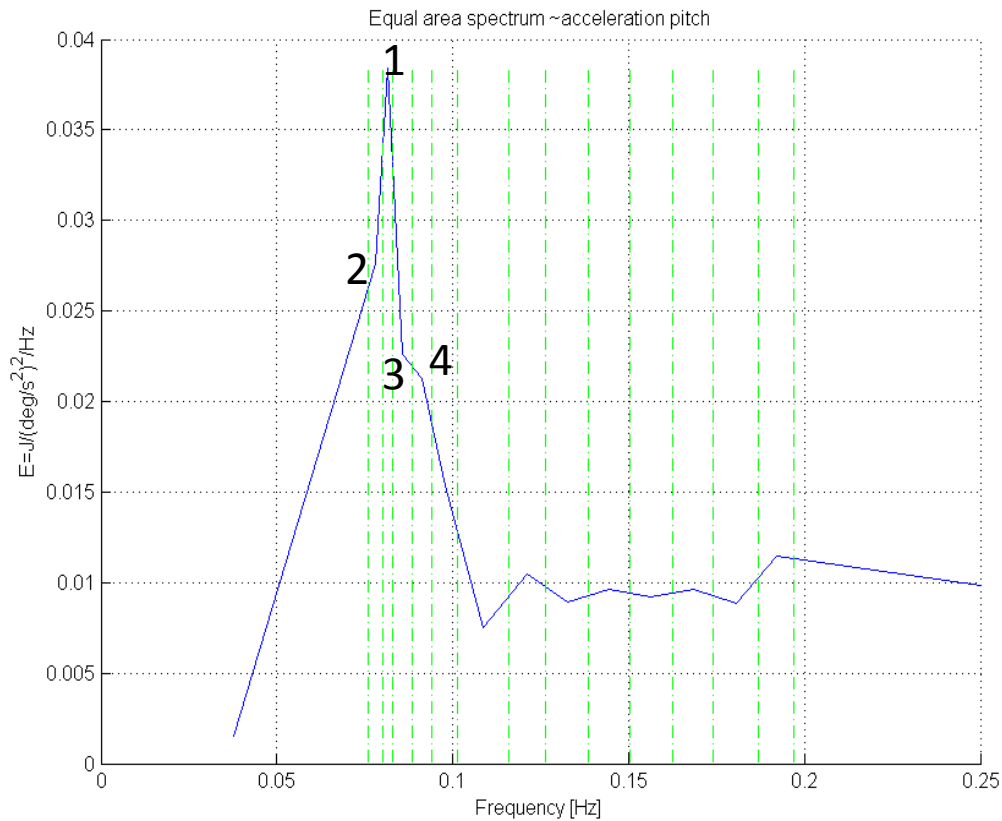


Figure 5.8 Binned frequency spectrum of the pitch acceleration. Numbers correspond with Table 5.3.

A review of the spectral plots, shows that the pitch acceleration has the most influence on the cable forces. This can already be seen by just reviewing the values given in Table 5.3. The pitch acceleration does however show a larger low frequency area and some high frequency noise emphasised by the differentiation of the displacement data. This emphasis is confirmed when comparing the displacement and acceleration frequency plots in Appendix C. This high frequency information is considered as noise since it is not seen in the frequency plot of the measured cable forces. More information on this high frequency content can be found in section 7.12.

5.6 COMPARISON OF TIME-DOMAIN DATA PLOTS

Apart from the comparison of frequency-domain plots another possibility is to transform the filtered data traces from the frequency-domain back to the time-domain using the inverse fast Fourier transform as described in section 5.3.4. In this analysis, the measured cable force time trace will be plotted against and compared with all centre of gravity accelerations in the 2-D situation, i.e. x,z-plane.

It should be pointed out that the only exception made on the assumption 2-D analysis is the fact that the roll motion is reviewed to check whether it is acceptable to consider a 2-D situation in this thesis. The time trace analysis shows that the roll motion has no similarities with the cable forces. This is as expected and confirms that 2-D analysis is sufficient to predict the cable forces, in the cases considered in this thesis. The roll motion time traces can be found in Appendix C.

Following from the frequency analysis, it was concluded that the pitch motion is the most influential motion in the system. This is why this section only considers the pitch motion for the sake of brevity. The normalised time trace of the pitch acceleration is shown in Figure 5.9. It is important to point out that the accelerations in the figure have been negatively plotted since the maximum positive angular acceleration coincides with the minimum cable force. This has been visualized as such, since it is easier to compare the data traces when the traces are not in anti-phase. It can be observed that, using this type of representation, the traces follow the same trend. However, there are differences concerning the shape, the frequency and possibly the phase. A type of prediction of the cable forces directly by the time traces of the motions in the centre of gravity is not considered accurate enough for the case considered.

Note that this plot contains the normalised version of the time traces. The normalisation has been performed using the time trace's own maximum, which is shown in equation 5.7. Therefore, the

amplitudes are greatly scaled in the time-domain plot considered here. In the next chapter, Chapter 6, this will be resolved by comparing the actual inertia force with the cable forces.

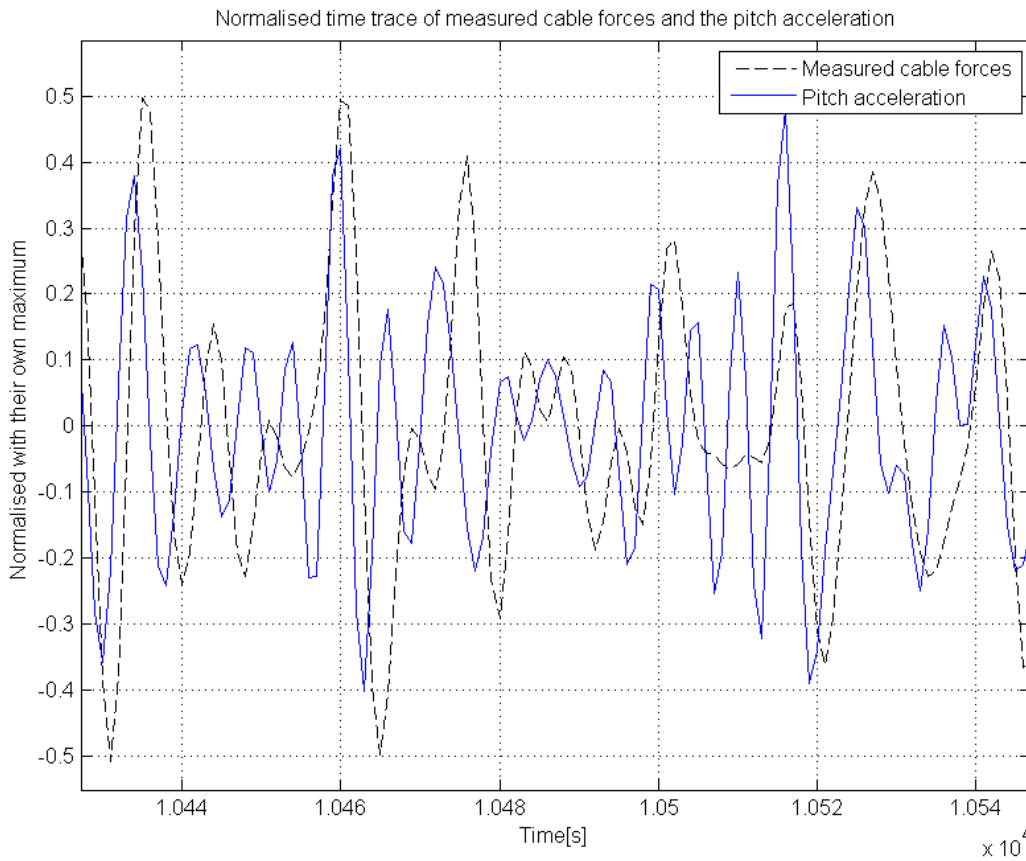


Figure 5.9 Normalised negative pitch acceleration [rad/s²] and normalised measured cable forces [kN].

$$\ddot{\theta}_{normalised}(t) = \frac{\ddot{\theta}(t) - mean(\ddot{\theta}(t))}{max(\ddot{\theta}(t) - mean(\ddot{\theta}(t)))} \quad 5.7$$

In which:

- $\ddot{\theta}_{normalised}$: Normalised pitch acceleration [rad/s²]
- $\ddot{\theta}$: Pitch acceleration in [rad/s²]

However, in this chapter, motions are compared with forces. It will be useful to compare actual inertial force values with the measured cable forces. Therefore, it will be worthwhile to review the spectra and the time traces of the motions and inertia of the stinger connection point. The stinger connection point is the point where the hang-off system is connected to the stinger. This comparison is performed in the next chapter, Chapter 6.

5.7 EVALUATION OF THE DATA ANALYSIS

From the previous chapter it can be concluded that the data processing through resampling and filtering yields better time trace data with less low and high frequency noise than the raw data. The standard deviation has improved from 311 kN to 268 kN (approximately 14% difference) because the noise was filtered from the data traces.

In the spectral plots it is observed what the peak frequencies in the system are and these frequencies can be compared showing that the pitch acceleration is the most influential motion concerning the cable forces which are measured.

The frequency plot and time trace plot of the roll acceleration and displacement both show that it is acceptable to maintain the 2-D analysis in further stages of the thesis instead of expanding to 3-D.

Through comparing the time traces it was found that the conclusions of the frequency analysis were confirmed and the pitch parameter is observed to be the most influential on the cable forces occurring. However the time trace still shows significant differences when compared with the measured cable force

data trace. A type of prediction of the cable forces directly by the time traces of the motions in the centre of gravity is not considered accurate enough. It will be useful to compare actual inertial force values with the measured cable forces. Therefore, it will be worthwhile to review the spectra and the time traces of the motions and inertia of the stinger connection point. This first model type is described in Chapter 6.

6. RIGID LINKS MODEL

In the previous chapter it was concluded that it would be valuable to compare the motion data of the stinger connection point to the measured cable forces in frequency- and time-domain. This means that the motions of the stinger connection point will need to be calculated with the motion data of the centre of gravity of the ship. To provide an overview of the ship, Figure 6.1 has been added. It shows the original motion locations in the centre of gravity (COG), the motion locations which will now be considered (stinger connection point) and the measuring point of the hang-off cable forces (Load cell SHS).

For this new location of interest new reviewing methods are introduced. This results in a more detailed base case analysis (including frequency- and time-analysis). The new reviewing methods are used to:

1. Compare the rigid links model results with the measured cable forces.
2. Compare the rigid links model results with the flexible links, which is performed in Chapters 7 and 8.

The flexible links model which will be introduced in a later stage (Chapter 7).

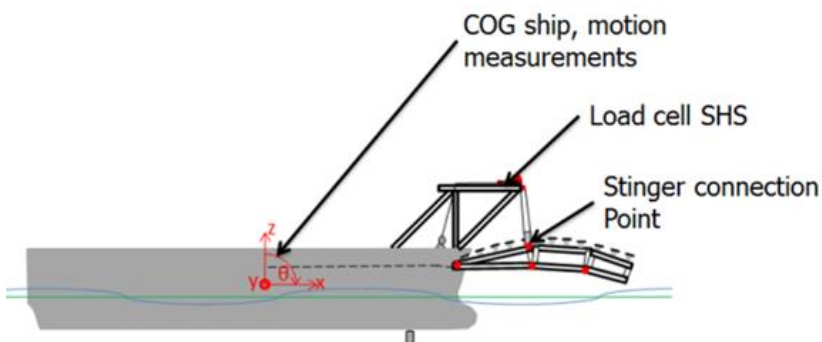


Figure 6.1 Sketch of the measurement motion locations and the measurement location of the cable forces.

6.1 MODEL OF A RIGID BODY WITH RIGID LINKS

To obtain the motions in this the stinger connection point (from now on: scp), linearized rigid body dynamics are used to build the rigid links model (hereafter called: RL model). The formulas, describing the motions in the scp, are given in equations 6.1 up to 6.3 [7]. Note that also in the equations "SCP" stands for stinger connection point.

A sketch of the RL model is given in Figure 6.2. The linearization can be justified by the fact that the angles are small. The maximum pitch angle has a value of approximately one degree, which confirms that the small angle approximation can be used (for this pitch angle). This model thus assumes:

1. The complete ship including the stinger and hang-off system is rigid.
2. The motion angles are small.

Furthermore, only the 2-D situation in vertical x,z -plane is considered in this thesis. This was justified in the previous chapter. The sway, roll and yaw angles are thus not included in the calculations, therefore they are indicated with a red colour.

The motion of interest in this chapter is the motion in the cable direction. The motion in cable direction is calculated through both the z_{scp} -motion and the x_{scp} -motion given in equations 6.1 and 6.3. When the motion in cable direction is obtained, the inertia force can be calculated using the stinger's masses and the acceleration term in this motion direction. The cable force prediction by this inertia force is hereafter referred to as the prediction of cable forces by the RL model.

$$x_{SCP} = x - y_b \cdot \psi + z_b \cdot \theta \quad \mathbf{6.1}$$

$$y_{SCP} = y + x_b \cdot \psi - z_b \cdot \varphi \quad \mathbf{6.2}$$

$$z_{SCP} = z - x_b \cdot \theta + y_b \cdot \varphi \quad \mathbf{6.3}$$

In which:

x	:	Surge in [m]
y	:	Sway in [m]
z	:	Heave in [m]
x_b	:	x-distance from centre of gravity to the stinger connection point in [m]
y_b	:	y-distance from centre of gravity to the stinger connection point in [m]
z_b	:	z-distance from centre of gravity to the stinger connection point in [m]
φ_r	:	Roll angle in [rad]
θ	:	Pitch angle in [rad]
ψ	:	Yaw angle in [rad]

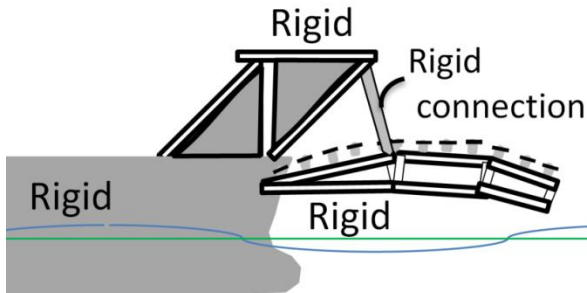


Figure 6.2 Sketch of the rigid body modelled with the linearized dynamical equations.

6.2 FREQUENCY -AND TIME TRACE ANALYSIS

This section contains the time- and frequency-analysis of the RL model. The first section, section 6.2.1, describes the advanced reviewing methods which will be used to visualise and quantify the RL model's prediction properties. Section 6.2.2 provides for the target values. In this thesis the target values are the properties of the measured cable forces. Targets are set for all reviewing methods applied and generate time-trace properties such as mean force and standard deviation. The third section, section 6.2.3, presents the actual time- and frequency-analysis. Note that this chapter's time- and frequency-analysis is used as comparison with the measured cable forces. The comparison with the flexible links model will be performed in Chapters 7 and 8, as stated at the beginning of this chapter.

6.2.1 REVIEWING METHODS

The resulting data traces of all models are reviewed using various methods. These methods are an addition to the observation technique of the time-domain plots. They are used in order to perform a more (detailed) quantitative investigation of the data. The methods are:

1. Normalised cross-covariance over the complete data trace.
2. Standard deviation of the cable force time-traces.
3. Correlation of peak amplitudes.
4. Mean peak amplitude difference.
5. Mean peak time difference.
6. Minimum distance method.
7. Frequency plot and spectrogram.

The first two reviewing methods and the last reviewing method consider the complete time traces. In this thesis it is, however, of interest to be able to predict the peak amplitudes with sufficient accuracy, rather than the dynamic response in the small amplitude region, as stated in the problem definition in section 2.3. This is why reviewing methods are introduced based on only peak values in the predicted and measured time traces. They will give a clearer overview of the best model to use for the prediction of the cable forces.

To achieve this, firstly the peak values of extremes above a chosen threshold value are found for both the predictive data trace and the measured data trace. Subsequently, the peak values should be paired and saved using Matlab [8]. The minimum peak amplitude or threshold value set for the paired peaks is 190 kN, which is a value that excludes all irregular low-amplitude information. Note that this peak finding method is used for all peak correlation types of reviewing methods.

NORMALISED CROSS COVARIANCE PLOTS

This function calculates the covariance of the traces and shifts one of the traces by 1 time step, which in this thesis is 1 second, after each covariance calculation. By calculating the normalised cross-covariance the similarity in shape (and thus behaviour) of the plots is quantified. A value of 1 would mean perfect

correlation, a value of -1 would mean perfect correlation in anti-phase and a value of 0 would mean no correlation.

The function is calculated using equation 6.4 and 6.5 [9]. It should be pointed out that the test does include influence by the low amplitude irregularities. In the lower amplitude region of the time traces shown in the upcoming section 6.2.3, irregular behaviour can be seen, while the larger amplitudes show better correlation. This means the function results can be "distorted" when compared with a case where only peak values are reviewed. The small amplitudes are thus expected to have a negative effect on the total correlation.

$$c_{xy}(ml) = \begin{cases} \sum_{n=0}^{Nl-ml-1} \left(x_{n+ml} - \frac{1}{Nl} \sum_{i=0}^{Nl-1} x_i \right) \left(y_n^* - \frac{1}{Nl} \sum_{i=0}^{Nl-1} y_i^* \right), ml \geq 0 \\ \overline{c_{yx}^*(-ml)}, ml < 0 \end{cases} \quad 6.4$$

$$c_{xy,normalised}(ml) = \frac{c_{xy}(ml)}{\max(c_{xy}(ml))} \quad 6.5$$

In which:

- C_{xy} : The cross covariance of data traces x and y for a time shift of ml
- x_i, y_i : Data trace values of data trace x and data trace y. Note that the *-symbol indicates the use of a complex conjugate.
- Nl : Length of the data traces
- ml : The time shift or also called the lag

STANDARD DEVIATION

The standard deviation is applied over the complete time trace and defines the amount of variation or dispersion of the amplitude values from the mean value over the total data trace. The standard deviation value can be compared with the standard deviation target value. The target standard deviation (set by the measured cable forces) thus indicates the amount of variation expected from the models. The function which is used to calculate the standard deviation is given in equation 6.6 [10].

$$S = \sqrt{\frac{1}{N-1} \sum_{i=1}^N |A_i - \mu|^2} \quad 6.6$$

In which:

- S : Standard deviation of a data trace in [kN]
- N : Vector length of the data trace
- A_i : Amplitude of vector value i of data trace A in [kN]
- μ : Mean value of the data trace in [kN]. An index indicates the specific data trace of which the mean value was taken.

CORRELATION OF PEAK AMPLITUDES

The correlation coefficient is applied on the vectors of paired peaks only. The function is essentially the division of the covariance of the two vectors by the multiplication of each vector's standard deviation. The correlation coefficient is the measure of linear correlation between the vectors. This reviewing method can take up values between -1 and +1 in which -1 indicates a negative correlation, +1 a positive correlation and 0 indicates no correlation at all. It should be pointed out that this correlation type does not indicate the slope of the linear function related to the two vectors. It indicates the rate of spreading about the best fit line through the scatter plot of the two vectors. So, when the correlation coefficient takes a value of 1, this essentially means that the behaviour of the traces is the same. The equation of the normalised correlation coefficient is given in equation 6.7. [11]

$$\rho(A, B) = \frac{1}{N-1} \sum_{i=1}^N \left(\frac{A_i - \mu_A}{\sigma_A} \right) \left(\frac{B_i - \mu_B}{\sigma_B} \right) \quad 6.7$$

In which:

- ρ : Normalised correlation coefficient of peak values, also called the normalised covariance of peak values. The closer the value is to 1 the better the correlation.

- A_i/B_i : Amplitude of vector value i of data trace A or B in [kN]
- $\mu_{-/A/B}$: Mean value of the data trace in [kN]. An index indicates the specific data trace of which the mean value was taken
- $\sigma_{A/B}$: Standard deviation of data trace A or B in [kN]

MEAN PEAK AMPLITUDE DIFFERENCE & TIME DIFFERENCE

The mean of the difference in amplitudes and time of the peak values provide an idea of the average values with which the predicted peaks are off target. The mean peak amplitude difference indicates how accurately the amplitudes are predicted by the model and the mean time difference indicates the mean delay of the model prediction when compared with the measured data trace. The equations of both reviewing methods are given in equation 6.8 and 6.9.

$$\Delta A_{mean} = \frac{1}{N} \sum_{i=1}^N A_{peak,i} - A_{peak,target} \tag{6.8}$$

$$\Delta t_{mean} = \frac{1}{N} \sum_{i=1}^N t_{peak,i} - t_{peak,target} \tag{6.9}$$

In which:

- ΔA_{mean} : Mean peak amplitude difference in [kN]. The smaller this value is the closer the two peaks are in amplitude .
- Δt_{mean} : Mean peak amplitude difference in [s]. The smaller this value is the closer the two peaks are in time.

MINIMUM DISTANCE METHOD

The idea of this reviewing method is that each pair of Δt and ΔA values (obtained through equation 6.8 and 6.9) can be plotted in a graph. For each peak comparison the graph has the peak of the measured data trace as its origin and on the graph the peak of the predicted data trace is plotted. Figure 6.3 has been provided for clarification of this method. This predicted peak quality is defined by a certain time and amplitude difference and thus lies at a certain distance from the origin. This distance is defined by the square root of the square values, as shown in equation 6.10. For each pair of peaks a certain distance can be found. The smaller this mean distance value is, the better the overall correlation is of the data traces.

$$Corr_{t\&A} = \frac{1}{N} \sum_{i=1}^N \sqrt{\Delta t_{peak,i}^2 + \Delta A_{peak,i}^2} \tag{6.10}$$

In which:

- $Corr_{t\&A}$: Peak correlation based on minimum distance. The closer to 1 this value is, the better or thus smaller the average distance between two corresponding peaks.

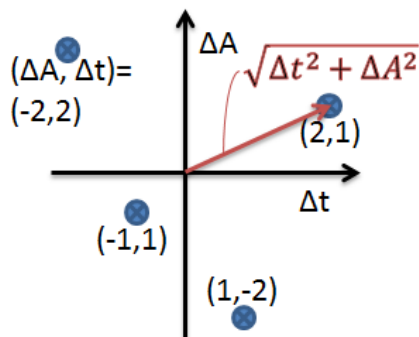


Figure 6.3 Example of Δt and ΔA in a graph. The basis for calculation of the peak correlation in time and amplitude.

FREQUENCY PLOT AND SPECTROGRAM

The last type of reviewing method used is the use of a spectrogram and with that a frequency plot. The spectrogram is used to view the data trace both in the frequency-domain and in the time-domain simultaneously. The time-frequency representation not only shows the frequencies that are governing, but, additionally, provides insight into which frequencies are present during the maxima that occur in the time-domain. In other words, the time-frequency plot shows the evolution of the frequency spectrum with time. Background on the spectrogram and its windowing function can be found in Appendix G. The

characteristics of the frequency plot itself have already been elaborated on in section 5.3.3, therefore no further explanation is given on this plotting type.

6.2.2 THE TARGET VALUES

Before the model prediction's accuracy can be quantified one needs to set target values to compare the model results with. These target values are based on the characteristics of the measured data trace, the time plots and the frequency plots of measured cable forces. This section provides for these plots and target values.

The plots given are the frequency spectrum and the spectrogram of the measured cable forces. They are shown in Figure 6.4 and Figure 6.5 respectively. The time trace of the measured cable forces can be found in the all plots of all models their force prediction time traces. Some specifications of the measured cable forces time traces are shown in Table 6.1.

The frequency plot of Figure 6.4 shows that most of the energy is concentrated at the frequency region of 0.07 Hz up to 0.1 Hz. The spectrogram confirms this but also shows that the largest amplitudes occur when:

1. The multiple sinusoids in the lower frequency range experience a maximum at the same time, and/or:
2. The multiple sinusoids in the higher frequency range experience a maximum at the same time.

However, it could be that the windowing function used in the spectrogram, the hamming window, causes a very low frequency periodic sinusoid visible in the spectrogram. It can be seen that approximately every 800 seconds some maxima are visible in the time traces. There is no natural explanation for a wave with a frequency thus low that its period is 800 seconds. Therefore, it should be kept in mind that this low frequent behaviour could be caused by the windowing function used.

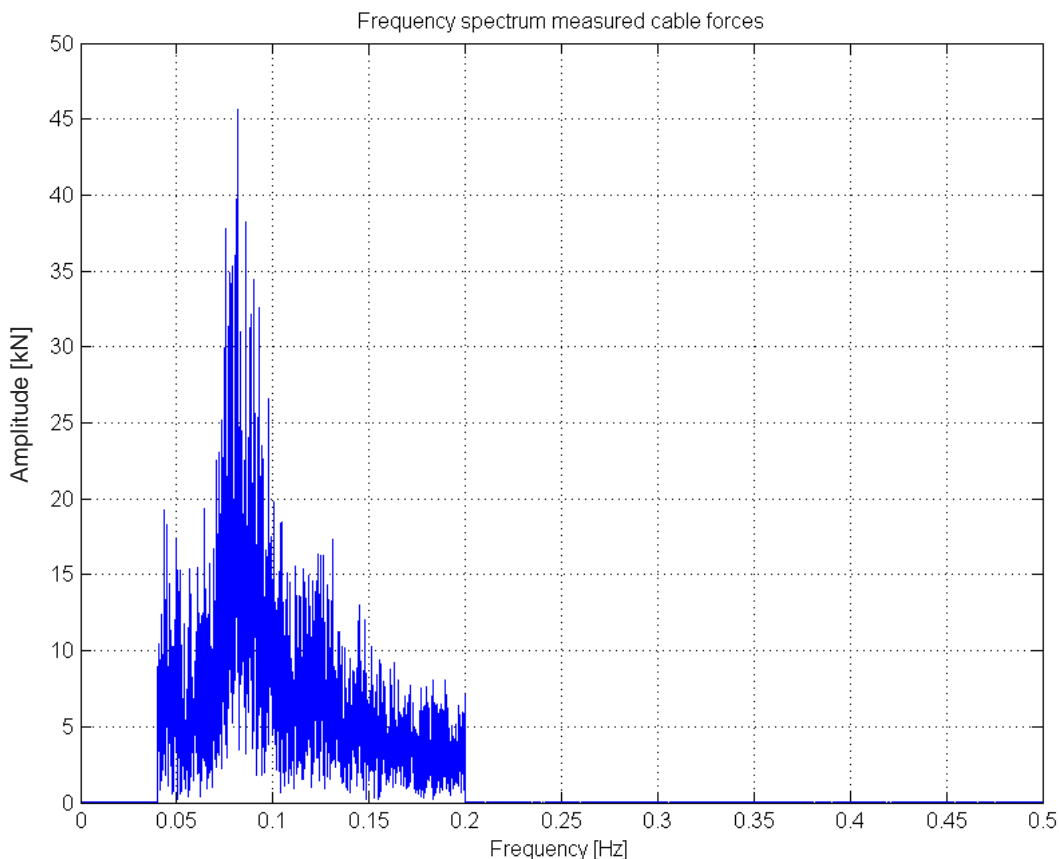


Figure 6.4 Frequency plot of the measured cable forces. The spectrum is non-binned but has been filtered.

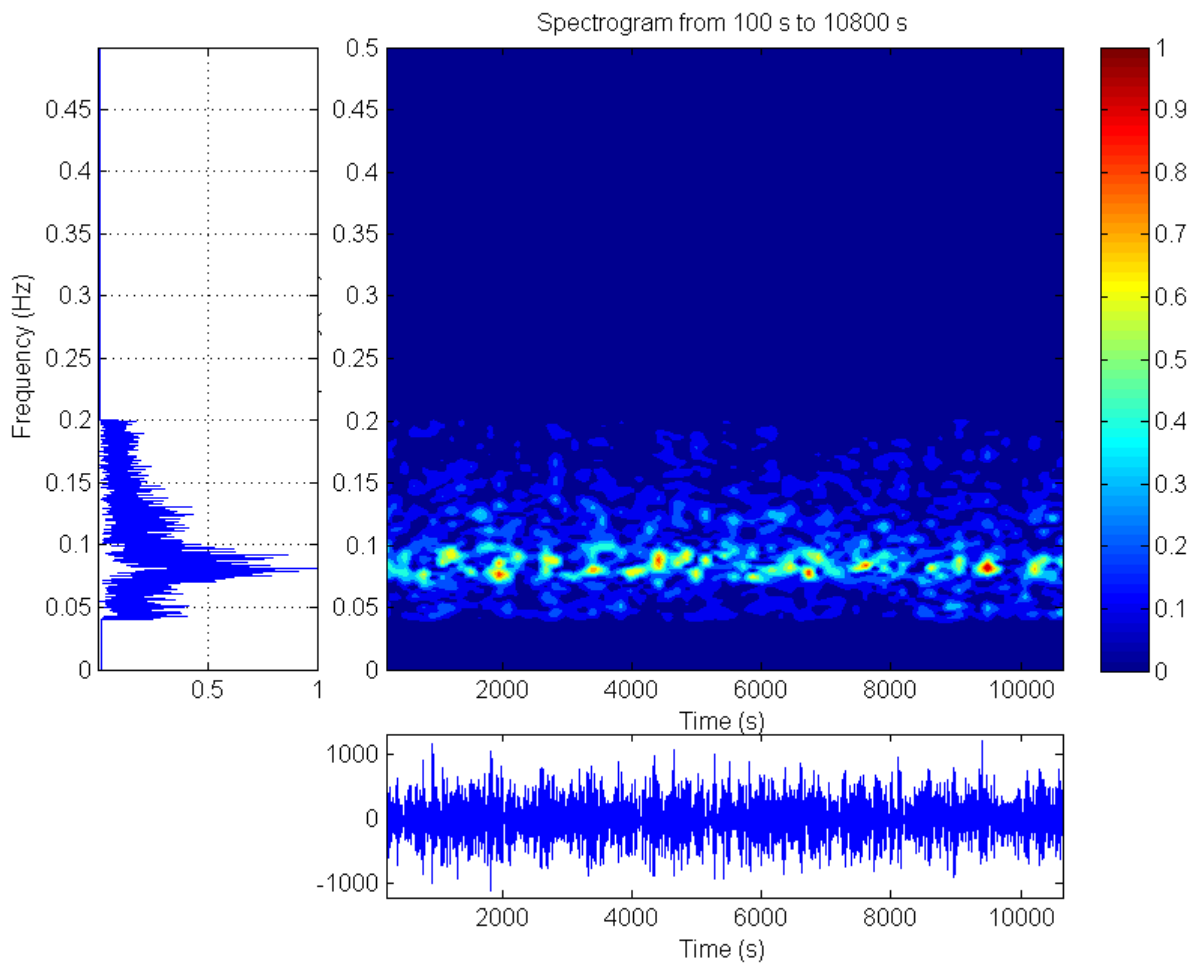


Figure 6.5 Spectrogram of the measured cable forces, using a hamming windowing function. Note: The frequency plot on the left hand side is normalised.

Target Values in[kN]	Standard deviation
Mean	1.894E4 kN
Standard deviation	267.7 kN
Max	2.016E4 kN
Min	1.782E4 kN

Table 6.1 Properties of the measured cable forces.

6.2.3 RL MODEL ANALYSIS

The RL model's cable force predictions are based on the inertia force in cable direction. It is therefore based on the motions of the scp point as described in section 6.1. In this section the reviewing methods of section 6.2.1 will be applied to determine the fit of the RL model with the measured cable forces.

Firstly, the time traces are reviewed. Secondly, a frequency analysis is performed after which thirdly the simultaneous time-frequency analysis is elaborated on.

TIME-DOMAIN ANALYSIS

The time trace of Figure 6.6 shows that the predictions follow the trend of the measured cable forces. It is thus observed that there is a clear correlation between the predicted cable forces and the measured cable forces. However, there seems to be a frequency difference present since it is observed that sometimes the predictive time trace and the measured time trace are in line and sometimes they are not. Additionally, it is visible that cable force prediction by the RL model underestimates the cable force values. The evidence of the underestimation of amplitude can be seen in the 2nd row of Table 7.2. This table further more includes other general properties of the time trace of the RL model.

The underestimation of the force amplitude is confirmed by the fact that the standard deviation of the cable force predicted by the RL model is 212 kN, while the standard deviation of the measured cable forces is 268 kN. The current standard deviation error is 20.8% when reviewing the standard deviation values of the RL model and the measured cable forces. It should be pointed out that this chapter does not include an uncertainty analysis. This analysis has been performed for the RL model in section 7.10.1.

If the worst case scenario by input errors is included, as found in section 7.10.1, The error in standard deviation grows to 22,2%.

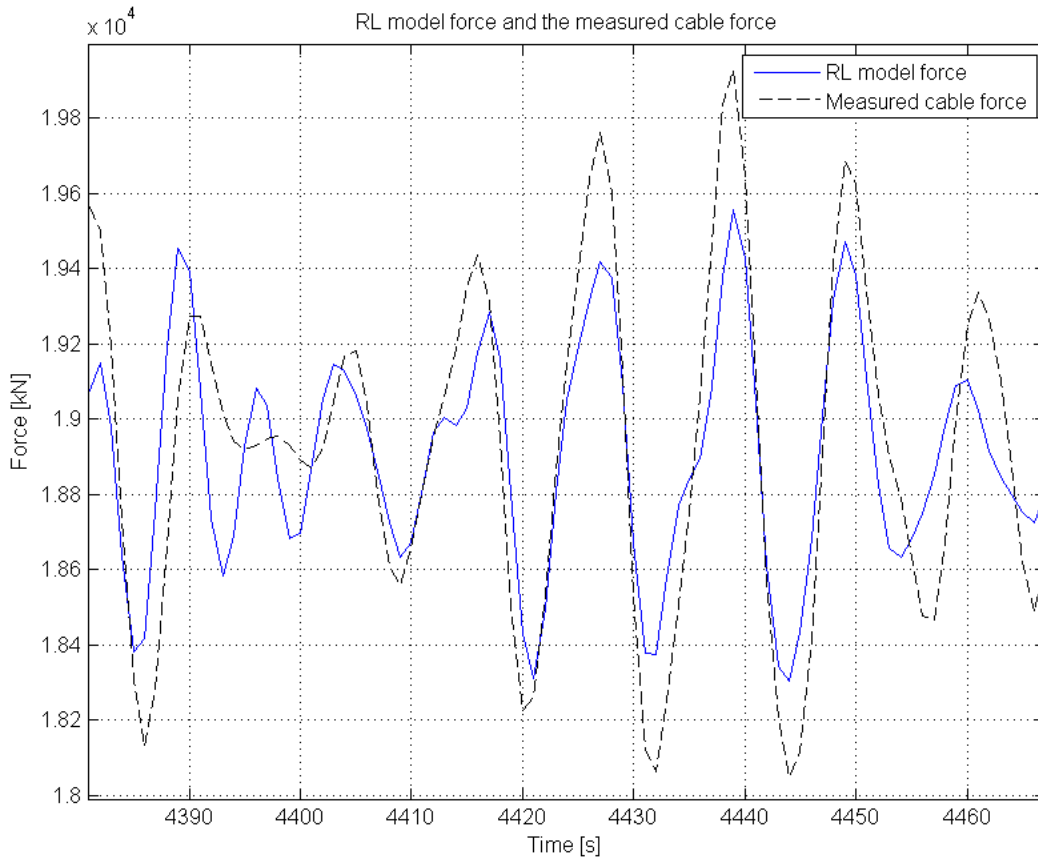


Figure 6.6 Time trace of the RL model and the measured cable force.

Property	Standard deviation	Mean	Maximum	Minimum
Values in [kN]	212 kN	1.8925E4 kN	2.0105E4 kN	1.7752E4 kN
Difference with measured values in [kN]	-55.3 kN	-12.9 kN	-52.4 kN	64.3 kN

Table 6.2 Time-trace properties of the RL model.

To further quantify the model’s performance, the normalised cross-covariance is applied to the cable force prediction of the RL model and the measured cable forces. To clarify the normalised cross-covariance function Figure 6.7 is added of the function’s results for the RL model predictions and the measured cable forces. For the sake of brevity this is the only figure to visualise the function. In later stages of the thesis only the resulting numbers of the function are given. It can be observed in Figure 6.7 that the predicted cable forces show strong similarities with the measured cable forces.

The cross-covariance plot shows the best correlation lies at -1 second. Considering the time plot in this section this -1 second must be an average delay value (of the constantly varying delay of the plot’s peaks) caused by the frequency difference. The cross-covariance plot’s peak value has the coordinates (-1, 0.721). This confirms the frequency difference in the time-trace as opposed to the presence of a phase difference, as a presence of only a phase difference would cause the normalised cross-covariance function to reach a value of nearly 1 at one specific time shift.

The results of all other quantitative reviewing methods are shown in Table 6.3. The average time shift indicated by the cross-covariance function is confirmed by the mean peak time difference. It should be noted that the minus sign of both time indications means that the time trace of the measured cable forces is on average approximately 1 second “behind” on the predicted time trace.

The mean peak amplitude difference confirms that the RL model underestimates the cable force amplitudes, just as previously concluded when reviewing the standard deviation of the RL model’s predictions. The peak amplitude correlation and the correlation in time & amplitude are noted for comparison with the FL model in a later stage.

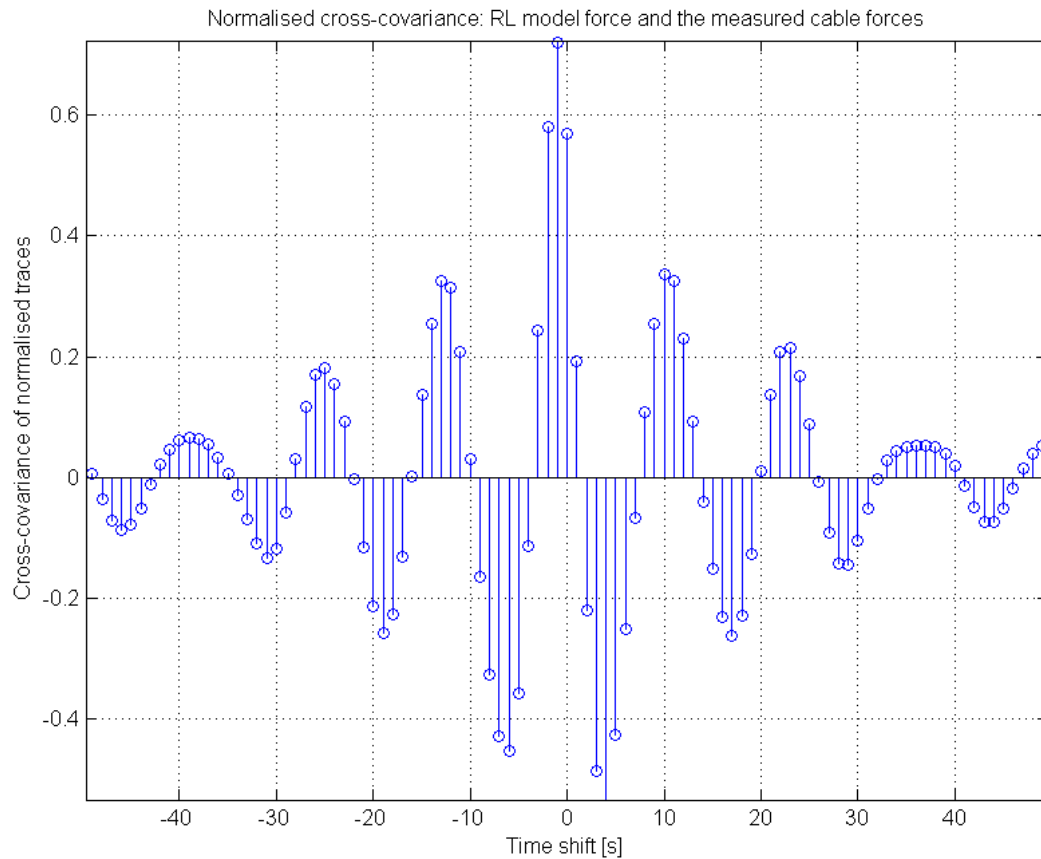


Figure 6.7 Cross covariance of the force prediction by the RL model and the measured cable forces.

Reviewing method	Result
Normalised cross-covariance complete	(-1, 0.721)
Standard deviation	212 kN
Peak amplitude correlation	0.601
Mean peak amplitude difference	-92.2 kN
Mean peak time difference	-1.1 s
Correlation in time & amplitude	140.98

Table 6.3 Results of the reviewing methods for the RL model.

FREQUENCY-DOMAIN ANALYSIS

In the previous section it was concluded that the RL model's prediction show to contain a amplitude and frequency difference when compared with the measured cable forces. The frequency spectrum of the RL model's predictions confirms this, as shown in Figure 6.8. It is evident that the frequency difference manifests itself through the abundance of high frequency information (in the range of 0.13 Hz up to 0.2 Hz) in the RL model prediction.

The maximum amplitudes are, however, present in the same frequency range as the measured cable forces, which is as expected. However, the peak amplitudes are lower than those found in the frequency plot of the measured cable forces (see Figure 6.4), which is in line with the conclusion of amplitude underestimation in the previous section.

The presence of high frequency content can have multiple causes, one of which is described in section 5.4 and section 5.5. Other causes could for example be some component transferred by the rigid character of the RL model are in reality damped out by the sheaves or the cables. That would be the cause of these higher frequencies not being visible in the measured cable forces. However, there are multiple other reasons why these high frequencies are present in the RL model's predictions. This is researched in section 7.12.

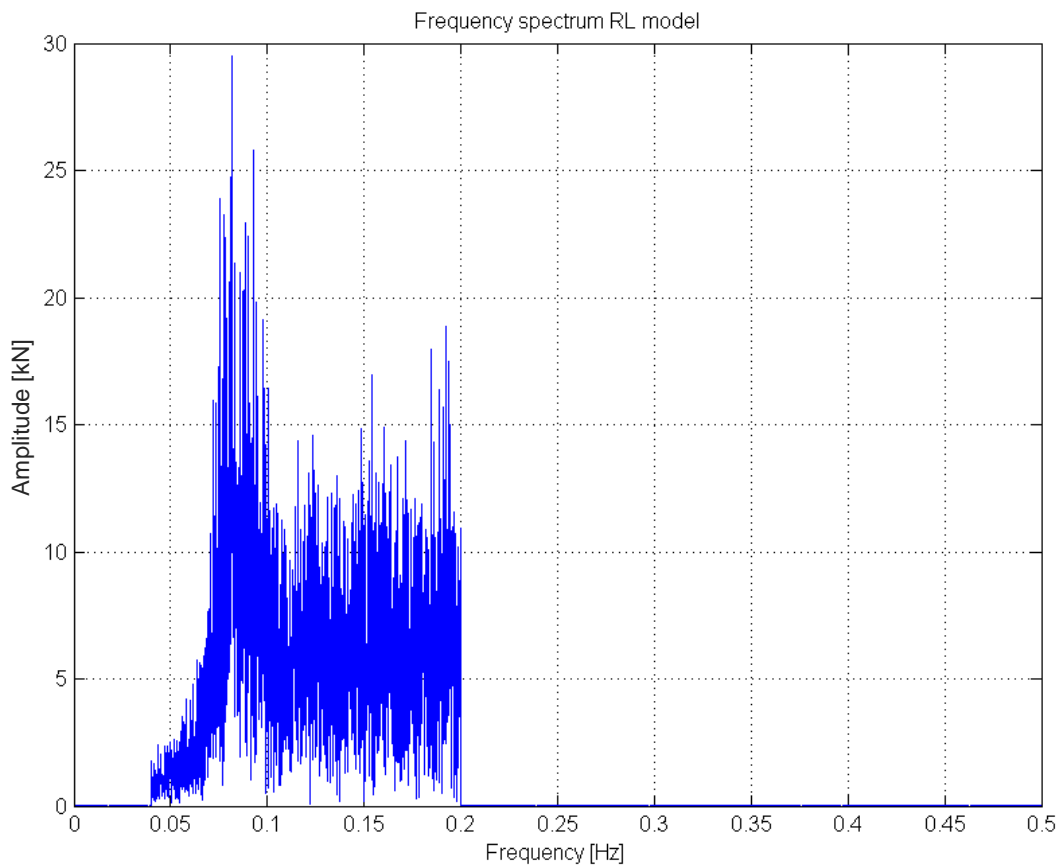


Figure 6.8 The frequency spectrum of the RL model. The spectrum is non-binned but has been filtered.

TIME- & FREQUENCY-DOMAIN ANALYSIS

In Figure 6.9 the spectrogram of the RL model is shown. The spectrogram shows that the largest frequency amplitudes occur in the region between 0.06 Hz and 0.1 Hz, which is conformed in Figure 6.8. This is in line with the spectrogram of the measured cable forces. Furthermore, maximum energy peaks in the spectrogram of the RL model coincide with the maximum energy peaks in the spectrogram of the measured cable forces. However, the RL model again shows to contains more high frequency information.

It can be observed that the peaks in time traces occur at points where a large number of frequencies contain energy. This would mean that the different sinusoids containing these frequencies would contain approximately the same phase delay which builds up the energy in these frequencies at the same approximate time. It is also visible that "lumps" of energy peaks in the time trace of the adjusted FL model coincide with medium-sized maxima of the lower frequencies.

In the regions where a large number of frequencies contain energy the RL model shows much more distinct maxima in the time-trace visible below the spectrogram. The distinct peaks are, however, overall smaller in amplitude than those visible in the spectrogram of the measured cable force. The accumulation of energy over a range of frequencies could thus "mimic" the peak amplitude, while in general the prediction time trace of the RL model underestimates the amplitudes.

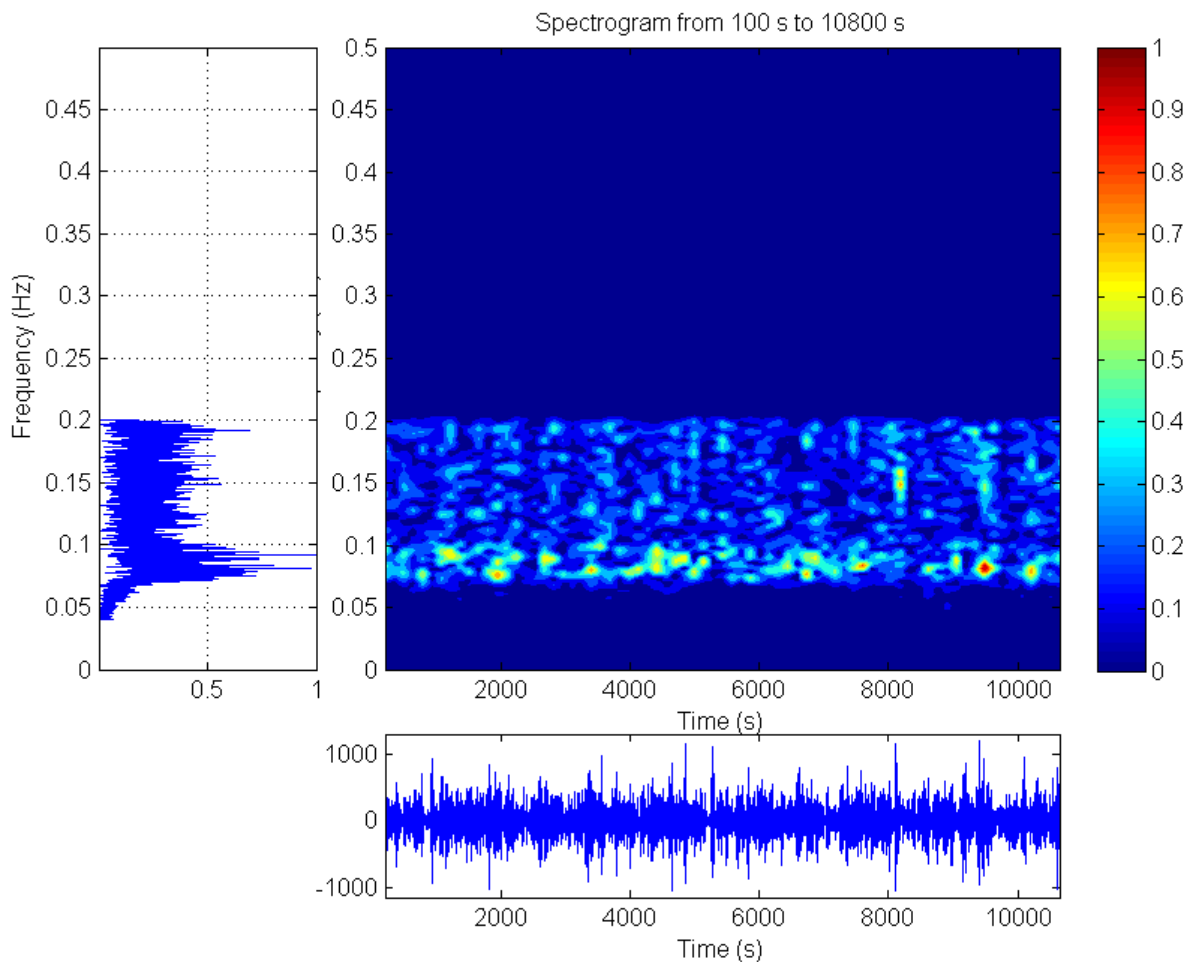


Figure 6.9 Spectrogram of the RL model, using a hamming windowing function. Note: The frequency plot on the left hand side is normalised.

6.3 EVALUATION OF THE RL MODEL ANALYSIS

Using the advanced reviewing methods it was found that the RL model is significantly correlated. However, the force prediction of the RL model shows to contain a frequency difference when compared with the measured cable forces. Additionally, the predicted force amplitudes are underestimated.

The frequency difference is caused by the high frequency content visible in the RL model's frequency plots. The cause of this is (as of yet) not known and will be researched in section 7.12. The current standard deviation error is 20.8% when reviewing the standard deviation values of the RL model and the measured cable forces. This number does not include the influence of input uncertainty of the model. The input uncertainty has been researched in section 7.10.1.

Considering that the ultimate goal is prediction of a chance of uplift based on statistical properties of the predictions, it can be deemed insufficient that the standard deviation of the total data trace considered is over 22% off target. Another reason that more accuracy is required is that, currently, the cable force predictions are for a situation where the stinger of Audacia is lifted from the water. A slight difference between predicted cable forces and measured cable forces can become larger when the stinger is considered in the submerged situation. In that case there is a range of additional factors influencing the cable forces. A difference in predicted and measured traces in such case is even harder to explain. Therefore understanding the current situation with a non-submerged stinger is crucial for the further exploitation of the physics of the situation in which the stinger is fully submerged in water.

Unfortunately, the limitation of the RL model is that it is not possible, using this model, to see the interaction between the stinger and the sheaves, while the load cell which measures these cable forces could actually be influenced by these sheaves and their interactions with the equipment. Furthermore, the cables are now assumed rigid but in reality can behave as springs and as such allow relative motion of the stinger and the ship. Lastly, the model does not account for any damping. Furthermore, the model does not allow for expansion or the adjustment of model parameters. Since the RL model does not

accurately describe the peak forces, therefore, a more detailed model which can cover the different parameters in the system more accurately is required.

To understand the dynamics of the hang-off system and with that try to acquire a better prediction of the cable forces than the RL model, a M-degree of freedom (hereafter: MDOF) dynamic model is produced. This MDOF flexible links model (hereafter FL model) is described in Chapter 7. This model accounts for:

7. FLEXIBLE LINKS MODEL

7.1 MODEL OF A RIGID BODY WITH FLEXIBLE LINKS

In the previous chapter it was concluded that it is desirable to more accurately predict the cable forces based on ship motions through an MDOF system. Therefore, the goal of the flexible links model (FL model) is to accurately predict the cable forces occurring as consequence of the ship motions. Similar to the RL model, the FL mode thus uses ship motions at the centre of gravity of the ship as input and uses measured cable forces for validation of the predicted time traces.

The FL model describes stinger motions, sheave motions and cable forces as consequence of ship motions in the 2-D plane, i.e. the x,z -plane. Naturally, the static components are an important input factor as well. A schematisation of this is shown in Figure 7.1. Note that α is the parameter indicating sheave rotation angle and ϕ is the parameter indicating the stinger motion (see Figure 7.2.). A schematisation of the model is provided in section 7.2.

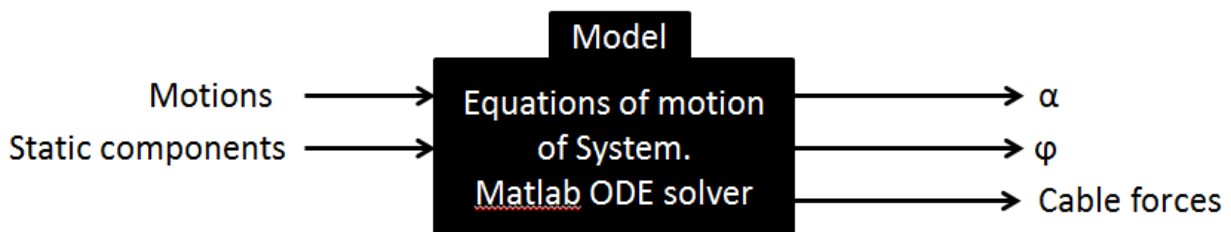


Figure 7.1 Schematisation of the model functionality. Note: α is the sheave rotation angle & ϕ is the stinger rotation angle.

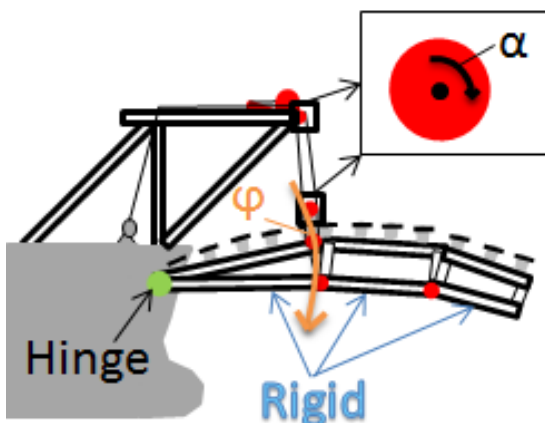


Figure 7.2 Output parameters of the model and some model characteristics.

7.2 MODEL SCHEMATISATION AND DESCRIPTION

It will be easier to understand the schematisation if first the lay-out of the actual stinger hang-off system is shown. Figure 7.3 shows the hang-off system and indicates the points of interest. The numbering used in the equations of motion is also shown. The large numbers on the cable parts running to the winches indicate cable numbers. The sheaves are numbered separately. At the leftmost top sheave the numbering starts at 1, then runs from left to right in all top sheaves. The numbering stops at sheave 24, the top right sheave of the system. Consequently, the bottom sheave blocks' sheaves were numbered in the same way from left to right, starting at 25 and ending at 44. Note that sheaves 6, 7, 18 and 19 are the sheaves connected with the load cells. Sheave 1, 14 and 19 in Figure 7.3 are indicated as clarification for equations 7.39 up to 7.42.

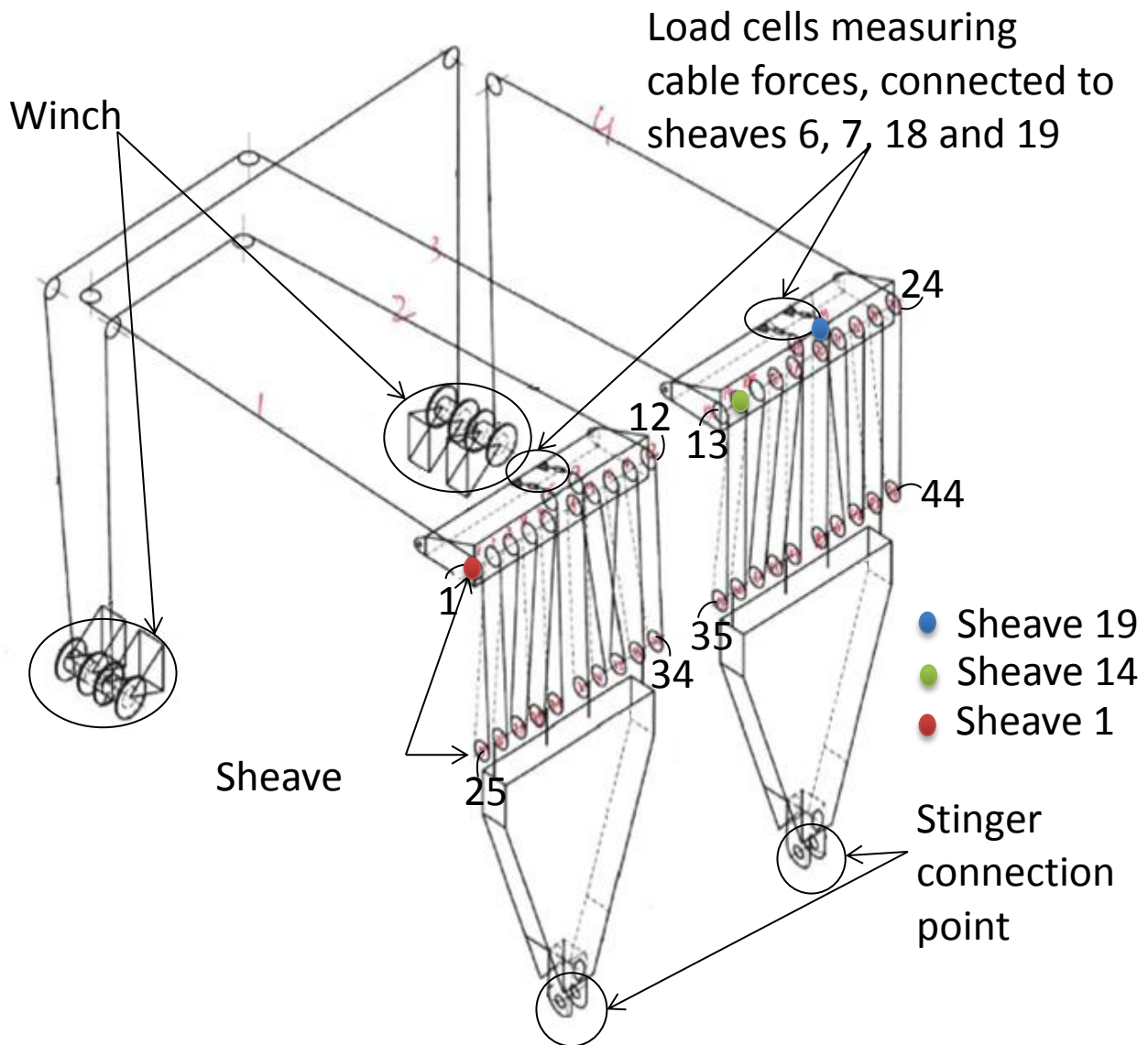


Figure 7.3 Hang-off system layout. Additionally cable and sheave numbering is given.

Some assumptions were made before schematising the FL model. Note that points mentioned are described in Figure 7.4. The assumptions are:

1. The ship itself is modelled as being rigid.
2. The stinger sections are modelled as being rigid.
3. The three stinger sections are modelled as separate rigidly connected rigid bodies.
4. The sheaves are assumed rigid.
5. The hang-off structure on which the cables and top sheaves are mounted is considered rigid.
6. The cables are modelled as springs.
7. The cables are modelled as being connected to the sheaves.
8. The ship's motion angles and the stinger motion angles are presumed to be small angles.
9. Point A, the main hinge, is a hinge connection.
10. The model only considers a 2-D situation, i.e. the x,z -plane. *However, in Figure 7.3 it can be seen that the cables leading to the winches have different lengths and thus these cables have different stiffness values. Therefore, all sheaves will be modelled separately to allow effects by these different cables.*
11. The winches are modelled as a type of rigid connection.
12. The rigid sheave blocks distribute the stinger weight evenly over the sheaves they contain.
13. The structural elements connecting the stinger connection point and the lower sheave block, *the lower block structures* (see Figure 1.2 and Figure 1.6), are assumed to always stay parallel with β . β is defined as the angle between the vertical in point C and the straight line connecting the top sheaves (point C) and the stinger connection point (point B). It is thus assumed that the weight of these elements does not influence the direction of the cables (see section 7.6.1. for calculation). Note that in line with this assumption, it is assumed sufficient to model the weights of the lower sheave blocks and the lower block structure in point B.

The sheaves leading the cables to the winches, which are located after sheaves 1, 12, 13 and 24, are not accounted for in the current model. Also note that during the calculation of several system characteristics additional assumptions are made. These are listed in section 7.5. Some assumptions are verified. This is explained in section 7.6.

The assumptions listed above were applied to the hang-off system shown in Figure 7.3 and resulted in the schematisation of the system shown in Figure 7.4. This schematisation also contains the chosen positive directions of the system. To clarify the figure an enumeration of the parameters with explanation is given in Table 7.1.

Motions	Description	Unit
α	The sheave rotation	rad
ϕ	The stinger angular motion	rad
θ	Pitch angle	rad
$Z_{A/C/D}$	Heave motion in A, C and D	m
$X_{A/C/D}$	Surge motion in points A, C and D	m
Geometry		
L_0	Distance from main hinge to the stinger connection point	m
L_A	Distance from the centre of gravity to point A	m
L_C	Distance from the centre of gravity to point C	m
β	Hang-off angle	rad
γ	Main hinge angle	rad
δ	Section 2 angle relative to the main hinge angle	rad
η	Section 3 angle relative to the angle of section 2	rad
L_1	Length of section 1	m
L_2	Length of section 2	m
L_3	Length of section 3	m
R	Radius of the sheaves.	m
Weight		
K_1	Spring stiffness of the wire rope between point D and point C	N/m
K_2	Spring stiffness of the wire rope between point C and point B	N/m
$K_{3\#}$	Spring stiffness of the wire rope running to winch number $\# = 1, 2, 3$ or 4	N/m
M_1	Mass of the stinger section 1	Kg
M_2	Mass of the stinger section 2	Kg
M_3	Mass of the stinger section 3	Kg
M_w	Mass of the wires acting on the load cells. This mass is has been taken as a point mass in point B of Figure 7.4. This choice is conservative since it overestimates the influence of your cable weight on your cable forces.	Kg
M_{LBS}	Mass of the structural element connecting the lower sheave block with the stinger connection point. This mass is has been taken as a point mass in point B of Figure 7.4.	Kg
m_{sh}	Mass of a sheave	Kg

Table 7.1 Schematisation parameters.

V : Potential energy in the system in [J]

The equations of motions are differentiated with respect to the chosen generalised coordinates as in equations 7.3 and 7.4 below:

$$\frac{d}{dt} \frac{\delta L}{\delta \dot{\varphi}} - \frac{\delta L}{\delta \varphi} = 0 \quad 7.3$$

$$\frac{d}{dt} \frac{\delta L}{\delta \dot{\alpha}_n} - \frac{\delta L}{\delta \alpha_n} = 0, \text{ for } n = 1, 2, \dots, 44 \quad 7.4$$

In which

$\dot{\alpha}$: Rotational velocity of sheaves in [rad/s]
 $\dot{\varphi}$: Rotational velocity of the stinger in [rad/s]

For all 44 sheaves and the stinger expression 7.3 and 7.4 are used, resulting in a system of 45 coupled equations of motion. To set-up these equations all kinetic and potential terms in equation 7.1 need to be considered.

7.3.2 THE KINETIC AND POTENTIAL ENERGY

Using Figure 7.4 the various terms contributing to the kinetic and the potential energy are defined. The general formulation of the kinetic terms can be found in equations 7.5 up to 7.7. These equations are based on the energy carried by a point mass (or rigid body experiencing translational motion) with a velocity in x- or z-direction or the rotational inertia of the sheaves with their angular velocity.

$$E_{kinetic, horizontal} = \frac{1}{2} m \dot{x}^2 \quad 7.5$$

$$E_{kinetic, vertical} = \frac{1}{2} m \dot{z}^2 \quad 7.6$$

$$E_{kinetic, rotational} = \frac{1}{2} I_{sheave} \dot{\alpha}^2 \quad 7.7$$

In which:

m : Mass in [kg]
 I_{sheave} : Rotational inertia of a sheave in [kg m²]
 \dot{x} : Velocity in x-direction in [m/s]
 \dot{z} : Velocity in z-direction in [m/s]

The general formulation of the potential terms can be found in equations 7.8 and 7.9. Here the potential terms are caused by the gravitational field and the elongation of the springs which describe the hang-off cables. Therefore these general terms are based on the masses times the gravitational inertia and z-elevation of the centre of gravities of the masses. The spring term is the multiplication of the spring stiffness with the elongation of the spring.

$$E_{potential} = mgz \quad 7.8$$

$$E_{pot, spring} = \frac{1}{2} K_{part} (\Delta u)^2 \quad 7.9$$

In which:

g : Gravitational acceleration in [m/s²]
z : Vertical displacement in [m]
 K_{part} : Spring coefficient of the hang-off cables in [N/m]
 Δu : Differential stretch of the hang-off cables in [m]

KINETIC ENERGY

The kinetic terms found using equations 7.5 up to 7.7 are described in the enumeration below:

1. Stinger section 1 in vertical & horizontal motion. In the equations this component is indicated with the abbreviation "M1".
2. Stinger section 2 in vertical & horizontal motion. In the equations this component is indicated with the abbreviation "M2".

3. Stinger section 3 in vertical & horizontal motion. In the equations this component is indicated with the abbreviation "M3".
4. The top sheaves in vertical & horizontal motion.
5. The bottom sheaves in vertical & horizontal motions. These masses are assumed to be located in point B.
6. The rotational inertia of all 44 sheaves.
7. The vertical & horizontal motions of the lower block structures. In the equations these components are indicated with the abbreviation "LBS". This is the structural connection between the lower sheave blocks and the stinger. These masses are assumed to be located in point B.

Before formulating all terms some constants are introduced to make the kinetic terms easier to read. The definitions of these constants are given in equation 7.10 up to 7.12. The kinetic terms in sequence of the above enumeration are given in equations 7.13 up to 7.22. Please note that definitions on all these parameter meanings are given in Table 7.1 and in the list of symbols at the start of this thesis report.

$$r_1(l) = l \quad 7.10$$

$$r_2(l) = \sqrt{L_1^2 + 2L_1l \cos(\eta) + l^2} \quad 7.11$$

$$r_3(l) = \sqrt{L_1^2 + L_2^2 + 2L_1L_2 \cos(\eta) + 2L_1l \cos(\eta - \delta) + 2L_2l \cos(\delta) + l^2} \quad 7.12$$

$$T_{M1,z} = \int_0^{L_1} \frac{M_1}{2L_1} (r_1(l) \cos(\gamma) \cos(\varphi) \dot{\varphi} - \dot{z}_A)^2 dl \quad 7.13$$

$$T_{M1,x} = \int_0^{L_1} \frac{M_1}{2L_1} (r_1(l) \sin(\gamma) \cos(\varphi) \dot{\varphi} + \dot{x}_A)^2 dl \quad 7.14$$

$$T_{M2,z} = \int_0^{L_2} \frac{M_2}{2L_2} (r_2(l) \cos(\gamma) \cos(\varphi) \dot{\varphi} - \dot{z}_A)^2 dl \quad 7.15$$

$$T_{M2,x} = \int_0^{L_2} \frac{M_2}{2L_2} (r_2(l) \sin(\gamma) \cos(\varphi) \dot{\varphi} + \dot{x}_A)^2 dl \quad 7.16$$

$$T_{M3,z} = \int_0^{L_3} \frac{M_3}{2L_3} (r_3(l) \cos(\gamma) \cos(\varphi) \dot{\varphi} - \dot{z}_A)^2 dl \quad 7.17$$

$$T_{M3,x} = \int_0^{L_3} \frac{M_3}{2L_3} (r_3(l) \sin(\gamma) \cos(\varphi) \dot{\varphi} + \dot{x}_A)^2 dl \quad 7.18$$

$$T_{Top\ sheaves\ x,z} = \sum_{n=1}^{24} \frac{1}{2} m_{sh,n} (\dot{z}_C^2 + \dot{x}_C^2) \quad 7.19$$

$$T_{Bottom\ sheaves,z} = \sum_{n=25}^{44} \frac{1}{2} m_{sh,n} (L_0 \cos(\gamma) \cos(\varphi) \dot{\varphi} - \dot{z}_A)^2 \quad 7.20$$

$$T_{Bottom\ sheaves\ x} = \sum_{n=25}^{44} \frac{1}{2} m_{sh,n} (\dot{x}_A + \sin(\gamma) \cos(\varphi) \dot{\varphi} L_0)^2 \quad 7.21$$

$$T_{Sheaves} = \sum_{n=1}^{44} \frac{1}{2} I_{sh,n} \dot{\alpha}_n^2 \quad 7.22$$

$$T_{LBS,z} = \frac{1}{2} m_{LBS} (L_0 \cos(\gamma) \cos(\varphi) \dot{\varphi} - \dot{z}_A)^2 \quad 7.23$$

$$T_{LBS,x} = \frac{1}{2} m_{LBS} (\dot{x}_A + \sin(\gamma) \cos(\varphi) \dot{\varphi} L_0)^2 \quad 7.24$$

In which:

T	:	Kinetic energy in [J]
L_0	:	Length to stinger connection point, point B in [m]
L_1	:	Length of stinger section 1 in [m]
L_2	:	Length of stinger section 2 in [m]
L_3	:	Length of stinger section 3 in [m]
l	:	Length along a stinger section in [m]
γ	:	Hinge angle 1, angle of stinger section 1 and the x-axis in [rad]
η	:	Hinge angle 2, angle of stinger section 1 and stinger section 2 in [rad]
δ	:	Hinge angle 3, angle of stinger section 2 and stinger section 3 in [rad]
M_1	:	Mass of stinger section1 in [kg]
M_2	:	Mass of stinger section2 in [kg]
M_3	:	Mass of stinger section3 in [kg]
$m_{sh,n}$:	Mass of sheave number n in [kg]
m_{LBS}	:	Mass of the lower block structures in [kg], modelled as present in point B
$I_{sh,n}$:	Rotational inertia of sheave number n in [kg m ²]
x_A	:	Motion in x-direction of point A (the main hinge) in [m]. Note that the dots indicate the derivative(s) in the time domain.
z_A	:	Motion in z-direction of point A (the main hinge) in [m]. Note that the dots indicate the derivative(s) in the time domain.
x_C	:	Motion in x-direction of point C (the main hinge) in [m]. Note that the dots indicate the derivative(s) in the time domain.
z_C	:	Motion in z-direction of point C (the main hinge) in [m]. Note that the dots indicate the derivative(s) in the time domain.
a_n	:	Angular motion of sheave number n in [rad]. Note that the dots indicate the derivative(s) in the time domain.
φ	:	Angular motion of the stinger in [rad]. Note that the dots indicate the derivative(s) in the time domain.

The total kinetic energy can be found using equation 7.25.

$$T_{total} = \sum_{i=1}^{12} T_i \quad 7.25$$

POTENTIAL ENERGY

The potential terms found using equation 7.8 and 7.9 are described in the enumeration below:

1. Stinger section 1 elevation changes.
2. Stinger section 2 elevation changes.
3. Stinger section 3 elevation changes.
4. Bottom sheave block elevation changes. These masses are assumed to be located in point B.
5. Elevation changes of the lower block structures These masses are assumed to be located in point B.
6. Elevation changes of the top sheaves by pitch motion of the ship.
7. Spring potential of the top wire ropes leading to the load cells, with spring stiffness K1.
8. Spring potential of the top wire ropes leading to the winches, with spring stiffness K3.
9. Spring potential of the diagonal wire ropes leading to the stinger, with spring stiffness K2.

The potential terms are given in equations 7.27 up to 7.35. To clarify the terms an additional function has been given. This function can be found in equation 7.26. Please note again that definitions on all these parameter meanings are given in Table 7.1.

$$f(\varphi) = L_0 \sin(\varphi) \cos(\gamma) \cos(\beta) - (L_C - L_A) \cos(\beta) \theta \quad 7.26$$

$$V_{M1} = - \int_0^{L_1} \frac{M_1}{L_1} g(r_1(l) \cos(\gamma) \sin(\varphi) - z_A) dl \quad 7.27$$

$$V_{M2} = - \int_0^{L_2} \frac{M_2}{L_2} g(r_2(l) \cos(\gamma) \sin(\varphi) - z_A) dl \quad 7.28$$

$$V_{M3} = - \int_0^{L_3} \frac{M_3}{L_3} g (r_3(l) \cos(\gamma) \sin(\varphi) - z_A) dl \quad 7.29$$

$$V_{Bottom\ sheaves} = - \sum_{n=25}^{44} m_{sh,n} g (L_0 \cos(\gamma) \sin(\varphi) - z_A) \quad 7.30$$

$$V_{Lower\ block\ structures} = -m_{LBS} g (L_0 \cos(\gamma) \sin(\varphi) - z_A) \quad 7.31$$

$$V_{Top\ sheaves} = \sum_{n=1}^{24} \frac{1}{2} m_{sheave,n} z_{C,n}^2 \quad 7.32$$

$$V_{Spring\ 1} = \frac{1}{2} K_1 R^2 (\alpha_6^2 + \alpha_7^2 + \alpha_{18}^2 + \alpha_{19}^2) \quad 7.33$$

$$V_{Spring\ 3} = \frac{1}{2} R^2 (K_{31} \alpha_1^2 + K_{32} \alpha_{12}^2 + K_{33} \alpha_{13}^2 + K_{34} \alpha_{24}^2) \quad 7.34$$

$$V_{Spring\ 2} = \frac{1}{2} K_2 ((f(\varphi) - R\alpha_1 + R\alpha_{25})^2 + \dots + (f(\varphi) + R\alpha_{44} - R\alpha_{24})^2) \quad 7.35$$

In which:

V	:	The potential energy [J]
β	:	The of the hang-off cables with the vertical through point C in [rad]
L_c	:	Distance along the x-axis of the centre of gravity to point C in [m]
L_a	:	Distance along the x-axis of the centre of gravity to point A in [m]
g	:	Gravitational acceleration in [m/s ²]
R	:	Sheave radius in [m]
K1	:	The spring stiffness of the cable leading from sheaves 6, 7, 18 and 19 to the dead ends of the cables containing the load cells in [N/m]
K2	:	The spring stiffness of the cable leading from the top sheaves (point C) to the stinger in [N/m]
K31	:	The spring stiffness of the cable leading from sheave 1 to the corresponding winch in [N/m]
K32	:	The spring stiffness of the cable leading from sheave 12 to the corresponding winch in [N/m]
K33	:	The spring stiffness of the cable leading from sheave 13 to the corresponding winch in [N/m]
K34	:	The spring stiffness of the cable leading from sheave 24 to the corresponding winch in [N/m]

Again, the total potential energy can be found using equation 7.36.

$$V_{total} = \sum_{i=1}^9 V_i \quad 7.36$$

7.3.3 DIFFERENTIATION AND LINEARIZATION

To obtain the equations of motion the summations of equation 7.25 and equation 7.36 were differentiated to their generalised coordinates, as described in equation 7.3 and equation 7.4. Note that the following terms fall away since they do not contain any generalised coordinate (thus they do not contain any q_n or ϕ). The terms that fall away when differentiating are:

1. The kinetic term of non-rotational velocity of the top sheaves. See equation 7.19.
2. The potential term of the top sheaves. See equation 7.32.

After differentiating these non-linear equations they will be linearized using the small angle approximation for the generalised coordinate φ . This means that the equation 7.37 and equation 7.38 were applied.

$$\cos(\varphi) \approx 1, \text{ for small } \varphi \quad 7.37$$

The complete set of resulting equations of motion can be found in Appendix D. It should be noted that these equations are the physical representation of the system and can be solved using multiple methods. In this thesis, two methods are used for solving this system of differential equations. The first method uses direct time-integration of the equations of motions whereas the second method utilizes the modal analysis approach. In principle both methods should yield the same answer. This section only elaborates on the equations of motions and solving them using direct time-integration algorithms. The modal analysis approach is introduced in section 7.4.

7.3.4 EQUATIONS OF MOTION

Examples of the original second order equations are given in Equation 7.39 up to Equation 7.42, before damping and friction are introduced. As stated in section 7.2, sheave 1, 14 and 19, which are indicated in Figure 7.3, are used as examples for clarification. Therefore the equations in this section contain text on which example sheave (among others) the equation applies. The complete system of equations of motion is given in Appendix D, as well as the definitions of all the remaining constants.

Equation 7.39 is given in a general form. As stated in the parameter descriptions the parameter "s" can take on multiple values, depending on the sheave one wants to consider. As an example, equation of sheave 19 one should use the value 19 for the parameter "s" and the corresponding "s2" value of 40. Hence, the equation of motion for sheave 19 is obtained.

Equation 7.40 works in the same way as described in the paragraph above. The parameter "m" can take on multiple values as indicated in the parameter descriptions below. The example equation of sheave 1 can thus be obtained through using the value 1 for "m" and using the corresponding "p" value of 1.

Equation 7.41 the parameter "x" in this equation can be utilized in the same way as described in the previous two paragraphs. This equation can be used for all other sheaves than those of Equation 7.39 and 7.40. Corresponding to each sheave number value of "x", the right hand side of the equation requires the sheave previous and sequential to the considered sheave in the wire rope system. The right hand side can thus describe a wide variety of sheave numbers corresponding to the parameter value of "x". In addition to that, the terms on the right hand side of the equation can be either positive or negative, depending on the sheave considered. Again, for the exact description of all equations of motion and their constants, please refer to Appendix D.

$$\ddot{\alpha}_s \cdot C_6 + \alpha_s \cdot C_7 = C_5 \cdot \varphi - C_8 \cdot \theta + C_9 \cdot \alpha_{s2} \quad \mathbf{7.39}$$

Applies on example sheave 19 for s=19

$$\ddot{\alpha}_m \cdot C_6 + \alpha_m \cdot C_{1p} = C_5 \cdot \varphi - C_8 \cdot \theta + C_9 \cdot \alpha_{m2} \quad \mathbf{7.40}$$

Applies on example sheave 1 for m=1

$$\ddot{\alpha}_x \cdot C_6 + \alpha_x \cdot 2 \cdot C_9 = \pm C_9 \cdot \alpha_{prev,x} \pm C_9 \cdot \alpha_{seq,x} \quad \mathbf{7.41}$$

Applies on example sheave 14 for x=14

$$\ddot{\varphi} \cdot C_1 + \varphi \cdot C_2 = \theta \cdot C_4 + (\ddot{z}_A + g) \cdot C_3 - \ddot{x}_A C_{10} + C_5 \cdot (\alpha_1 + \alpha_6 + \alpha_7 + \alpha_{12} + \alpha_{13} + \alpha_{18} + \alpha_{19} + \alpha_{24}) \quad \mathbf{7.42}$$

In which:

- s : Index which can take the values of 6, 7, 18 and 19
- s2 : Index which can take the values of 29 for s=6, 30 for s=7, 39 for s=18, and 40 for s=19
- m : Index which can take the values of 1, 12, 13, and 24
- m2 : Index which can take the values of 25 for m=1, 34 for m=12, 35 for m=13, and 44 for m=24
- p : Index which can take the values of 1 for m=1, 2 for m=12, 3 for m=13, and 4 for m=24
- x : Index which can take the value of 1 up to 44 with the exception of 1, 6, 7, 12, 13, 18, 19 and 24
- $\alpha_{prev,x}$: Index which indicates the previous sheave connected to the cable in the system. Corresponding to the parameter "x" with an value of 14, the sheave number of the previous sheave is 35. For this value of "x" the term should be positive. Refer to Appendix D for detailed definitions of the equations of motion.

- $\alpha_{seq,x}$: Index which indicates the sequential sheave connected to the cable in the system. Corresponding to the parameter "x" with an value of 14, the sheave number of the sequential sheave is 36. For this value of "x" the term should be positive. Refer to Appendix D for detailed definitions of the equations of motion.
- θ : Pitch at the COG in [rad]
- \ddot{z}_A : z-acceleration in point A (main hinge) in [m/s²]
- \ddot{x}_A : x-acceleration in point A (main hinge) in [m/s²]
- g : Gravitational acceleration in [m/s²]
- $C_{1...14}$: Constants containing mass terms, arms, angles and other factors. The values of these constants are described in Appendix D

Note that these equations not yet contain damping terms and friction terms. These terms are included in the equations during a later stage. Explanation on the addition of these terms can be found in the next sections. Information on the choice of the initial conditions is given in section 7.5.

STIFFNESS MATRIX

To make sure the derived equations of motions are correct one could check the symmetry of the stiffness matrix belonging to this system. The stiffness matrix of the system and its symmetry are shown in Appendix E.

NOTE ON THE CENTRE OF GRAVITY

The energy terms of equations 7.13 up to 7.18 and 7.27 up to 7.29 contain integrals. The derivation of the equations of motion using these integrals, assumes that the centre of gravity of the rigid sections lies at half the length of the corresponding section. However, the centre of gravity of the sections does not lie exactly at this location. Therefore the terms of the equation of motion containing the moment by the stinger weight are corrected by correcting the arms of the force in these constants.

ADDITION OF DAMPING

As stated earlier the damping terms are added in a later stage of the building of the model. When adding the damping terms the equations change as shown in the example equations 7.43 up to 7.46.

$$\ddot{\alpha}_s \cdot C_6 + \dot{\alpha}_x \cdot D_1 + \alpha_s \cdot C_7 = C_5 \cdot \varphi - C_8 \cdot \theta + C_9 \cdot \alpha_{y \neq s} \quad 7.43$$

Applies on example sheave 1

$$\ddot{\alpha}_m \cdot C_6 + \dot{\alpha}_x \cdot D_1 + \alpha_m \cdot C_{1p} = C_5 \cdot \varphi - C_8 \cdot \theta + C_9 \cdot \alpha_{y \neq m} \quad 7.44$$

Applies on example sheave 14

$$\ddot{\alpha}_x \cdot C_6 + \dot{\alpha}_x \cdot D_1 + \alpha_x \cdot 2 \cdot C_9 = C_9 \cdot \alpha_{y \neq x} \quad 7.45$$

Applies on example sheave 19

$$\ddot{\varphi} \cdot C_1 + \dot{\varphi} \cdot D_2 + \varphi \cdot C_2 = \theta \cdot C_4 + (\ddot{z}_A + g) \cdot C_3 - \ddot{x}_A C_{10} + \alpha_{s2} \cdot C_5 \quad 7.46$$

In which:

- $D_{1/2}$: Damping terms of type 1 and 2. Type 1 is related to the velocity of the sheaves and type 2 is related to the velocity of stinger. The damping terms are in [$\frac{kg \cdot m^2}{s \cdot rad}$]. It should be pointed out that the damping for each cable leading to a winch is different due to the various stiffness values in their equations. This is explained in the next few sections
- $\dot{\alpha}_x$: The velocity component of sheave x
- $\dot{\varphi}$: The velocity component of the stinger angular motion

It should be noted that when damping is applied like this, the damping by the wire ropes is not accounted for and the equations thus do not contain damping coupling terms. Since the damping in the system is unknown, a parameter is estimated and used in the FL model. However, as will be concluded in section 7.11 the damping is of less significance compared with the spring terms in the equations.

At first, for the base case, the values are estimated based on the mass and the stiffness of the equations of motion. It was decided to assume that the system experiences a critical damping ratio in the order of 5% as defined for a single degree of freedom system. However, it should be pointed out that this is not valid for a multiple degree of freedom system, thus the values represented by this equation are a rough estimation. The first estimation of damping was made to be approximately:

1. A D_1 has values within the range of 0.9E3 up to 1.5E3 $[\frac{kg \cdot m^2}{s \cdot rad}]$.
2. A D_2 value of 9.8E10 $[\frac{kg \cdot m^2}{s \cdot rad}]$.

Due to the large mass of the stinger this damping term was undoubtedly largely overestimated. This value of damping occurring in the stinger hinge is very unlikely. Furthermore, it should be pointed out that the type of damping thus introduced is of viscous nature, which can be unrealistic in describing the damping in this system. It is however a basic and mathematically convenient method to introduce a (linear) damping term which represents the overall dissipation occurring in the system. In addition, one needs to note that the viscous dissipation mechanism is essentially rate dependent, which means that is proportional to the velocity. The downside of working with velocity dependent damping is that the damping applies to all frequencies, so noise and motion information are equally influenced. It would be better to apply a frequency or mode dependent damping. That way certain frequency ranges can be damped more than the frequencies outside those ranges. Types of damping which would be better to apply are enumerated in section 9.3.

ADDITION OF SHEAVE FRICTION

The friction which will be added to the equations is rotational friction acting on the system via the cylindrical roller bearings. As assumed in section 7.2, it is expected to be more likely for the sheave to rotate as opposed to the situation where the steel wire rope starts to slip relatively to the sheave. Figure 7.5 shows a sketch of the motion inducing the friction.

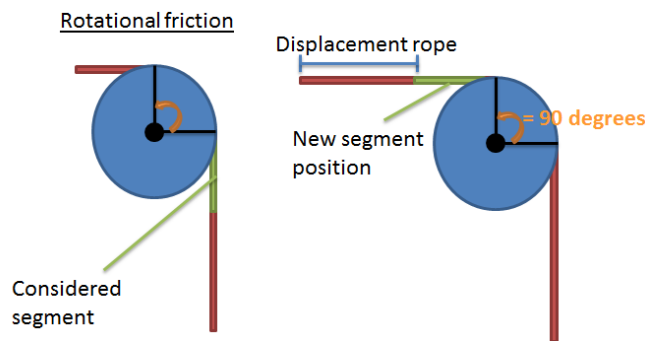


Figure 7.5 Rotational friction (left) and rotation by the sheave (right).

The bearing friction has been included in the equations of motion by the frictional moment term M_f , as can be seen in equations 7.47 up to 7.50.

$$\ddot{\alpha}_s \cdot C_6 + \dot{\alpha}_x \cdot D_1 + \alpha_s \cdot C_7 = C_5 \cdot \varphi - C_8 \cdot \theta + C_9 \cdot \alpha_{y \neq s} - M_f \quad 7.47$$

Applies on example sheave 1

$$\ddot{\alpha}_m \cdot C_6 + \dot{\alpha}_x \cdot D_1 + \alpha_m \cdot C_{1p} = C_5 \cdot \varphi - C_8 \cdot \theta + C_9 \cdot \alpha_{y \neq m} - M_f \quad 7.48$$

Applies on example sheave 14

$$\ddot{\alpha}_x \cdot C_6 + \dot{\alpha}_x \cdot D_1 + \alpha_x \cdot 2 \cdot C_9 = C_9 \cdot \alpha_{y \neq x} - M_f \quad 7.49$$

Applies on example sheave 19

$$\ddot{\varphi} \cdot C_1 + \dot{\varphi} \cdot D_2 + \varphi \cdot C_2 = \theta \cdot C_4 + (\ddot{z}_A + g) \cdot C_3 - \ddot{x}_A C_{10} + \alpha_{s2} \cdot C_5 \quad 7.50$$

In which:

M_f : Frictional moment term [Nm]

In the calculation of the rotational friction only a force related friction was included since the contribution of the term of the velocity dependent friction is small considering that it contains a factor of 10^{-7} [12] and that the normal force on the sheaves is considerably large. Therefore the velocity related friction would yield a less significant addition when compared with the force related dynamic friction in the equations of motion. The equations with which the friction is calculated are equation 7.51 [12] and equation 7.52. The axial force, or normal force, was calculated using equation 7.53 [13]. To clarify the calculations Figure 7.5 has been added, showing the calculation of the normal force acting on the sheave.

The addition of friction in this form reduces the mean value and the amplitude of the cable force prediction by the dynamic model. It however does not influence the phase of the time traces, which is logical since the friction as introduced is not velocity dependent. Note that because the effects were observed to be small and since the computational time increased gravely (order of hours), the friction is not included in the FL model analyses but the option to use the friction terms is present in the Matlab model as an option for usage.

$$M_f = g_f(\dot{\alpha}) \cdot fr \cdot \frac{d_{bore}}{2} \cdot N_o \quad 7.51$$

$$g(\dot{\alpha}) = \begin{cases} 1, & \text{for } \dot{\alpha} < 0 \\ -1, & \text{for } \dot{\alpha} > 0 \\ 0, & \text{for } \dot{\alpha} = 0 \end{cases} \quad 7.52$$

$$N = \sin\left(\frac{d\theta}{2}\right) \cdot (Te) + \sin\left(\frac{d\theta}{2}\right) \cdot (Te + dTe) = \sin\left(\frac{d\theta}{2}\right) \cdot (Te_x + Te_{x+1}) \quad 7.53$$

In which:

- fr : Frictional coefficient of the double cylindrical roller bearing
- d_{bore} : Bore diameter in [m]
- N_o : Normal force (or radial force) on sheave axis in [N]
- dθ : Contact angle of the wire in [rad]
- Te : Tension in the cable parts directly connected with the sheave concerned in [N]. Note that the tension in the cable is a function of α_x , $\alpha_{prev,x}$, $\alpha_{seq,x}$, Φ , θ (pitch) and the stiffness of the specific cable parts
- x : Sheave index number
- $g_f(\dot{\alpha})$: Velocity dependent function to give the friction component the right directional sign depending on the velocity of the sheave

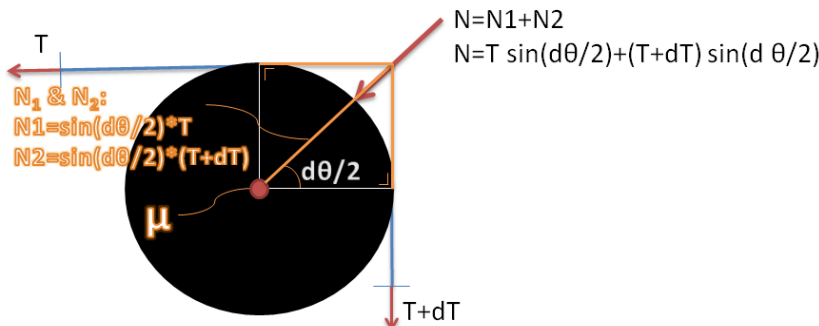


Figure 7.6 The calculation of normal force by the tensions of cables on both sides of the sheave.

7.3.5 STATIC BUOYANCY

Even though a non-submerged situation is reviewed, as stated in section 4.2, the model does contain the influence of the static buoyancy in the event one uses a stinger configuration input in the model, which includes a submerged stinger. The static buoyancy is accounted for by calculating the submerged volume of the stinger. Logically, the submergence means the hang-off cables will carry less load when the stinger is submerged.

It should be pointed out, however, that solely the static buoyancy term will not be sufficient to calculate the cable forces in a submerged state. There are multiple physical effects which must be defined to accurately predict the cable forces using the FL model.

7.4 SOLVING METHODS FOR THE EQUATIONS OF MOTION

The equations of motion can be solved using two methods. The first method is direct time-integration of the ordinary differential equations and the second method is the modal analysis. (Information on the solving of the equations in Matlab can be found in Appendix H.) Both methods are used in this thesis and both methods are solved using Matlab. The two approaches use the same equations of motion, however, the direct time integration uses the equations as defined in the previous section but the modal analysis solves the same equations after translation to the modal domain. This section will elaborate on this matter and give a general explanation on the modal analysis method.

The modal analysis is an alternative method for solving for a system with n degrees of freedom and thus n equations of motion. Essentially it is a method to represent the forced motion as a summation of normal modes (the normalised eigenvectors) of the free vibrations multiplied by the modal time function. The forced motion is called the generalized displacement. The equation is given in equation 7.54. This means that the generalized displacement is separated into a space and a time function. [14]

$$\underline{x}(t) = \sum_{i=1}^N \hat{\underline{x}}_i u_i(t) = \underline{E} \underline{u}(t) \quad 7.54$$

In which:

- \underline{x} : Generalized displacements of all degrees of freedom
- $\hat{\underline{x}}_i$: i^{th} Normal mode of the system
- $u_i(t)$: Modal time function
- \underline{E} : Eigen matrix containing all eigenvectors or normal modes

The eigenvectors and eigenvalues of the undamped n-degree of freedom system are obtained numerically through Matlab. When solving the eigenvalue problem it is assumed the eigenvectors are known but their amplitudes are undefined. These eigenvectors and eigenvalues are consequently used in the calculations of the modal equations of motion which are solved for the modal time function. Note that the eigenvectors in these calculations are mass normalised. However, the analysis is a mathematical representation of the system through which the actual physical response can be calculated using this notation for the generalised displacements.

The modal equations are obtained by substituting equation 7.54 in the equations of motion and pre-multiplying these equations the transposed eigenmatrix. These operations are shown in equation 7.55. Because of the orthogonality property of the eigenvectors, one obtains the uncoupled equations of motions containing the modal mass and modal stiffness matrices. The calculation of modal matrices is displayed by equations 7.56 and 7.57. It must be pointed out, however, that if damping is present in the system the off-diagonal elements of the modal damping matrix are generally non-zero. This means that the equations of motions cannot be uncoupled [14]. However, due to the way damping is introduced, as a percentage of critical damping of a certain mode, it is possible to obtain a diagonal modal damping matrix.

$$\underline{E}^T \underline{M} \underline{E} \ddot{\underline{u}} + \underline{E}^T \underline{K} \underline{E} \underline{u} = \underline{E}^T \underline{F} \quad 7.55$$

$$\underline{M}^* = \underline{E}^T \underline{M} \underline{E} \quad 7.56$$

$$\underline{K}^* = \underline{E}^T \underline{K} \underline{E} \quad 7.57$$

In which:

- \underline{M}^* : Modal mass matrix
- \underline{K}^* : Modal stiffness matrix
- \underline{M} : Physical mass matrix
- \underline{K} : Physical stiffness matrix
- \underline{F} : Force vector with forces acting on each degree of freedom

In this thesis the modal matrixes have been calculated by using mass-normalised eigenvectors. They are calculated using equation 7.58. This means that the modal mass matrix is equal to the identity matrix of size 45x45. For the equations of motion the type of normalisation does not, in principle, matter since the matrices are all post- and pre-multiplied by the correspondent eigenvector matrix. Some numerical issues that come into play while performing the modal analysis are described in Appendix F.

$$\underline{E}_{\text{Normalised}} = \frac{\underline{E}}{\sqrt{\underline{E}^T \underline{M} \underline{E}}} \quad 7.58$$

The damping used in the system in this thesis is an estimation. For the modal analysis the damping has been defined as a percentage of the critical damping. The critical damping is first calculated using the modal mass and modal stiffness matrixes. Subsequently, a constant value equal to 5% of the critical damping over all modes was used as base case. The most significant modes' percentages have been

varied in order to find a better fit. The critical damping of each mode has been calculated using equation 7.59. The actual damping was consequently calculated using equation 7.60. This equation will return a fully populated damping matrix.

$$d_{ii}^{critical} = 2\sqrt{k_{ii}^* m_{ii}^*} \quad 7.59$$

$$d_{ii}^* = 0.05 \cdot d_{ii}^{critical} \quad 7.60$$

In which:

$d_{ii}^{critical}$: Critical modal damping of mode i
 k_{ii}^* : Modal stiffness of mode i
 m_{ii}^* : Modal mass of mode i
 d_{ii}^* : Modal damping of mode i

With the diagonal modal damping matrix, the damping of each separate modal equation can be varied on its own. To find the physical damping which corresponds to the chosen modal damping matrix, equation 7.61 can be used. With that equation the physical meaning of the applied damping can thus be found.

$$D_{physical} = MED^* E^{-1} \quad 7.61$$

In which:

$D_{physical}$: Physical damping matrix derived from the modal damping matrix
 D^* : Modal damping matrix

When using the modal analysis the differential equations will be solved for the modal system. The equations will be solved for $\underline{u}(t)$, the unknown time function. Then, to obtain the generalized displacements one still needs to apply equation 7.54 to the solved differential equations.

The modal analysis method should yield the exact same result with the direct time-integration method provided that the damping is applied the same in the two methods.

7.5 PREPARATORY CALCULATIONS

Before solving the equations of motion it is necessary to define multiple system parameter values. The first section of this chapter describes how these parameter values are obtained. The second section of this chapter describes which calculations are performed with the solutions of the ordinary differential equations. Both sections include assumptions made additional to those in section 7.2. A more detailed elaboration on Matlab settings and limitations are given in Appendix H.

7.5.1 DEFINING SYSTEM PARAMETERS

The parameters of the system which need to be defined before the equations of motions can be solved are:

1. The stiffness values of the cable parts in the hang-off system.
2. All weights of all (pieces of) equipment.
3. The static buoyancy of all (pieces of) equipment.
4. The rotational inertia of the sheaves.
5. The definition of the initial conditions.
6. Solving of some Matlab related difficulties (which is described in more detail in Appendix H).

STIFFNESS VALUES

The stiffness of the cables is calculated using equation 7.62.

$$K_{part} = \frac{E_y A}{l_{unstretched}} \quad 7.62$$

In which:

K_{part} : Stiffness of a cable part in [N/m]
 E_y : Youngs Modulus in [N/m²]
 A : Area in [m²]
 $l_{unstretched}$: Original unstretched rope length of parts in [m]

The calculation of the unstretched cable lengths is necessary to acquire the stiffness values of the various wire rope parts. Note that $l_{unstretched}$ is calculated via the total strain in the wires. The total strain is calculated through the static weight of the stinger (including all equipment) and the self-weight of the cables, see equation 7.63. Note that the self-weight dependent strain is actually a factor 100 smaller than the strain by the static weight, therefore its contribution is relatively small compared to the static weight of the stinger. Combining equation 7.63 and 7.66, one can derive a second order equation with only ϵ_{tot} as unknown. This variable can be calculated for any stinger position. When the unstretched cable length is known it can then be used to calculate equation 7.62. Using these equations one can calculate all stiffness parameters of the cables parts modelled as springs. This yields spring stiffness K1, K2 and K3. The only difference in the calculations for stiffness value K1 and K3 is the sign of the self-weight force, another angle than beta and, of course, a different $l_{stretched}$.

$$\begin{aligned} \epsilon_{tot} &= \epsilon_{static} + \epsilon_{self-weight} \\ &= \frac{F_{static}}{E_y \cdot A} + \frac{mpm \cdot g \cdot l_{unstretched} \cdot \cos(\beta)}{2 \cdot E_y \cdot A} \end{aligned} \quad 7.63$$

$$l_{unstretched} = \frac{l_{stretched}}{(1 + \epsilon_{tot})} \quad 7.64$$

In which:

ϵ_{tot}	:	Total strain
ϵ_{Static}	:	Strain by the static weight in the cables
$\epsilon_{self-weight}$:	Strain by self-weight of the cable
mpm	:	Mass per meter cable in [kg/m]
$l_{stretched}$:	Stretched cable length of part cable considered in [m]

Assumptions made during the determination of the spring stiffness parameters are:

- Sheaves 1, 6, 7, 12, 13, 18, 19 and 24 are assumed to be of equal height (z-coordinate) as the top sheave blocks of the hang-off frame. The cables running to these sheaves are thus assumed to be of equal length as the rest of the windings.
- The rope sections running from sheaves 6, 7, 18, 19 to the solid connection point in the model, point D in Figure 7.4, are assumed to have the original length belonging to the original sheave positions of sheaves 6, 7, 18 and 19 (thus without the previous assumption).
- The winches are assumed to be rigid connections at the ends of the cables parts running from sheaves 1, 12, 13 and 24.

EQUIPMENT WEIGHTS, STATIC BUOYANCY AND ROTATIONAL INERTIA

The weight of the following equipment is calculated and included:

- The three stinger parts
- The lower block structure
- The lower sheave block
- The pup-pieces
- The rollerboxes
- The walkways
- The cables

The static buoyancy is included in the FL model. It accounts for the submerged volume of all previously enumerated parts depending on the stinger angle and the stinger configuration.

The calculation of the rotational moment of the sheaves has been performed using equation 7.65, the standard function for the rotational inertia of a solid cylinder.

$$I_{sheave} = \frac{1}{2} m_{sh} R^2 \quad 7.65$$

In which:

I_{sheave}	:	The rotational inertia of the sheave [kg·m ²]
m_{sh}	:	Mass of the sheave [kg]
R	:	Radius of the sheave [m]

The sheaves actually do not have a cylindrical shape since the wire rope is wound through the groove of the sheave. The depth of this groove is small compared to the radius so the influence of these extensions on both sides of the wire rope is considered insignificant for the total rotational inertia.

Therefore, the extensions have been accounted for using a solid cylinder (without the groove) with a slightly larger radius, representative for the volume distribution of the groove. A sketch of this is shown in Figure 7.7.

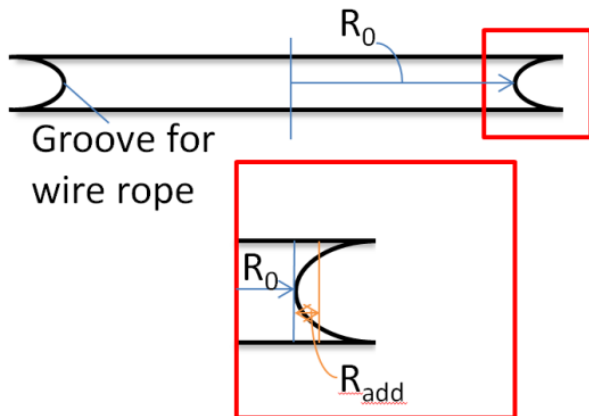


Figure 7.7 Representative radius for inertia calculations.

THE INITIAL CONDITIONS

In order to solve the equations of motion, initial conditions are defined. To prevent disturbance in the resulting motions by an initial displacement of the system, the static equilibrium of the system was calculated. This was done by finding the static solution of the dynamic equations using the static moments acting on the system and the K-matrix of the system. The equation resulting in the values of the static initial conditions is equation 7.66.

$$\underline{\underline{StatIC}} = \underline{\underline{K}}^{-1} \cdot \underline{\underline{M}}_{static} \quad 7.66$$

In which:

- $\underline{\underline{StatIC}}$: Static values of all DOF (Degree Of Freedom) to apply at t=0 when solving the ordinary differential equations
- $\underline{\underline{K}}$: Stiffness matrix of the system of equations
- $\underline{\underline{M}}_{static}$: Static force vector acting on the system

COMPLICATIONS CONCERNING MATLAB

When solving the equations of motions using Matlab there are some points which require attention. These points are explained in Appendix H and are various in nature. To summarise shortly, the difficulties found are:

1. The solver (the function that is used in Matlab to solve the differential equations) uses discontinuous internal time steps when solving. Since the input of ship motions is time-dependent, it is necessary to interpolate this input so a value is known for every internal time step used by the solver.
2. Due to an efficiency complication considering computational time an alternative ode-solver is used instead of the regular ordinary differential equation solver, *ode45* function.
3. Definitions of the tolerances which define the maximum allowable error of the solver predictions.

7.5.2 USING THE ORDINARY DIFFERENTIAL EQUATIONS RESULTS

The solver gives multiple outputs, as explained in Appendix H. These outputs can be used to define multiple variables which can be used for evaluation of the models. Also the cable force prediction itself will need to be calculated using the output values of the solver. The calculations are performed after obtaining the solutions to the equations of motion:

1. The cable forces at load cell locations (see Figure 7.3).
2. The total cable force.
3. The mean sheave frictional moment values.
4. The accelerations of all degrees of freedom.

The calculation of cable forces at the load cell positions was performed using equation 7.67. The idea is that since the cables are modelled as springs, the elongation of such a spring and the known stiffness values will yield the force in the cable.

$$F_{LC,n} = \alpha_x \cdot RK_1$$

for x = 6, 7, 18, 19

for n = 1 ... 4

7.67

In which:

- $F_{LC,n}$: Cable force at load cell number n [N]
R : Sheave diameter [m]
 K_1 : Spring stiffness of the rope sections running from sheaves 6, 7, 18, 19 to the solid connection point, point D in Figure 7.4, in [N/m]
x : Sheave number 6, 7, 18 or 19
n : Cable number 1, 2, 3 or 4

The total cable force was calculated with equation 7.68. Note that the factor 10 represents that each cable has 10 windings through the pulley system. To acquire the total load which acts on the hang-off system one needs to account for the fact that one such cable winding carries only a part of the total load.

$$F_{c,total} = (F_{LC,1} + F_{LC,2} + F_{LC,3} + F_{LC,4}) \cdot 10$$
7.68

In which:

- $F_{c,total}$: Total predicted cable force in [N]

The calculation of the mean sheave frictional moments was done using equation 7.69. For more detail on the calculation of frictional moment please refer to section 7.3.

$$M_f(\dot{t}) = \text{mean} \left(g_f(\dot{\alpha}) \cdot f \cdot \frac{d_{bore}}{2} \cdot N(\dot{t}) \right)$$
7.69

Accelerations were calculated using differentiation in frequency domain, as explained in section 5.4.

7.6 VALIDATION OF ASSUMPTIONS

This section elaborates on some of the assumptions made in section 7.2 and the proof of these assumptions being physically or mathematically correct.

7.6.1 SMALL ANGLE APPROXIMATION

The small angle approximation states that for small angles the equations of $\sin(\varphi)$ and $\cos(\varphi)$ can be approximated, as stated in equation 7.37 and 7.38. Reviewing the model results it can be seen that the maximum value of the stinger angle φ is 2.4 degrees and the mean value is 2.0 degrees. Using this maximum angle the error induced for the cosine function by the approximation is smaller than 0.09%. The error introduced for the sine function due to the approximation is smaller than 0.03%. Therefore it can be stated that the small angle approximation can be used for the parameter φ .

7.6.2 2-D-ANALYSIS APPROXIMATION

In Chapter 5 it was found that the roll motion has little to no common characteristics with the measured cable forces. This angular motion is estimated to be the most influential 3-D motion present in reality. Because this motion does not seem to have these common characteristics with the measured cable forces in this time trace and because the system is almost completely symmetric, it is not considered necessary to expand the model to 3-D for this thesis. An expansion of the model to 3-D configuration would be of interest only for cases, other than the one considered in this thesis, contain significant out-of-plane motions of the system.

7.6.3 CONTRIBUTION OF LOWER BLOCK STRUCTURE MASS

The lower block structure is the structural connection between the lower sheaves and the stinger connection point. This structure is indicated in Figure 7.8 for clarification. As stated in assumption 13 of section 7.2, the lower sheave block structure is included in point B of the schematisation of Figure 7.4. The length of these structures is 8.1 meters. Therefore they induce a moment which is carried by the hang-off cables. This means the actual force in the hang-off cables might be significantly different than accounted for in the current calculations, using assumption 13 of section 7.2. The additional force might be thus large that it cannot be assumed to be present in point. Therefore the assumption of placing its weight in point B is reviewed by calculating the static contribution of such a moment.

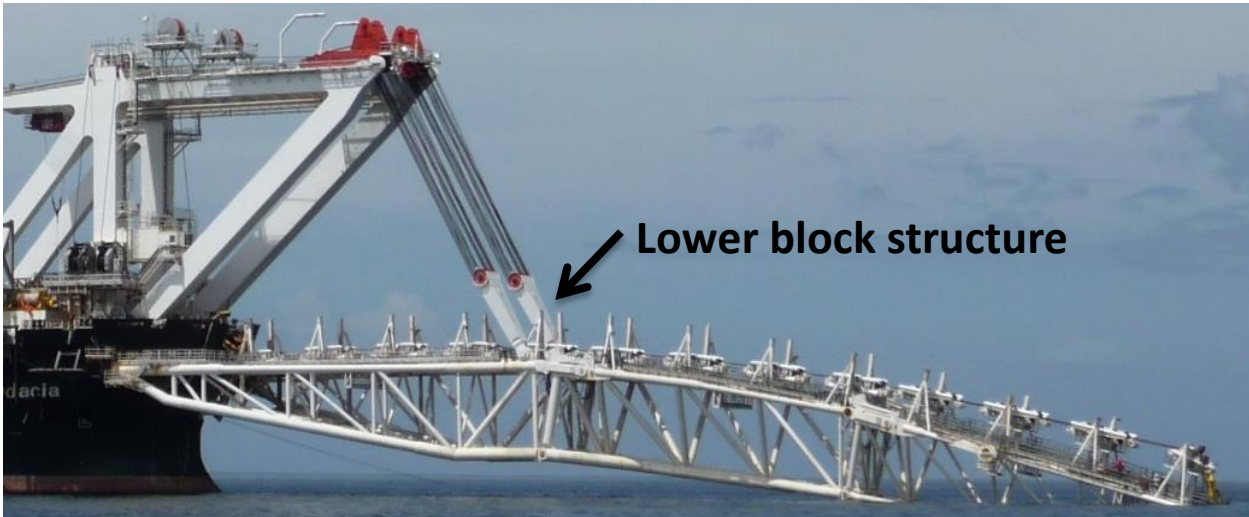


Figure 7.8 Reminder of the lower block structure location.

The results are given in Table 7.2. The increase of tension when accounting for this moment would be 0.353 kN. This would be a 14.1 kN increase (0.075% increase) on the original total static weight of 1.891E4 kN, which is used now. The calculations also show that the lower block structure's angle ($\Delta\text{ang}2$) and cable's angle ($\Delta\text{ang}1$) are respectively $8.34\text{E-}7$ radians and $4.30\text{E-}7$ radians. (For angle locations, see Figure I.1 in Appendix I.) The angles and the force increase show that it is fine to assume the sheave blocks and their structure to be in point B and in line with the angle β (assumption 13 of section 7.2). The information on how this moment contribution to the static cable force was calculated is given in Appendix I.

	Absolute increase of tension compared with NO sheave & block weight [kN]	Relative increase of tension compared with NO sheave & block weight [%]
Block and sheave weight in point B (original calculation)	+31.389	+7.11
Including Lower block structure moment	+31.742	+7.19

Table 7.2 Effects of the original and the new calculation on the cable tension (T) relative to the situation without the weight of the sheaves and the lower block structure.

7.7 VALIDATION FL MODEL USING DIRECT TIME-INTEGRATION

Prior to the use of the model for cable force predictions, it needs to be verified in order to check whether the results of the model are as expected and thus can be considered as reliable. Therefore, in this section, various cases are investigated in order to validate the model predictions. Note that all tests were performed without sheave friction

7.7.1 THE BASE CASE

Following from the previous chapters the modelled system is an a-symmetrical system which can be influenced by friction, inertia, cables as springs, external forcing and damping. The input motions considered here correspond to the base case in which measured motions are known at the centre of gravity of the ship, i.e. heave, surge and pitch motions.

The base case main variables are defined as:

- K_1 : Spring constant based on length of cables of type I, the distance of top sheave to load cell connection. K_1 has a value of $1.21\text{e}+06$ [N/m].
- K_2 : Spring constant based on length of cables of type II, the distance of top sheaves to the stinger sheave block. K_2 has a value of $5.9\text{e}+05$ [N/m].
- K_3 : Spring constants based on length of cables of type III, the distance of top sheaves to the winches. K_3 is a vector contain in four different values since every rope part leading to the winches has a different stiffness value. The vector values are: $10^5[1.53 \ 1.84 \ 1.61 \ 1.94]$ in [N/m].
- $D_{1/2}$: Damping is initially used as defined in section 7.3.4.

7.7.2 STATIC AND FREE VIBRATION TEST

In this section two tests are performed: a static test and an free vibration test with initial displacement. For the static test it is expected that when the system is found in the equilibrium position and provided that there are no forces acting on the system, all degrees of freedom will remain in their original position. For the free vibration test the original initial conditions are multiplied by a factor of 1.1. The expectation is that the degrees of freedom, due to the system being underdamped, will oscillate but damp out to their equilibrium positions. The tests and their expected results are listed in Table 7.3.

Test #	Test	Expectation
1	Static test	The result will be a constant shave angle and stinger angle, thus all degrees of freedom show and keep one value in the original position.
2	Free vibration test after initial displacement.	Some oscillation will be visible which will damp out to the static equilibrium values.

Table 7.3 Static tests 1 and 2 with their description and their expectations.

The results of both tests can be found in Figure 7.9 up to Figure 7.10. The results shown are as expected in Table 7.3.

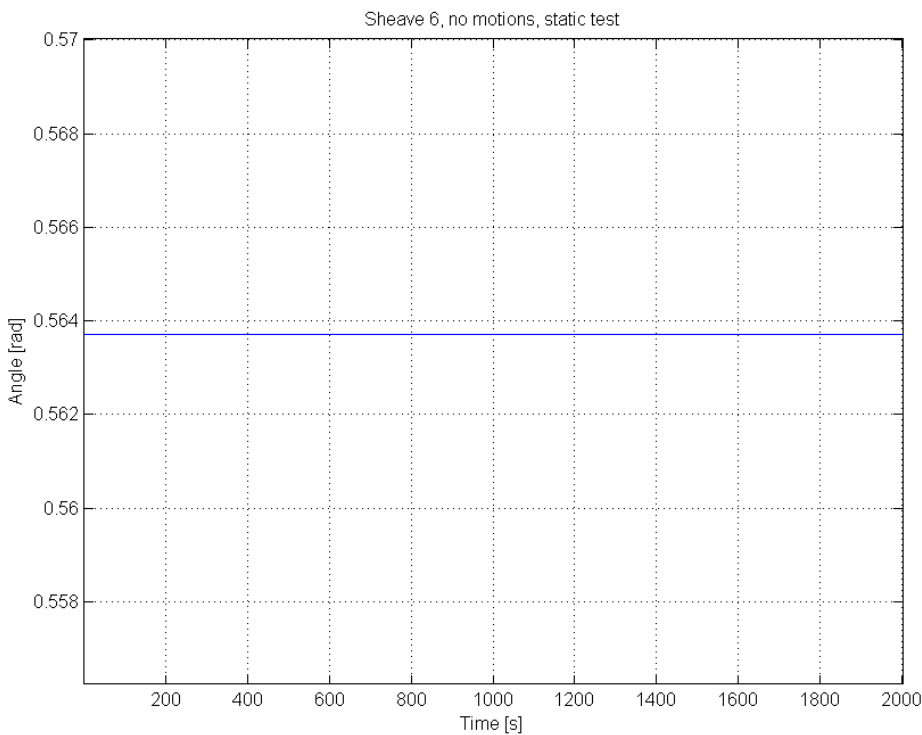


Figure 7.9 Results of static test 1. Sheave 6 also stays in equilibrium position, as expected.

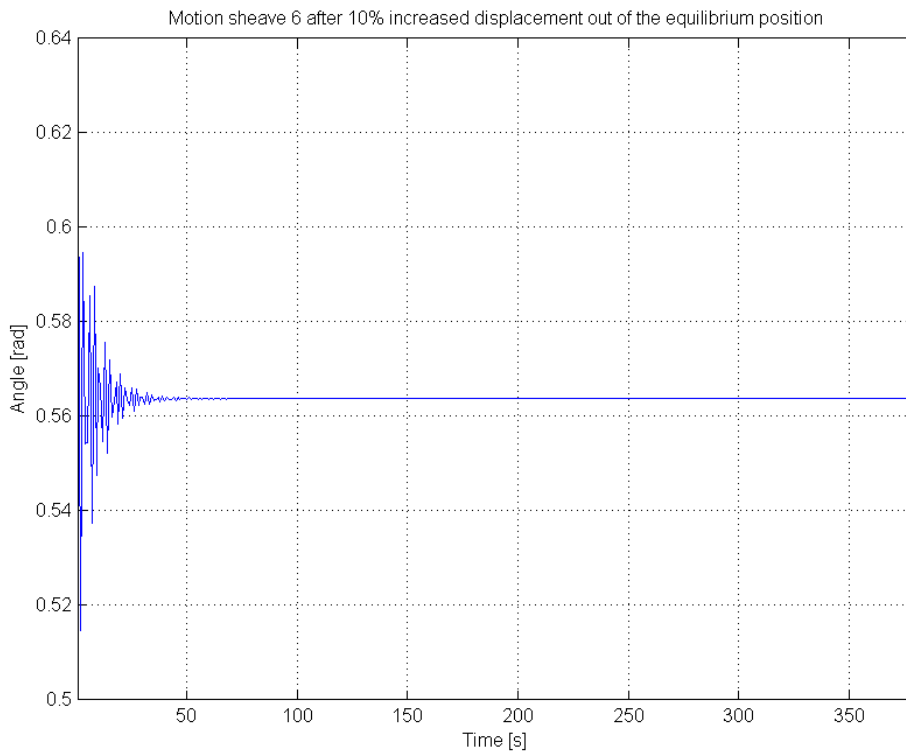


Figure 7.10 Result of the free vibration test. Sheave 6 shows oscillations after initial displacement of 10%, as expected.

7.7.3 HARMONIC EXCITATION TESTS

This section elaborates on the harmonic excitation testing performed in this thesis. Instead of using the measured ship motions as input an artificial pitch input has been used with a known frequency and amplitude. The chosen amplitude is 0.7 degrees, or 0.012 radians. The chosen amplitude value is large compared with the input data but it will be easier to analyse the response to this large input than to a small input. This artificial pitch equation is given in equation 7.70.

$$\theta_{custom} = B \cdot \sin(\omega t) \quad 7.70$$

In which:

- B : Chosen amplitude [rad]
- ω : Chosen frequency [rad/s]
- θ_{custom} : Artificial pitch input with chosen parameters

For the dynamic tests 1 up to 3 different values of the excitation frequency ω are chosen. The ω -values are chosen such to represent extremes. The artificial motions contain a very high frequency (larger than the highest frequency), a very low frequency (lower than the fundamental frequency) and the base resonance frequency. The range of system frequencies are separately found through the modal analysis approach. Table 7.4 shows all tests, the qualities of the artificial input motion and it shows the expectations of the test results.

Test #	Harmonic excitation test	Expectation
1	High frequency custom θ excitation. ($A=0.7^\circ$, $\omega=700$)	The excitation contains a frequency above the highest natural frequency of the system, it lies within the mass dominated regime of the FL model. Because of the stinger's large inertia it does not have enough time to respond with an angular motion as consequence of the high excitation frequency.
2	Low frequency custom θ excitation. ($A=0.7^\circ$, $\omega=0.007$)	Because the pitch motion influences the spring forces in the springs with stiffness K_2 , a low frequency pitch motion will result in a slow quasi-static stinger angle motion. This is to be expected as the extreme low frequency excitation lies far below the first natural mode of the system.
3	Natural frequency custom θ excitation. ($A=0.7^\circ$, $\omega=2.22$)	With the artificial pitch motion containing the base natural frequency, the system's response should show resonance.

Table 7.4 Harmonic excitation tests 1, 2 and 3: Their description and their expectations.

The results of the tests can be found in Figure 7.11 and Figure 7.13. As indicated in their titles: The results are as expected in Table 7.4.

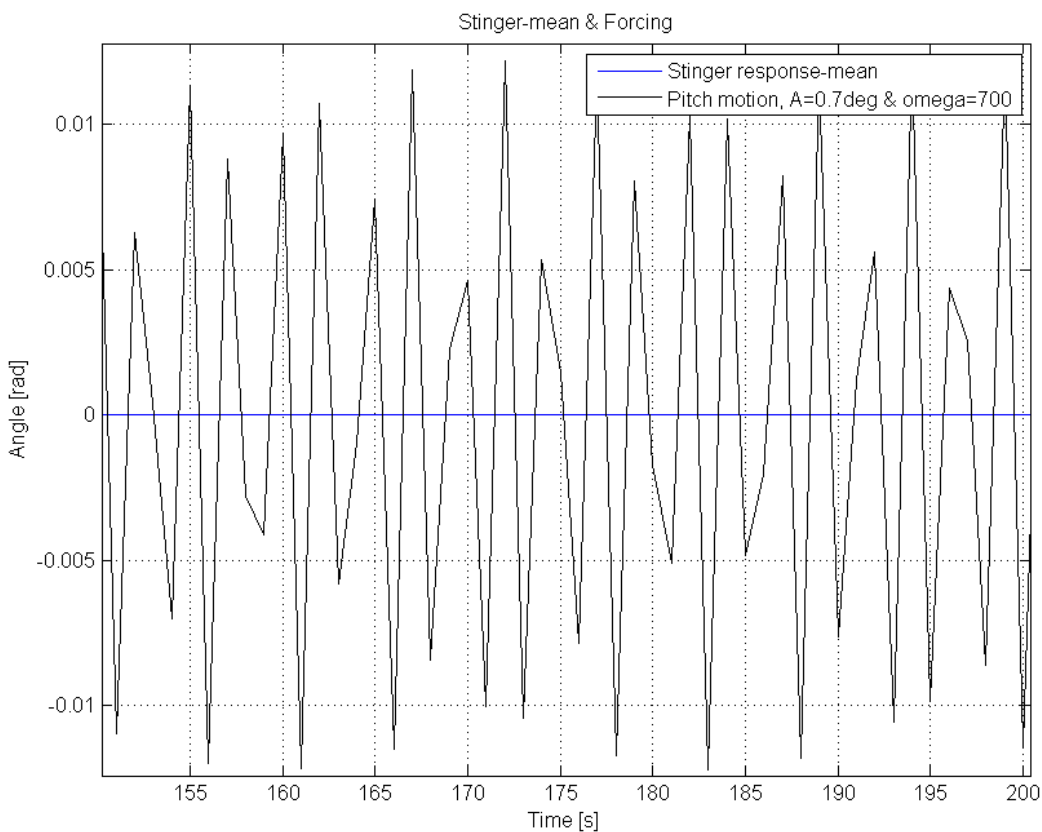


Figure 7.11 Results of dynamic test 1. The stinger shows little to no displacement by the excitation far into the mass-dominated regime, thus the high frequency custom θ excitation. The results are as expected.

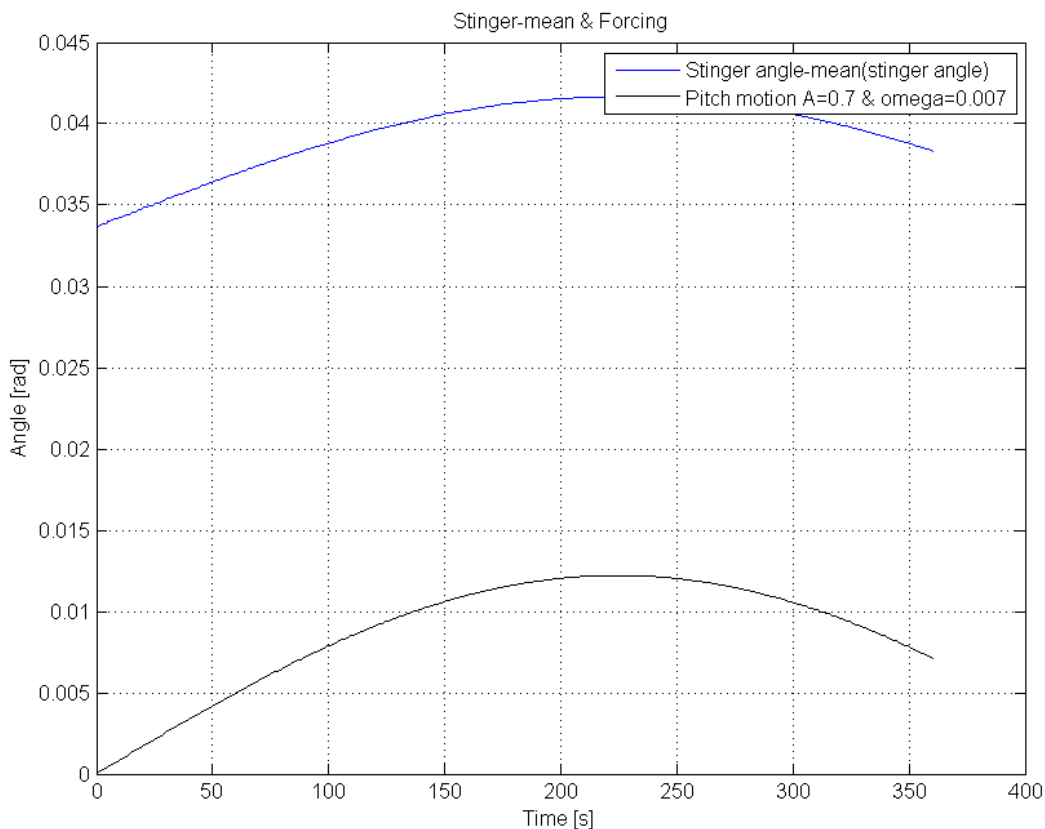


Figure 7.12 Results of dynamic test 2. The stinger reacts quasi-static to the low frequency custom θ excitation. As expected.

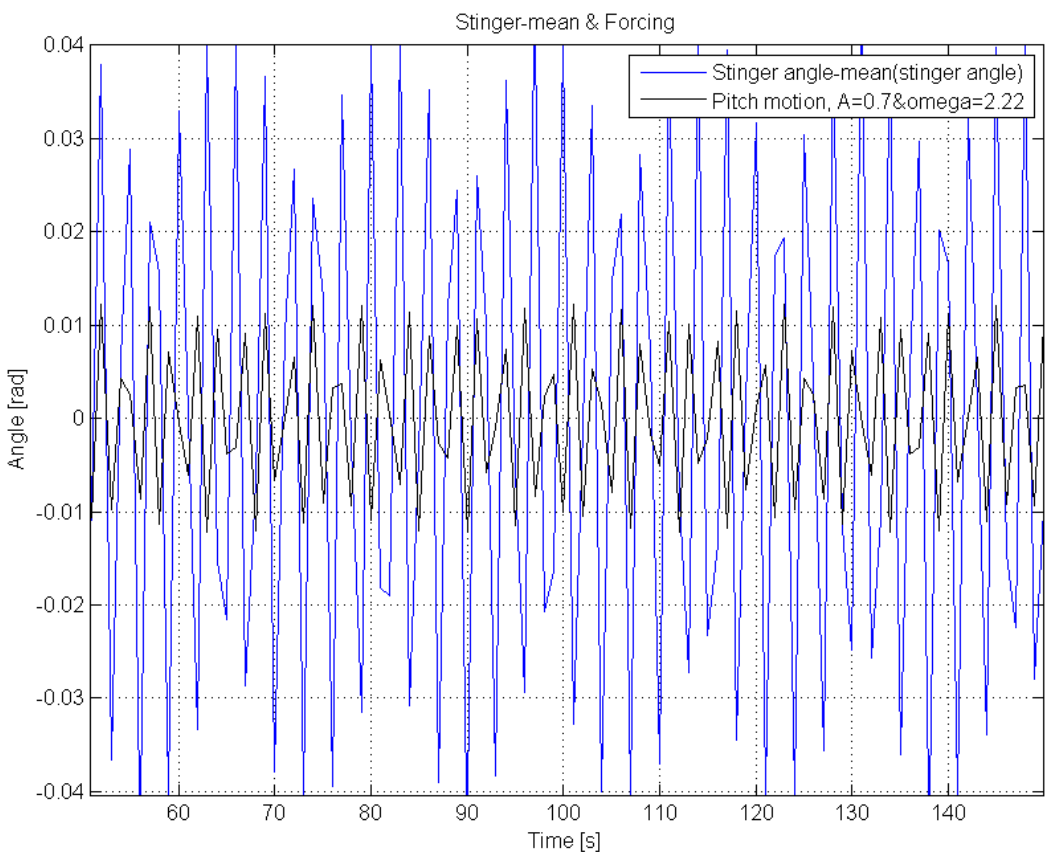


Figure 7.13 The stinger's response to an excitation in the natural frequency, as expected.

7.8 BASE CASE ANALYSIS

This section elaborates on the previously described models and methods and gives the base case results of these models and methods. The base case of a model is the starting point of the model's settings. For the RL model the base case is the only case possible since its parameters cannot be changed. For the FL

model there are multiple parameter settings possible. Therefore, the FL model is at this point first analysed for its base case as described in section 7.7.1. The analysis is performed for both the direct time-integration technique and the modal analysis. The results are presented using the same graphs and reviewing methods as in section 6.2.3, in which the RL model was analysed.

7.8.1 REVIEWING METHODS RECAPITULATION

The resulting data traces of all models are reviewed using different methods. As explained in section 6.2.3 the results of the FL model will both be quantitatively as qualitatively analysed. The methods used are:

1. Normalised cross-covariance over the complete data trace.
2. Standard deviation of the cable force time-traces.
3. Correlation of peak amplitudes.
4. Mean peak amplitude difference.
5. Mean peak time difference.
6. Minimum distance method.
7. Frequency plot and spectrogram.

As they have already been explained in detail in section 6.2.1, no further elaboration is given on the reviewing methods at this point.

7.8.2 THE TARGET VALUES RECAPITULATION

A complete analysis of the measured cable forces was performed in section 6.2.2. Therefore, this section will only recap the analysis by providing for the target values and plots. Those can be used to compare the FL model results with. The frequency spectrum and the spectrogram are shown in Figure 7.14 and Figure 7.15 respectively. Specifications of the measured cable forces' time-domain are shown in Table 7.5.

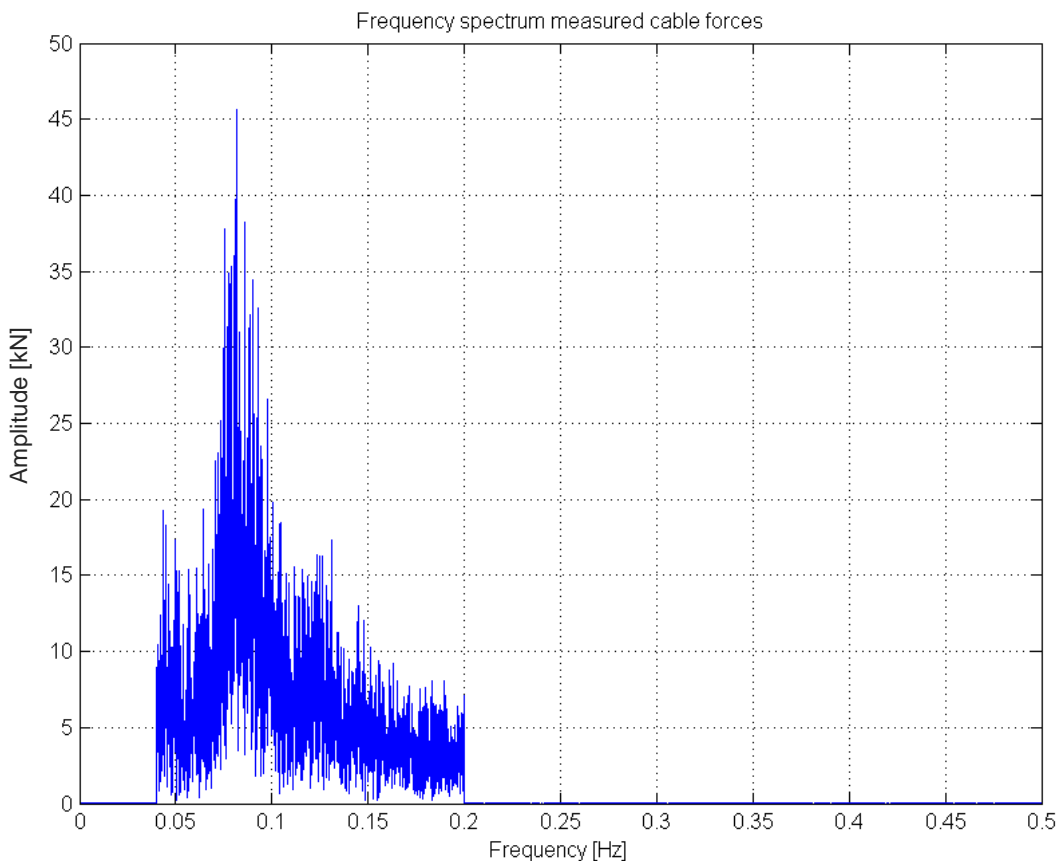


Figure 7.14 Frequency plot of the measured cable forces. The spectrum is non-binned but has been filtered.

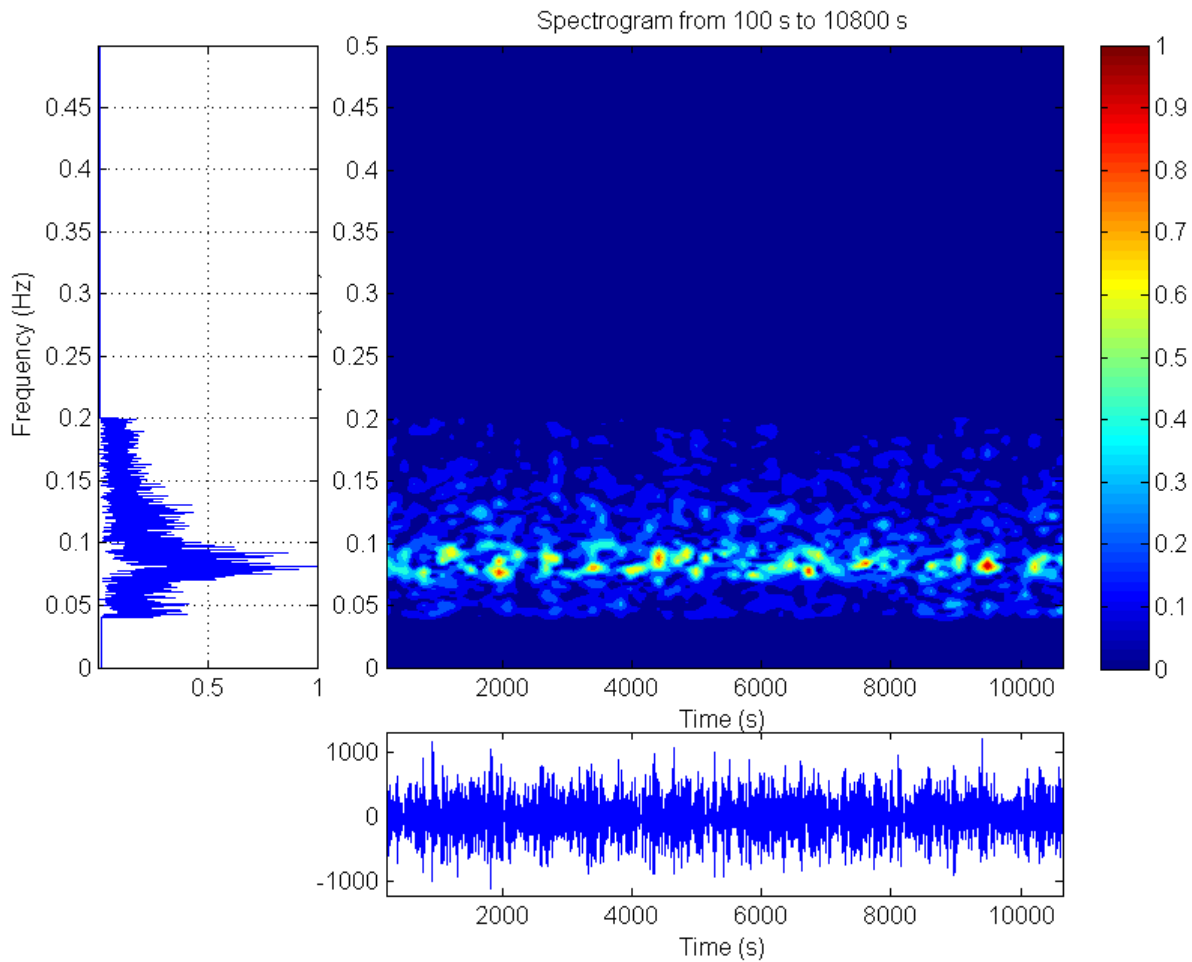


Figure 7.15 Spectrogram of the measured cable forces, using a hamming windowing function. Note: The frequency plot on the left hand side is normalised.

Target Values in[kN]	Standard deviation
Mean	1.894E4 kN
Standard deviation	267.7 kN
Max	2.016E4 kN
Min	1.782E4 kN

Table 7.5 Properties of the measured cable forces.

7.8.3 RL MODEL RECAPITULATION

The RL model analysis was already performed in section 6.2.3. For a detailed analysis please refer to this section. The current section will only recap the results of the RL model analysis. Since the time trace of the RL model is present in all time-domain plots of the FL model, the time-domain plot of the RL model is not shown as it is unnecessary to do so. The general time trace properties can, however, be found in Table 7.6. The results of all quantitative reviewing methods are shown in Table 7.7. In order to compare frequency analysis results of the FL model with the RL model's frequency results the frequency spectrum is given in Figure 7.16. In Figure 7.17 the spectrogram of the RL model is shown for comparison with the time-frequency results of the FL model.

In section 6.2.3 it was that the RL model is significantly correlated but showed to contain a frequency difference. Additionally it is apparent that the predicted force amplitudes are underestimated. The frequency difference is caused by the high frequency content visible in the RL model's frequency plots. The current standard deviation error is 20.8% when reviewing the standard deviation values of the RL model and the measured cable forces. This number does exclude the influence of input uncertainty of the model, which can be found in section 7.10.1.

Property	Standard deviation	Mean	Maximum	Minimum
Values in [kN]	212 kN	1.8925E4 kN	2.0105E4 kN	1.7752E4 kN
Difference with measured values in [kN]	-55.3 kN	-12.9 kN	-52.4 kN	64.3 kN

Table 7.6 Time-trace properties of the RL model.

Reviewing method	Result
Normalised cross-covariance complete	(-1, 0.721)
Standard deviation	212 kN
Peak amplitude correlation	0.601
Mean peak amplitude difference	-92.2 kN
Mean peak time difference	-1.1 s
Correlation in time & amplitude	140.98

Table 7.7 Results of the reviewing methods for the RL model.

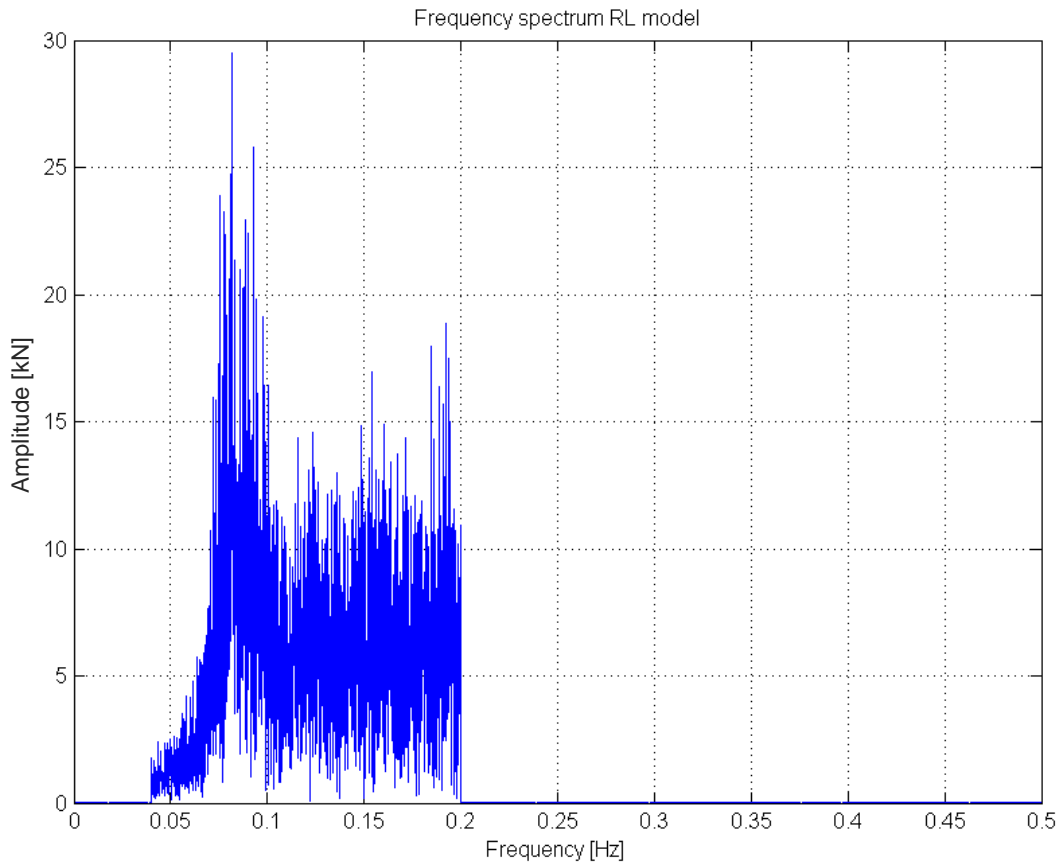


Figure 7.16 The frequency spectrum of the RL model. The spectrum is non-binned but has been filtered.

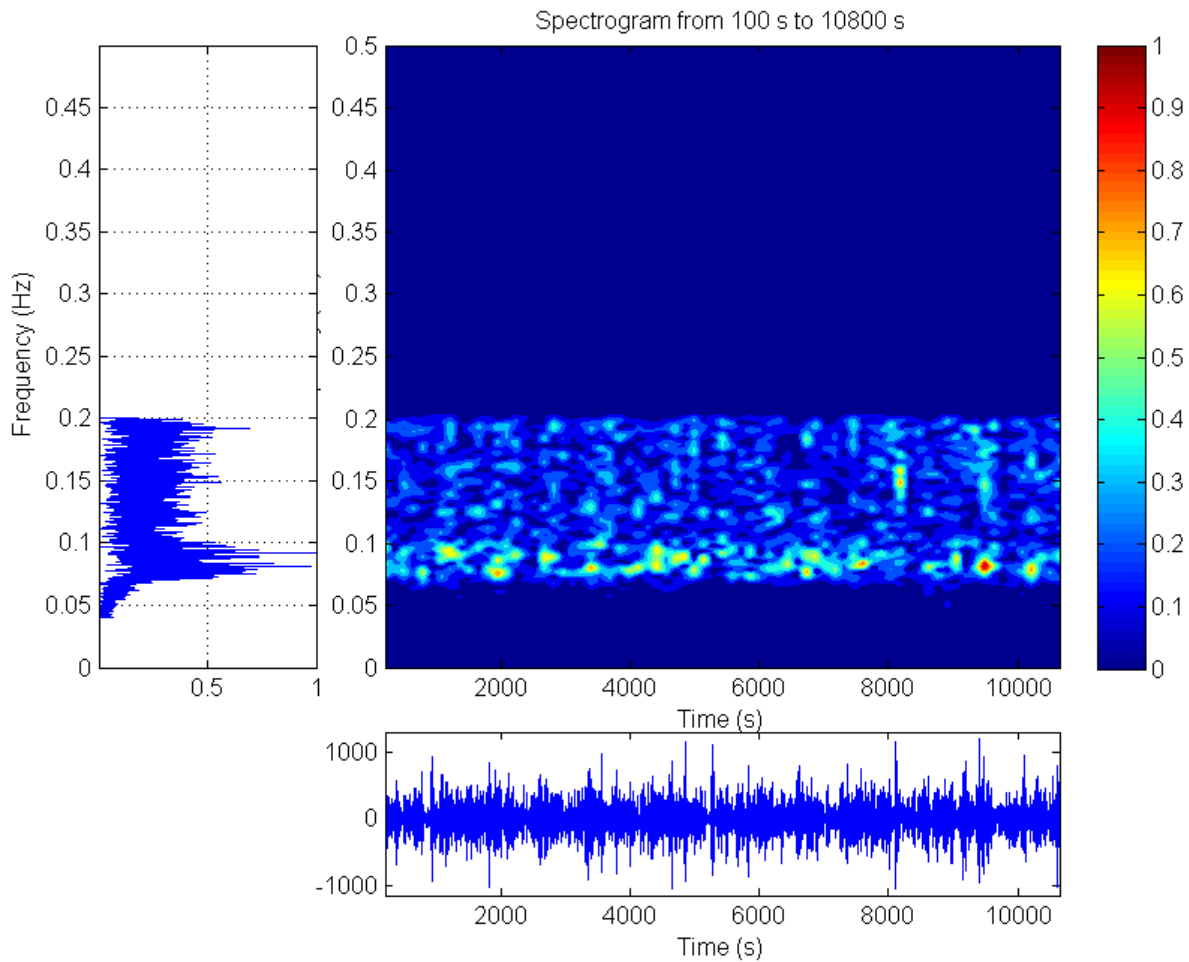


Figure 7.17 Spectrogram of the RL model, using a hamming windowing function. Note: The frequency plot on the left hand side is normalised.

7.8.4 FL MODEL USING DIRECT TIME-INTEGRATION

This section will provide the results of the observations of the FL model using direct time-integration. The reviewing of its performance is done in the same way as the RL model. The time traces can be found in Figure 7.18. They show that the trend is followed well and that the amplitude is larger than that of the RL model. However, it can be seen that there is still a frequency difference present.

Some general properties of the time trace of the FL model can be found in Table 7.8. It can also be seen that there are larger differences than the RL case for all values, except the mean value, with the measured cable forces than the differences observed for the RL model. The FL model shows overall larger amplitudes than the measured data trace. Considering that the parameters are variable for the FL model it is deemed viable to find a better fit to the measured data.

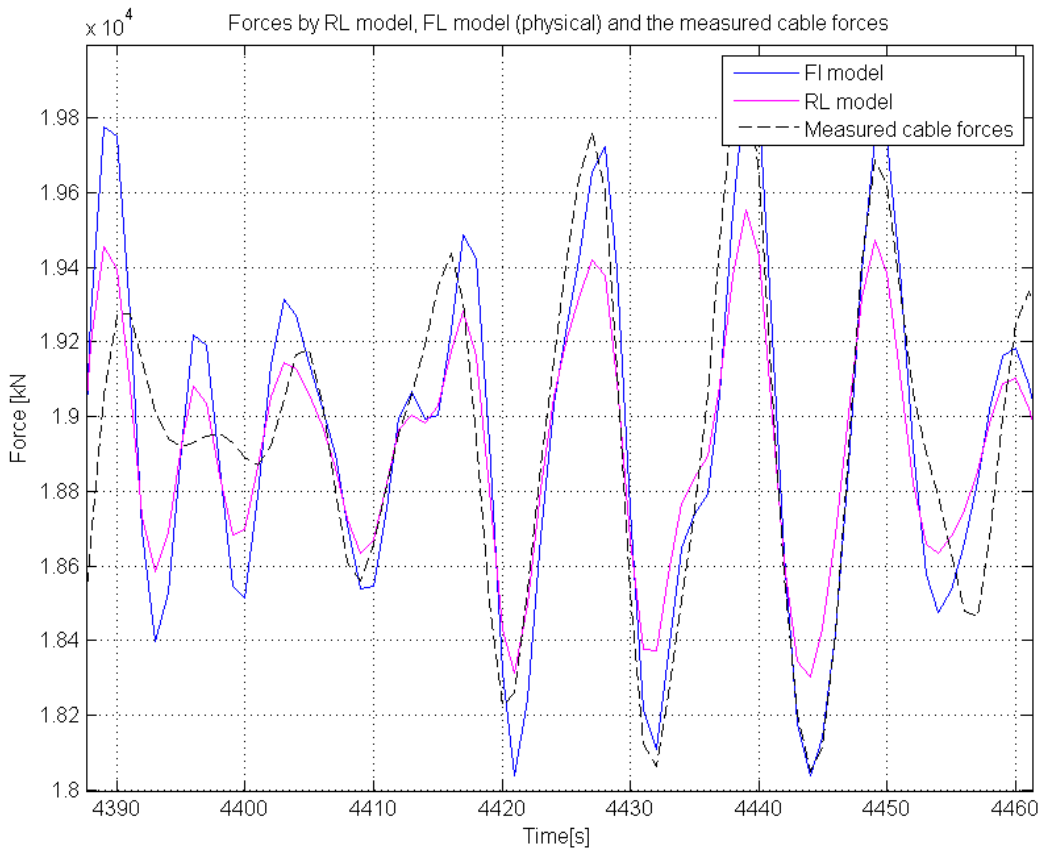


Figure 7.18 Time trace of the FL model using the direct time-integration method. The figure also includes the time trace of the RL model for comparison.

Property	Standard deviation	Mean	Maximum	Minimum
Values in [kN]	334.9	1.8925E4 kN	2.075E4 kN	1.720E4 kN
Difference with measured values in [kN]	67.2 kN	-12.9 kN	594.7 kN	614.6 kN

Table 7.8 Time-trace properties of the FL model using direct time integration.

The frequency plot of the FL model, shown in Figure 7.19, is in shape alike that of the RL model frequency plot. Again, the frequency plot confirms the fact that there is more high frequency information present in the FL model data traces than in the measured cable force data trace. The maximum magnitudes are in the expected region and it is observed that the FL magnitudes fit those of the measured cable forces better than the RL model magnitudes in the frequency plots.

In addition, it can be observed that the relative noise amplitude, when compared with the highest peak in the frequency spectrum, is larger than visible in the RL model frequency plot. One of the reasons can be, as is apparent in Figure 7.19, that the frequencies closer to the fundamental frequency of the system (which is defined in section 7.8.5) show more response than both the RL model and the measured cable forces in this frequency range.

Furthermore, it must be pointed out that the input data of the FL model is filtered just as for the RL model. Since the input data is filtered, as described in section 5.3, the range beyond a frequency of 0.2 Hz should not contain any amplitude information. Those frequencies were cut-off in the filtering process. However, there is some response visible at the fundamental frequency of the system in the frequency spectrum of the FL model. This can be contributed to the fact that some numerical errors can be generated by the Matlab ode-solver, which react at this natural frequency.

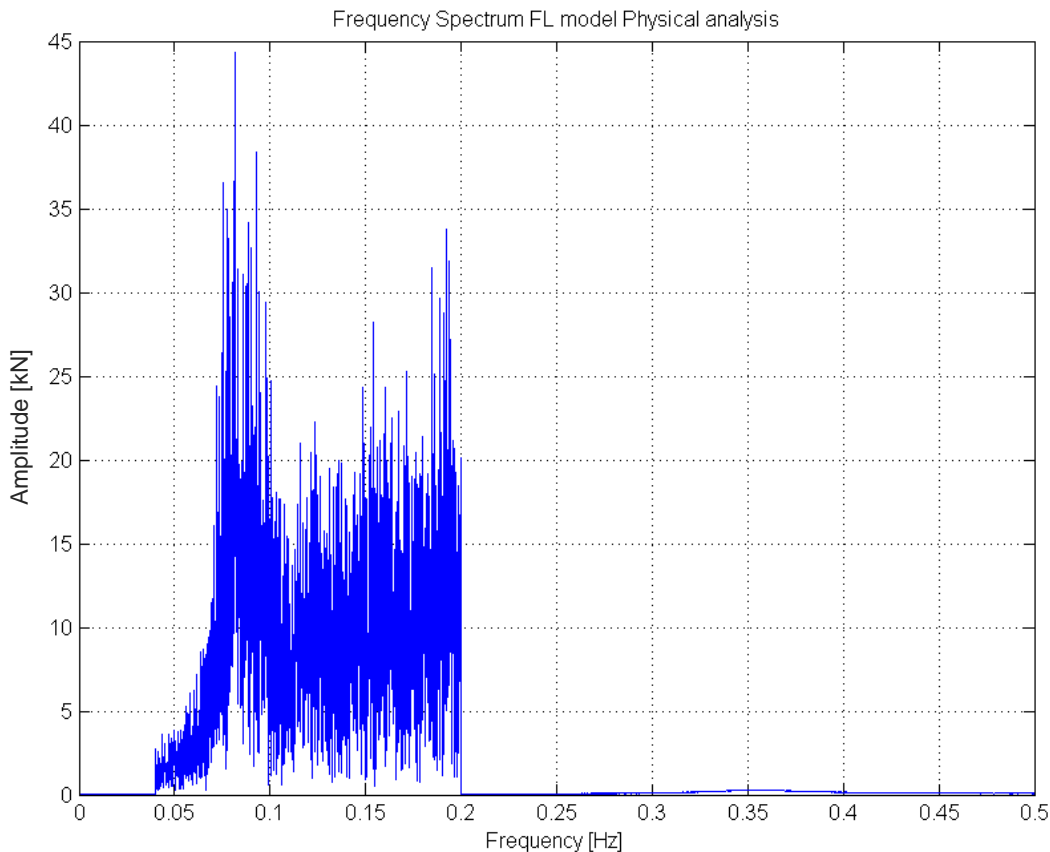


Figure 7.19 Non-binned, filtered spectrum of the FL model using the direct time-integration method.

The results of all quantitative reviewing methods are shown in Table 7.9. The cross-covariance's time shift is again confirmed by the mean peak time difference. It can be seen that the total normalised cross-covariance has a lower maximum value. There are multiple reasons why the normalised cross-covariance gives a lower value for the FL model than for the RL model. The first reason is that the shape of the time trace is different than the RL model's time trace. However, when reviewing the shapes of the RL model and the FL model's time traces in Figure 7.18, they appear equally well. Therefore, this does not seem to be the reason for the difference in cross-covariance value. The second reason for the lower normalised cross-covariance values is that the calculation uses time steps of exactly one second when shifting the time traces as explained in section 6.2.1. The mean peak time difference indicates that overall the trace is 0.8 seconds off when compared with the measured data traces. If the optimum cross-covariance would occur at 0.8 seconds shift instead of a 1 second shift it is logical that the cross-covariance calculated is lower than when the shift would be 0.8 seconds. This has been sketched in Figure 7.20. Note that the sketch shows an exaggerated situation. It can be seen that logically the coloured parabola with its peak closest to the shifted measured peak will give the better correlation.

Further analysis of the results in Table 7.9 shows that the mean peak amplitude difference is larger and the correlation in time and amplitude is larger than that of the RL model. The only parameter which shows improvement is the peak amplitude correlation. When purely considering the matched peak's amplitudes (the peak amplitude correlation) it is observed that the FL model shows slightly better results.

In Figure 7.21 the spectrogram of the FL model using the time-integration is shown. It is confirmed that there is more high frequency information in the system than the measured cable force and it is confirmed that relatively the FL model contains more high frequency noise than the RL model as the frequency plots on the left hand side of the spectrogram is normalised. The further time-frequency behaviour is not very different when compared with the RL model's spectrogram, in section 6.2.3.

When adjusting the stiffness values of the FL model it can be seen that for low stiffness values the higher frequency region (of 0.13 Hz up to 0.2 Hz) of the FL model shows more reaction with the first natural mode of the system. This can be explained by the fact that lowering the stiffness values of the system also lowers its natural frequencies. As the natural frequencies draw closer to the excitations, the FL model will show "fake" response which is actually resonance due to the proximity of the first mode. If the stiffness values are increased the opposite effect is seen. Proof of this is given in section 7.11.

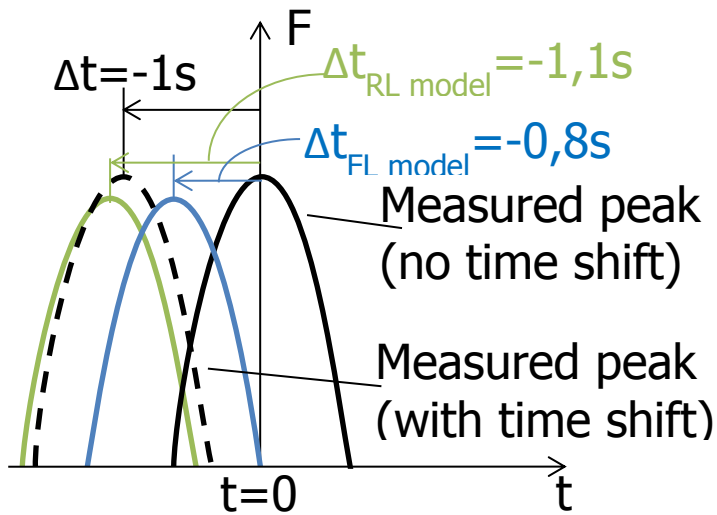


Figure 7.20 Sketch of the cross-covariance time steps and its influence on the resulting cross covariance value.

Reviewing method	Result
Normalised cross-covariance complete	(-1, 0.683)
Standard deviation	334.5 kN
Peak amplitude correlation	0.603
Mean peak amplitude difference	105.8 kN
Mean peak time difference	-0.8 s
Correlation in time & amplitude	161.7

Table 7.9 Results of the reviewing methods for the direct time-integration FL model.

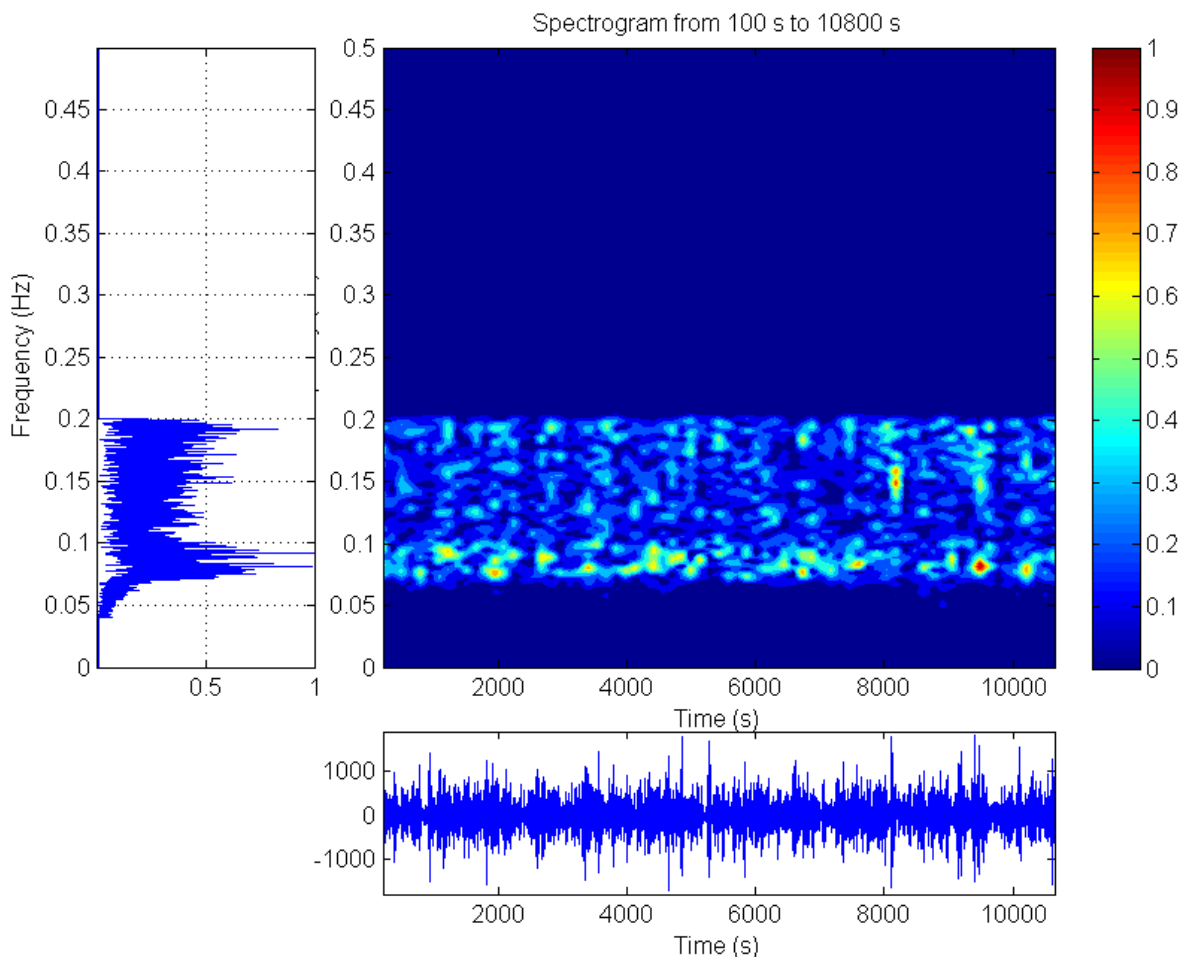


Figure 7.21 Spectrogram of the FL model using the direct time-integration method. Note: The frequency plot on the left hand side is normalised.

In summary the current results of the FL model indicate that the base case is not an improvement to the RL model. However, the FL model's parameters can be varied and in a later stage a better fit is given of the data which will show improved results of the FL model.

Lastly it should be pointed out that it is beneficial to find the cause(s) for the high frequency noise which is present in both models. Multiple possible causes of this high frequency noise were already stated in Chapter 6. One additional hypothesis on the cause of the high frequency noise is that it is caused by reaction with the first natural mode of the system (for the FL model only). It is therefore valuable to consider the FL model results using the Modal analysis. One is then able to increase the damping for this specific mode in order to "suppress" the reactions in the higher frequency range of the data. Other causes of the high frequency information are sought for and listed in section 7.9. There the most influential methods of mitigating the high frequency noise are given.

7.8.5 FL MODEL USING MODAL METHOD

The modal analysis method is applied for two reasons:

1. To apply a less "randomly" chosen damping by using percentages of the critical modal damping.
2. To apply different percentages of damping to different modes. Since each mode is influential around a certain frequency range, it is a controlled method to insert damping at different frequencies.

This method should not yield very different results from the direct time-integration method, provided that the amount of damping is similar in both models. Because this is not the case, this would explain why the two methods give slightly different results in the same model.

When damping certain modes, one should keep in mind that each modal damping represents a physical damping which applies to all frequencies in the system. Each mode has a different amount of influence on the different frequencies. By damping the closest mode(s) to these higher frequencies one might be able to alter the shape of the frequency spectrum (and thus the shape of the time-domain plot) in order to find a better fit of the predicted data with the measured data. It should be pointed out that this section is the base case analysis of the FL model using the modal analysis method. Therefore the base case of 5% of the critical damping is utilized in this chapter. No specific attempt of damping certain modes is as of yet made. This principle is however applied in section 7.9.2.

The FL model using the modal analysis method is reviewed in the same manner as in the previous sections. First the time plots are reviewed in Figure 7.22. The properties of the new method's results within the FL model are shown in Table 7.10. The modal analysis method with a 5% critical damping as damping term yields approximately the same results as the direct time-integration method. It is evident that the modal analysis method also overestimates the dynamic amplitudes of the cable forces, just like the FL model using the direct time-integration method. Additionally, it shows the same type of frequency difference. Table 7.10, which contains the general properties, confirms this. Since the modal analysis is part of the FL model it is still deemed viable to find a better fit to the measured data.

The frequency plot in Figure 7.23 confirms the fact that there is more high frequency information present in the data traces than in the measured cable force data trace. The maximum magnitudes are in the expected region frequency region but have a larger magnitude even than the FL model using a direct time-integration method, which also explains the slightly larger values shown in the Table 7.10. The spectrum also shows a slight response at the natural frequency of the base case system, which is the natural frequency corresponding to the first mode of the system. This fundamental natural frequency has a value of 0.35 Hz. The natural frequencies corresponding to next four higher modes are 1.15 Hz, 1.16 Hz, 1.19 Hz and 1.20 Hz. The last four natural frequency values are thus close, since the system is nearly symmetric. If the system was symmetric you would expect the four symmetric cables to show the same natural frequencies and modes.

Finally, it is interesting to point out that apparently the RL model seems to exhibit no response of noise to the natural frequency of the system (which is visible in section 7.8.4). This can be because the RL model's natural frequency is infinite due to the infinite stiffness of this entirely rigid system. Both FL models show response in the higher frequencies to the first mode of the system. Proof of this is given in section 7.11.

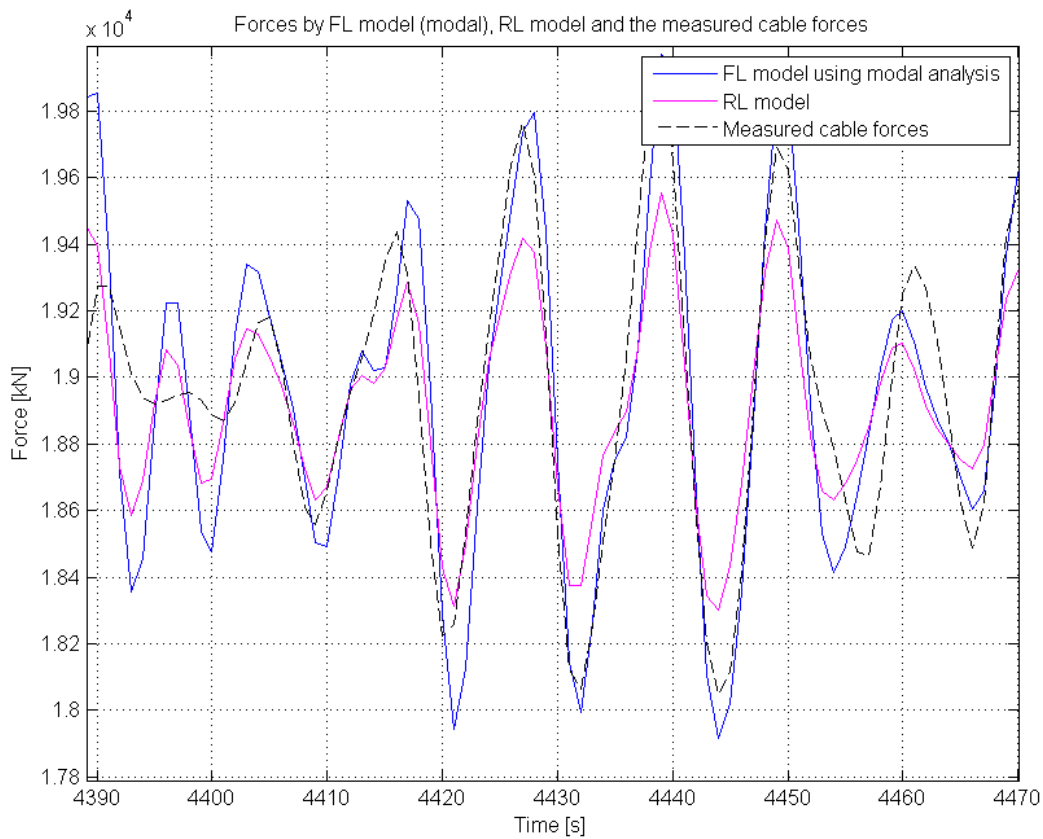


Figure 7.22 Time trace of the FL model using the modal analysis method. The figure also includes the time trace of the RL model for comparison.

Property	Standard deviation	Mean	Maximum	Minimum
Values in[kN]	364.7	1.8925E4 kN	2.091E4 kN	1.702E4 kN
Difference with measured values in [kN]	97.0 kN	-12.9 kN	757.0 kN	799.0 kN

Table 7.10 Time-trace properties of the FL model using the modal analysis approach.

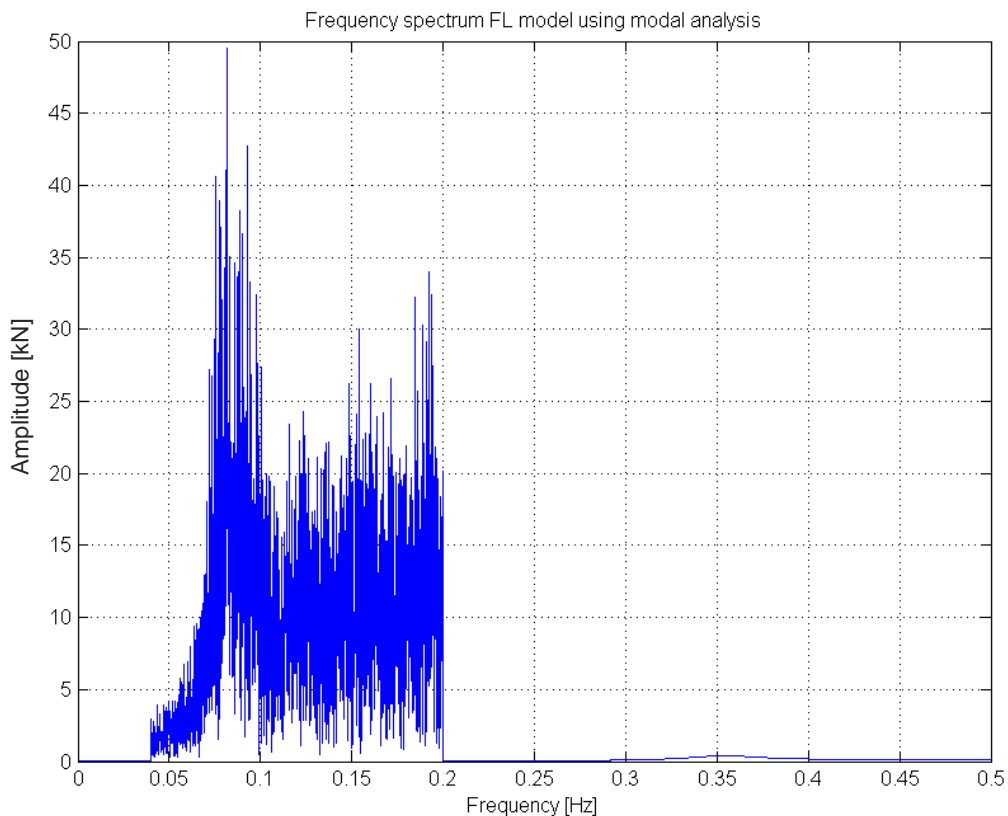


Figure 7.23 Non-binned, filtered spectrum of the FL model using the modal analysis approach.

The results of all quantitative reviewing methods are shown in Figure 7.10. It can be seen that the total normalised cross-covariance has a lower maximum value than the RL model for the same reasons as explained in the previous section.

In Figure 7.24 the spectrogram of the FL model using the modal analysis is shown. It is observed that the modal solving method and its slightly different application of damping show slightly less relative noise than the FL model using direct time-integration, when compared with the maximum frequency magnitude. Maxima in the spectrogram occur for the same reasons as explained in section 6.2.3.

Reviewing method	Result
Normalised cross-covariance complete	(-1,0.691)
Standard deviation	364.7 kN
Peak amplitude correlation	0.619
Mean peak amplitude difference	149.6 kN
Mean peak time difference	-0.8 s
Correlation including normalised time & amplitude	187.0

Table 7.11 Results of the reviewing methods for the direct time-integration FL model.

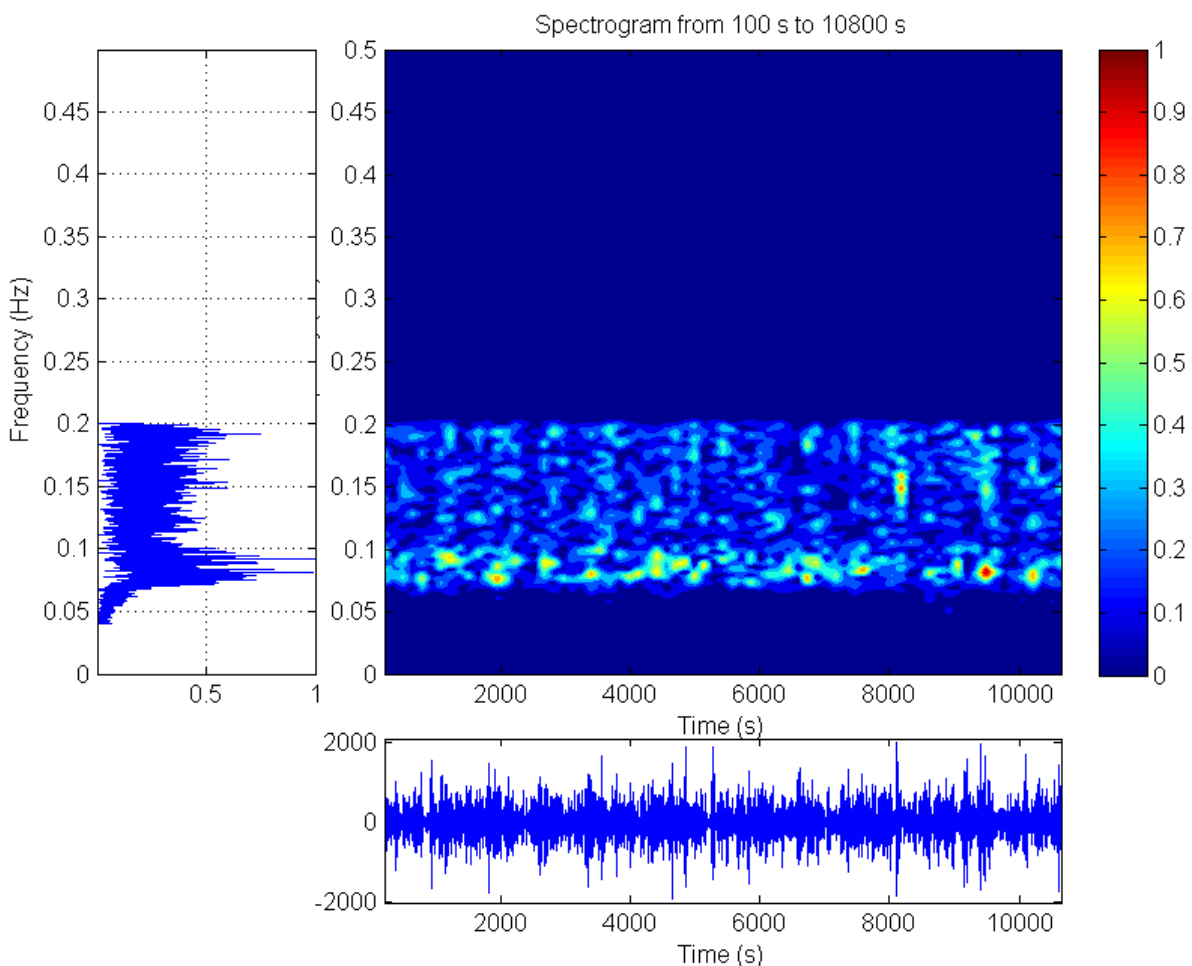


Figure 7.24 Spectrogram of the FL model using the modal analysis method. Note: The frequency plot on the left hand side is normalised.

It is observed that find a better fit must be found, just as concluded in the previous section.

7.8.6 PARAMETER IMPROVEMENT FOR BASE CASE MODELS

During the analysis in the following sections it was found that the current stiffness values of the FL model were underestimated. The adjusted model results are presented in section 7.9. The newly defined stiffness values are however not the exact solution because the stiffness values depend on the differential stresses and direction of the stresses in the wires, which both influence the Young's modulus [15] and the differential diameter by the tension of the wires. Since the tension continuously varies there is not 1 specific stiffness value which describes the system properly. These are non-linear effects which

are not accounted for in this thesis. It should also be pointed out that, even if one accounts for all these effects, all these parameters are valid for a new and intact cable. Since no aging was accounted for thus it can be expected that an ideal stiffness value which accounts for all previous effects will still not be the real stiffness value of the system. The impact of all these factors is significant since already only based on the non-linear effect of the Young's modulus the stiffness values between -2% and +7% of the values now used in section 7.9. These are percentages, calculated using a graph relating stresses and a steel wire rope (of equal quality) Young's modulus [15]. These percentages thus do not account for all other effects stated in this section.

If one would like to investigate further the stiffness parameters of the system, one should account for the bends around the sheaves and its effect on stiffness. However, this effect is expected not to yield a largely different value. Also, hysteresis is not accounted for in this thesis. Possible unequal load distribution and thus stress differentials within one cable and its windings are not accounted for in this thesis as well. These are all effects which would need to be taken into account should one like to investigate the exact stiffness value of the wires.

7.9 FL MODEL WITH PARAMETER IMPROVEMENT

In this section the stiffness values are adjusted to their new estimation. Both the result of the FL model using direct time-integration and the modal analysis are added with their data characteristics.

7.9.1 ADJUSTED FL MODEL USING DIRECT TIME-INTEGRATION

The adjusted model parameters are given in Table 7.12. The results are again compared with the measured data trace of the cable force. The sequence of comparing is the same as in section 7.8. The time traces are shown in Figure 7.25. The time trace qualities can be found in Table 7.13.

The time trace similarity is good when compared with the measured cable forces. All time trace parameters, as observed in Table 7.13, show improvement. It should be pointed out that the current "accuracy" of the standard deviation lies below the error margin by the input errors possible defined in section 7.10. Therefore this small differential standard deviation has no significance. Instead, the accuracy of the FL model using the time-integration method is the 9.9 kN of uncertainty in the standard deviation accuracy of the model. The mean value does seem to be slightly more off target than in the previous FL model. This can be caused because the larger stiffness value allows less elongation for the same static force. Hence, the centre of gravity of the stinger structure and the moment it causes is slightly smaller than in previous analyses.

Even though the parameters have been adjusted there is still a frequency difference present which is also visible in the frequency plot in Figure 7.26. It can be seen, however, in the frequency plot of the adjusted FL model, shown in Figure 7.26, that there is relatively less high frequency noise present in the region between 0.13 Hz and 0.2 Hz when compared with Figure 7.19. Since the result of the adjustment is based on the same input as that of the original results in section 7.8.4 and 7.8.5, one reason for the reduction of higher frequency noise is the increase of the fundamental natural frequency. The frequency difference between the excitations and the first mode has grown and therefore there is less (resonance) response of the noise to the first mode. This is confirmed in section 7.11 and by the fact that the noise left over resembles the noise magnitudes of the RL model (which in theory contains an infinite stiffness). The leftover noise is thus caused by other effects. Other possible reasons for this noise are given in section 7.12.

The maximum magnitudes in the frequency plot are again present in the expected and they have the approximate expected height conform the measured cable forces.

Parameter	Parameter value
K1	3.52E7 in [N/m]
K2	1.71E7 in [N/m]
K3 _{1 up to 4}	[4.44E6 5.34E6 4.68E6 5.64E6] in $\frac{kg \cdot m^2}{s \cdot rad}$
Damping uniform	4.2E4 in $\frac{kg \cdot m^2}{s \cdot rad}$

Table 7.12 Adjusted parameter values of the adjusted FL model using direct time integration.

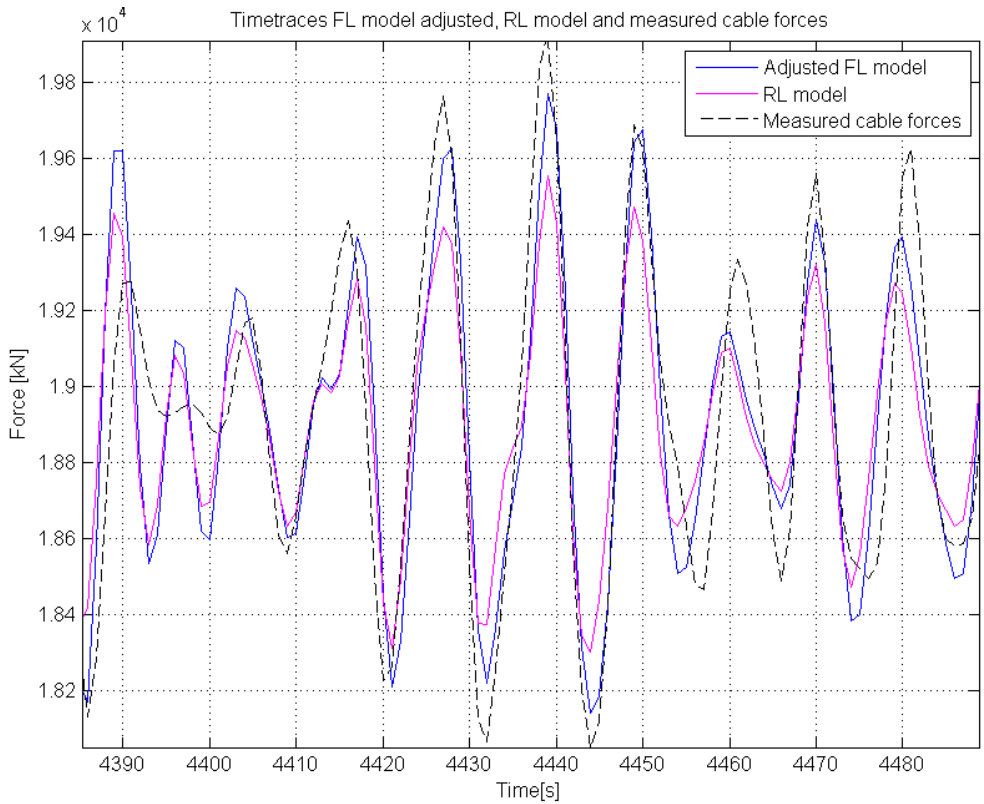


Figure 7.25 Time trace of the FL model using the direct time-integration method with adjusted parameters. The figure also includes the time trace of the RL model for comparison.

Property	Standard deviation	Mean	Maximum	Minimum
Values in [kN]	270.6	1.8924E4	2.036E4	1.745E4
Difference with measured values in [kN]	2.9 kN	-13.5 kN	201.5 kN	-368.3 kN

Table 7.13 Time-trace properties of the adjusted FL model using the direct time-integration method with adjusted parameters.

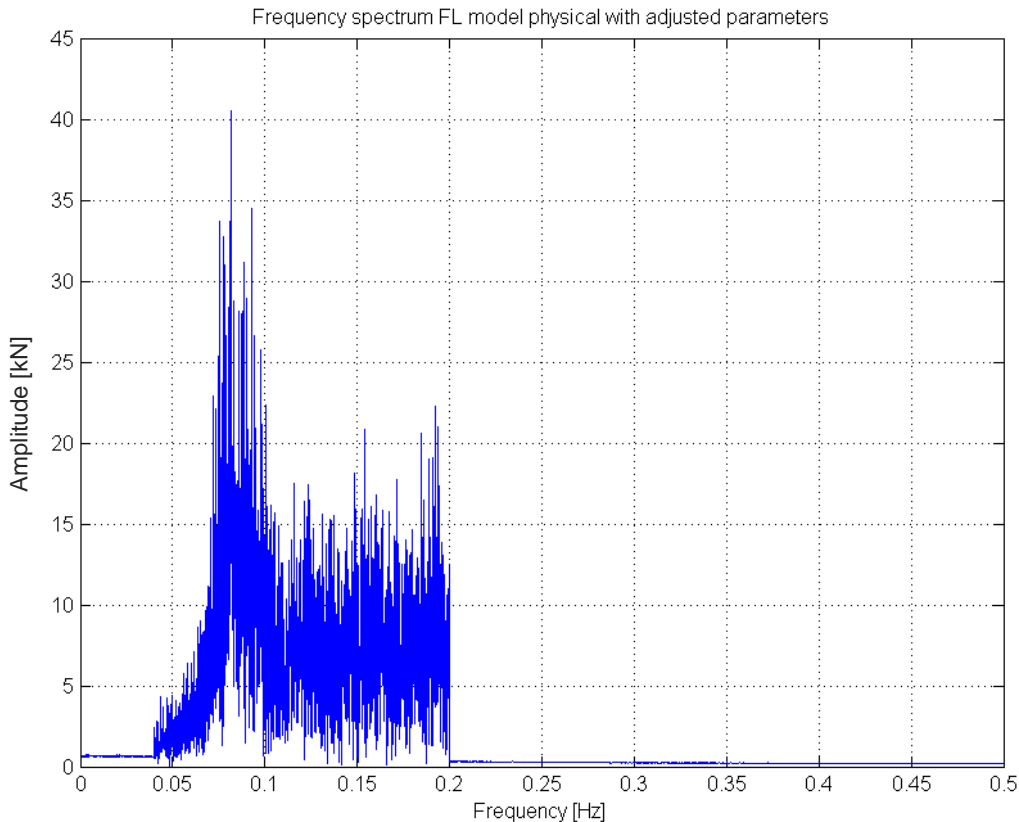


Figure 7.26 Non-binned, filtered spectrum of the adjusted FL model using the direct time-integration method.

All results of the reviewing methods are shown in Table 7.14. Even though the mean peak time difference indicates the cross covariance should provide an unfavourable result, as was seen in the previous model reviews, the cross covariance is larger than the cross-covariance value of the RL model.

In Figure 7.27 the spectrogram of the adjusted FL model is shown. The reduction in relative noise is also visible here. The spectrogram looks more alike the spectrogram of the measured cable forces with relatively less high frequency presence. Maxima in the spectrogram occur for the same reasons as explained in section 6.2.3

Reviewing method	Result
Normalised cross-covariance complete	(-1, 0.732)
Standard deviation	270.6 kN
Peak amplitude correlation	0.635
Mean peak amplitude difference	8.12 kN
Mean peak time difference	-0.74 s
Correlation in time & amplitude	118.4

Table 7.14 Results of the reviewing methods for the direct time-integration adjusted FL model.

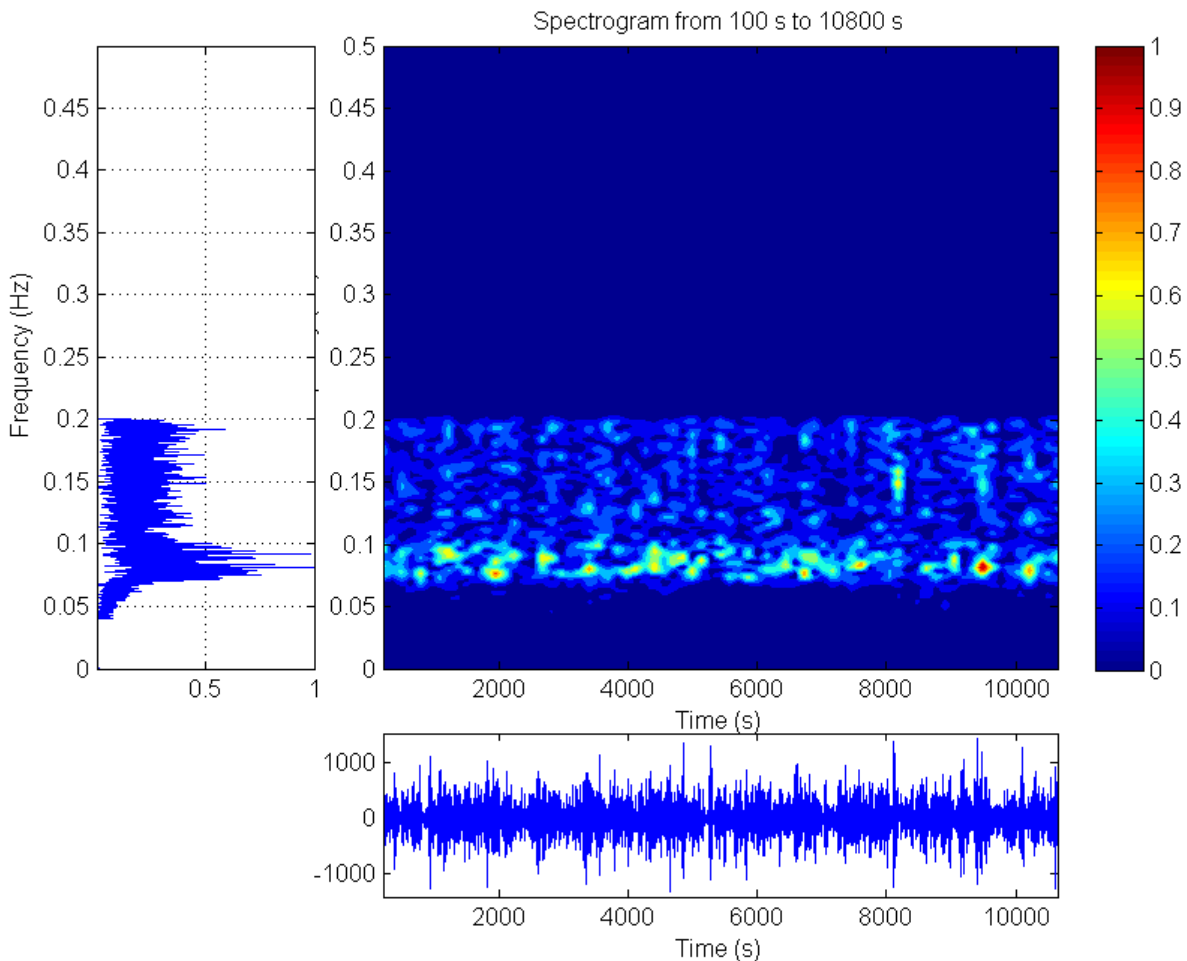


Figure 7.27 Spectrogram of the adjusted FL model using the direct time-integration method. Note: The frequency plot on the left hand side is normalised.

In conclusion it can be stated that the FL model as presented in this section currently has a good fit (the best so far in this thesis) for the measured data in the time traces considered. It accurately describes the cable forces in time and has the best frequency spectrum when comparing with the measurements. The next section, section 7.9.2, will elaborate on the modal analysis variant of the adjusted FL model.

7.9.2 ADJUSTED FL MODEL USING MODAL METHOD

The adjusted FL model using modal analysis is further adjusted to improve the fit with the measured data. The main improvement concerns the reduction of high frequency noise in the system by suppressing the reactions at these frequencies. The parameters are given in Table 7.15. The new results of the FL model using modal analysis method are again compared with the measured data trace of the cable force. Firstly, the time traces are compared in Figure 7.28 and the general properties of the FL

model predictions using modal analysis can be found in Table 7.16. The results are similar to the adjusted FL model of the previous section, including the standard deviation accuracy as explained in the previous section.

The frequency spectrum is shown in Figure 7.29. Despite the fact that there is less noise in the higher frequencies between 0.13 Hz and 0.2 Hz, as compared to the previous cases, some noise is still present. When varying the damping percentages of modes 1 to 5, it can be seen that the damping influences the amount of response seen in the higher frequencies. It should be pointed out that the damping of mode 2-5 is preferred since they have less influence on the main peaks of the response spectrum. The maximum magnitudes are again present in the region where the measured cable forces also show to contain their maximum magnitude. In addition, the fundamental frequency has a value of 1.9 Hz. This means that the excitation frequencies are much smaller in value when compared with the first natural frequency, that the response of the system can be viewed as quasi-static. In the sensitivity analysis of section 7.11, it is therefore expected that the adjusted FL model should be stiffness dominated.

Parameter	Parameter value
K1	3.52E7 in [N/m]
K2	1.71E7 in [N/m]
K3 _{1 up to 4}	[4.44E6 5.34E6 4.68E6 5.64E6] in [N/m]
Damping mode 1	0.12 factor of critical damping mode 1 in $\frac{kg \cdot m^2}{s \cdot rad}$
Damping mode 2-5	0.01 factor of critical damping mode 2 up to mode 5 in $\frac{kg \cdot m^2}{s \cdot rad}$
Damping mode 6-45	0.11 factor of critical damping mode 6 to mode 45 in $\frac{kg \cdot m^2}{s \cdot rad}$

Table 7.15 Adjusted parameter values of the adjusted FL model using modal analysis.

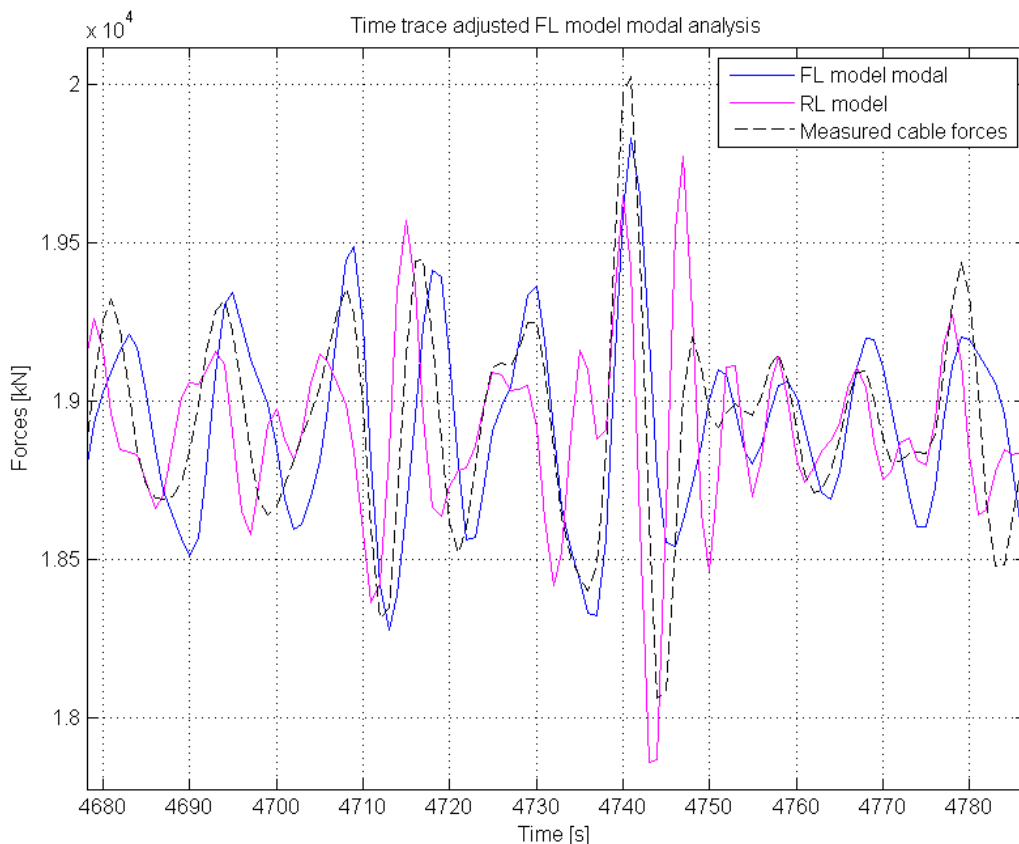


Figure 7.28 Time trace of the FL model using the modal analysis method with adjusted parameters. The figure also includes the time trace of the RL model for comparison.

Property	Standard deviation	Mean	Maximum	Minimum
Values in [kN]	268.0	1.8925E4	2.037E4	1.7815E4
Difference with measured values in [kN]	0.3 kN	-13.1 kN	210 kN	-5 kN

Table 7.16 Time-trace properties of the adjusted FL model using modal analysis.

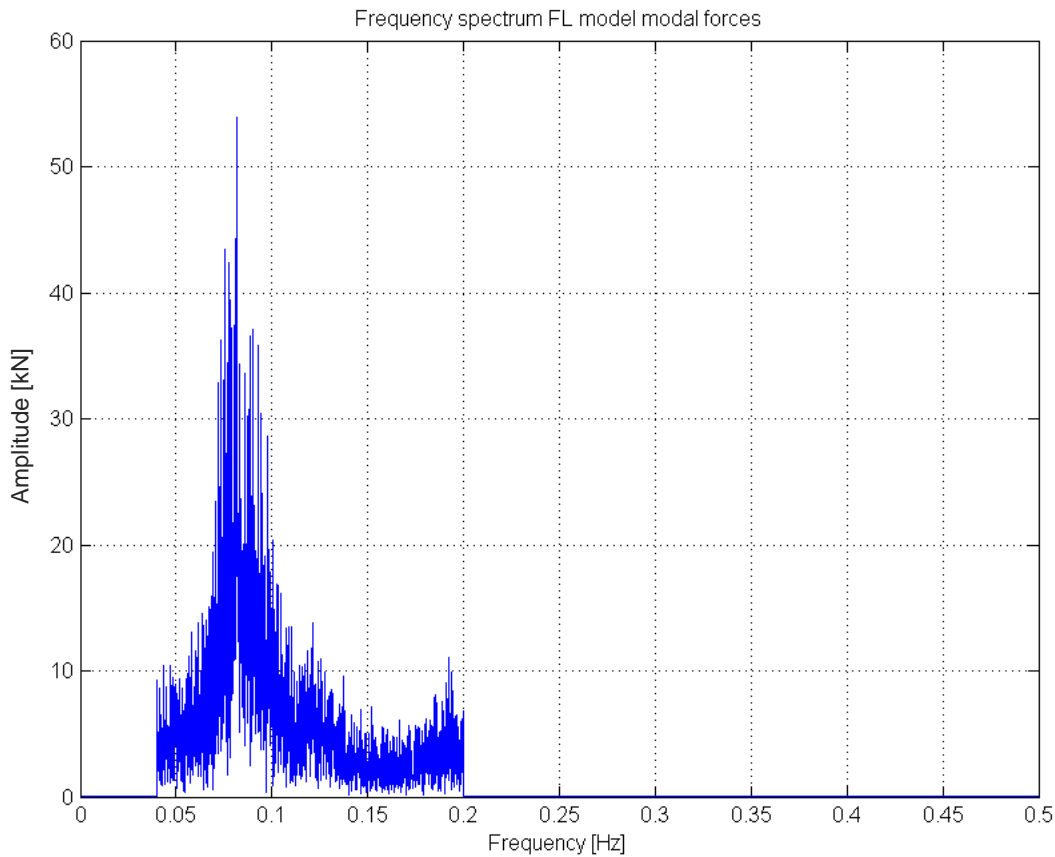


Figure 7.29 Non-binned, filtered spectrum of the FL model using the modal analysis method.

The results of all reviewing methods are shown in Table 7.17. As can be seen, the results are again comparable to those of the adjusted FL model using direct time-integration.

Reviewing method	Result
Normalised cross-covariance complete	(2, 0.735)
Standard deviation	268.0 kN
Peak amplitude correlation	0.569
Mean peak amplitude difference	-14.5 kN
Mean peak time difference	2.1 s
Correlation in time & amplitude	125.7

Table 7.17 Results of the reviewing methods for the modal analysis method FL model.

In Figure 7.27 the spectrogram of the adjusted FL model is shown. It can be seen that the spectrogram shows less dominance of the higher frequency region, as concluded from Figure 7.29. The shape matches the frequency plot of the measured cable forces better than any other model type or setting until now. Also here, it can be seen that the peaks in time traces occur at points where a large number of frequencies contain energy. This would mean that the different sinusoids containing these frequencies would contain approximately the same phase delay which builds up the energy in these frequencies at the same approximate time. It is also visible that "lumps" of energy peaks in the time trace of the adjusted FL model coincide with medium-sized maxima of the lower frequencies. As stated earlier (section 6.2.2), this periodicity can also be caused by the hamming window used for the creation of the spectrograms. It is not possible that there is a periodic natural motion which is approximately 800 seconds of period.

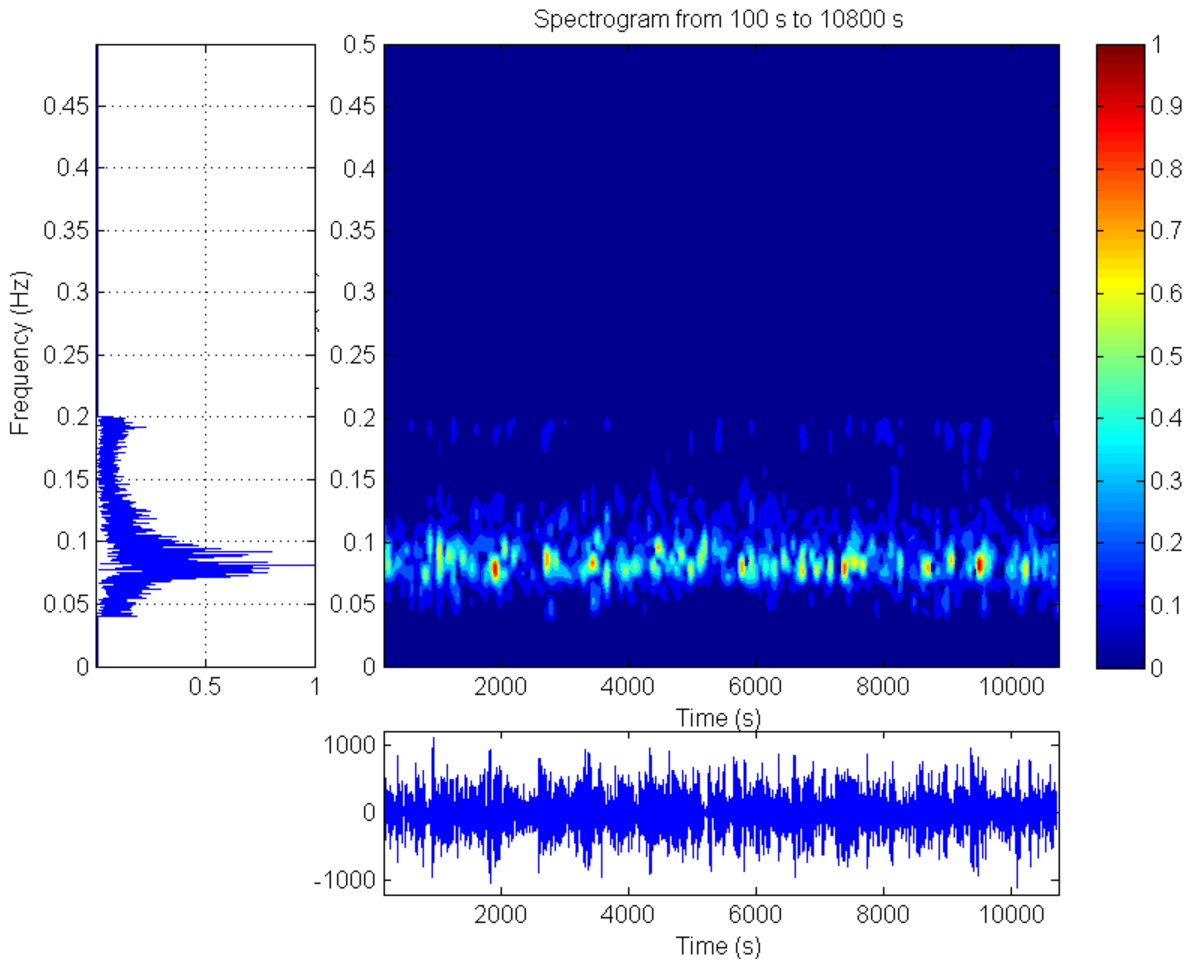


Figure 7.30 Spectrogram of the adjusted FL model using the modal analysis method. Note: The frequency plot on the left hand side is normalised.

7.9.3 SUB RESULT OF RL AND FL MODEL COMPARISON

In conclusion to the model comparisons, it can be stated that the general FL model as presented in this section has the best fit for the measured data in the time traces considered. It accurately describes the cable forces in time and has the best fit in the frequency domain when comparing with the measurements. It is, however, still of interest to review how the high frequency noise influences the frequency spectrum since this could reveal additional ways of improving the model. Furthermore, it is good to think of possible causes of the high frequency noise found in the previous model versions. This point is researched in section 7.12.

7.10 UNCERTAINTY ANALYSIS BY INPUT ERRORS

The uncertainty analysis performed involves assessing the largest measurement errors which can occur and the extent of their influence on the resulting cable forces. The maximum increase and decrease of the (centre of gravity) motion data traces have been calculated using equation 7.71 up to 7.73, which are percent uncertainties [16].

$$x(t) = x(t) \left(1 \pm \frac{0.025}{|x(t)|} \right) \text{ OR} \quad 7.71$$

$$x(t) = x(t)(1 \pm 0.025), \quad \textit{Whichever is larger}$$

$$z(t) = z(t) \left(1 \pm \frac{0.025}{|z(t)|} \right) \text{ OR} \quad 7.72$$

$$z(t) = z(t)(1 \pm 0.025), \quad \textit{Whichever is larger}$$

$$\theta(t) = \textit{pitch}(t) \left(1 \pm \frac{0.01}{|\theta(t)|} \right) \quad 7.73$$

The error margins of the measured data are given in Chapter 5, Table 5.1. The results have been noted in section 7.10.1 up to 7.10.4. It should be pointed out up front that it is highly unlikely that the measurements all experience a maximum or minimum at the exact same time.

7.10.1 RL MODEL

In Table 7.18 the cable forces are given of three cases:

1. Inertia forces resulting from the maximum input motion values due to the maximum measurement errors.
2. Inertia forces resulting from the minimum input motion values due to the maximum measurement errors.
3. The original inertia forces from the base case situation, using the measured value without the errors.

Case number	Force calculated	Standard deviation	Percentage
1	Force due maximum input motions due to maximum error	217	+2.4%
2	Force due maximum input motions due to minimum error	209	-1.4%
3	Force FRB base case	212	-

Table 7.18 Results of uncertainty analysis, RL model.

As mentioned at the beginning of the chapter, it is highly unlikely that the measurement points all contain the maximum possible error. Additionally, it can be concluded from Table 7.18 that the magnitude of this error is relatively small with a maximum of 5.1 kN deviation from the base case situation. Therefore it can be stated that for the RL model the influence of measurement errors in the input data is insignificant when compared with the shortage in standard deviation the RL model has relative to the measured cable forces standard deviation.

7.10.2 FL MODEL USING DIRECT TIME-INTEGRATION

In Table 7.19 the cable forces are given of three cases:

1. Hang-off cable forces resulting from the maximum input motion values due to the maximum measurement errors.
2. Hang-off cable forces resulting from the minimum input motion values due to the maximum measurement errors.
3. The original hang-off cable forces from the base case situation, using the measured value without the errors.

Case number	Force calculated	Standard deviation	Percentage
1	Force due maximum input motions due to maximum error	279.69	+3.4%
2	Force due maximum input motions due to minimum error	265.28	-2.0%
3	Force base case	270.6	--

Table 7.19 Results of uncertainty range, adjusted FL model using direct time-integration.

The error is for the FL model more significant since through the parameter variation the model can approach the "ideal" solution, where the predicted data trace matches the measured cable forces (almost) exactly. Because the accuracy of the standard deviation fall in the range of error induced by input error, the error percentage stated in the table above is of great importance. When using the FL model utilizing the direct time-integration method and when able to find a perfect fit for the target standard deviation of 267.7 kN, the uncertainty by the input error has a value 9.1 kN. This value does, however, not account for uncertainties in the measured cable forces. In section 7.10.3 the cable force uncertainty will be dealt with and the conclusion on this matter can be found in section 7.10.5.

7.10.3 ERROR IN THE MEASURED CABLE FORCE

As stated in section 5.1 the errors of the measured cable forces are 0.1% plus 0.01% per degree Celsius of the reading. For a 20°C environment the error is thus 0.3% of the reading in total. In Table 7.20 the maximum effects of this error are denoted. Again, first the maximum force due to a maximum error occurring on all data points is calculated after which the minimum force due to a maximum error occurring on all data points is calculated. The table also shows the actual measured data trace characteristics which are used for validation.

Force calculated	Mean	Standard deviation	Maximum	Minimum
Measured force maximum due to maximum error	1.900E4	268.5 ($\Delta=+0.8\text{kN}$)	2.022E4	1.787E4
Measured force minimum due maximum error	1.888E4	266.9 ($\Delta=-0.8\text{kN}$)	2.010E4	1.766E4
Measured force base case	1.894E4	267.7	2.016E4	1.782E4

Table 7.20 Total influence of the error on the values of the measured cable forces.

7.10.4 UNCERTAINTY IN MASS AND CENTRE OF GRAVITY

Several tests were performed to find the centre of gravities and masses of the different stinger sections. The last measurement has been performed in 2007, however the constant work on the stinger changes these two measured values constantly. The measurements have been validated by multiple parties so their values are considered a reliable reference. Since no range of uncertainty is given regarding these values, no analysis can be performed on this. A variation of 0.5% on the total mass on the stinger sections already changes the complete static and dynamic situation of the predicted cable forces. However, since the current calculations with the measured masses and centres of gravities yield a mean value or static force which differs only 0.079% from the measured cable forces' mean, the measured location of the mass and centres of gravity are considered accurate enough.

7.10.5 CONCLUDING FOR THE FL MODEL UNCERTAINTY

A 3.4% change in the standard deviation of the predicted cable force due to maximum measurement errors occurring over the complete input data traces, is significant. The fit of a prediction is quantified using, among other methods, the standard deviation to judge the amount of correlation between the predicted force trace and the measured force trace. When the input errors can cause the actual value of the predictive trace to be 3.4% off target, this has significant influence on the amplitudes and thus standard deviation. To clarify: a 3.4% deviation on an optimum best fit by the FL model with an standard deviation of 267.7 kN means the actual value can be 9.1 kN off target in standard deviation. Including the maximum error in the measured cable forces this uncertainty grows to a value of 9.9 kN.

In Chapter 6 it has been stated that the standard deviation without input error is 20.8% when reviewing the standard deviation values of the RL model and the measured cable forces. If the worst case scenario by input errors is included, as found in section 7.10.1, The error in standard deviation grows to 22,2%.

7.11 SENSITIVITY ANALYSIS BY PARAMETER VARIATION

The sensitivity or parameter variation is applied to the FL model using the direct time-integration. As mentioned in section 7.8.6, the stiffness value is calculated for an ideal rope condition and no non-linear effects are accounted for. It also was indicated earlier in this thesis that the damping term is an estimate. Because of the uncertainties in the stiffness values and the damping values, it has been decided to vary those in order to check the influence on the model results.

This section will review changes in the model parameters and will review the influence of the motion parameters. Each parameter is reviewed by changing its value and reviewing some results of the model and quantifying them. The results are noted in the sections below.

7.11.1 MODEL PARAMETERS

The stiffness values of the model are evaluated separately. The change in stiffness value is checked against the change in a degree of freedom of the system and the resulting force. The chosen degree of freedom is that of sheave 6 which is connected to both the spring with stiffness K2 and the spring with stiffness K1.

All the stiffness values of the springs are separately reduced by 2%. The results are as follows:

- A 2% reduction of the first spring stiffness (K1) results in a 1% change of the sheave motion and a 0.8% change in cable force standard deviation.
- A 2% reduction of the second spring stiffness (K2) results in a 12% change of the sheave motion and a 14% change in cable force standard deviation.
- A 2% reduction of the third spring stiffness (K3) results in no change of the sheave motion and of the cable force standard deviation.

It is evident that the second spring stiffness, the stiffness belonging to springs linking the top sheaves with the bottom sheaves and the stinger motion, is the most influential.

Finally, the damping values are uniformly reduced by 2%. This reduction results in a 0.2% change of the sheave motion and a 0.2% change in cable force standard deviation.

Now that the stiffness of the model is reviewed, it is interesting to confirm the findings as pointed out in section 7.9.1. The finding is that some of the high frequency noise in section 7.8.4 is caused by the reaction with the natural frequency of the first mode. Reducing the spring stiffness reduces the natural frequency value corresponding to the first mode. The finding will be tested by reducing the total stiffness of the system by two different factors, one so the first mode is in the vicinity of the excitations and one such that the first mode's frequency difference with the excitations is larger. The effects will be reviewed by reading the magnitude values of the frequency spectra of the results. As visible in Figure 7.31, there is noise present between 0.13 Hz and 0.2 Hz of increasing magnitude. For every test the minimum and maximum peak magnitude in this frequency range is noted.

When reducing the total stiffness of the system by a factor 35 the high frequency noise takes up a range of values from a magnitude of 16 up to a magnitude of 32. When the total stiffness of the system is reduced by a factor of 15 the high frequency noise takes up values from a magnitude of 11 up to a magnitude of 20. This trend is continued when again reducing by a smaller factor.

It can thus be seen that when the base natural frequency is closer to the high frequency noise it reacts with the first mode, as in the base case FL model described in section 7.9. When the first natural mode lies at a higher frequency this reaction by the high frequency noise in the excitation frequency region becomes less. The tests are visualised in the spectrograms of Figure 7.31 and Figure 7.32. Clearly the second spectrum, containing the higher natural frequency, shows less high frequency noise. It should be pointed out that the natural frequencies of the two plots are indicated by the black arrow present in the figures.

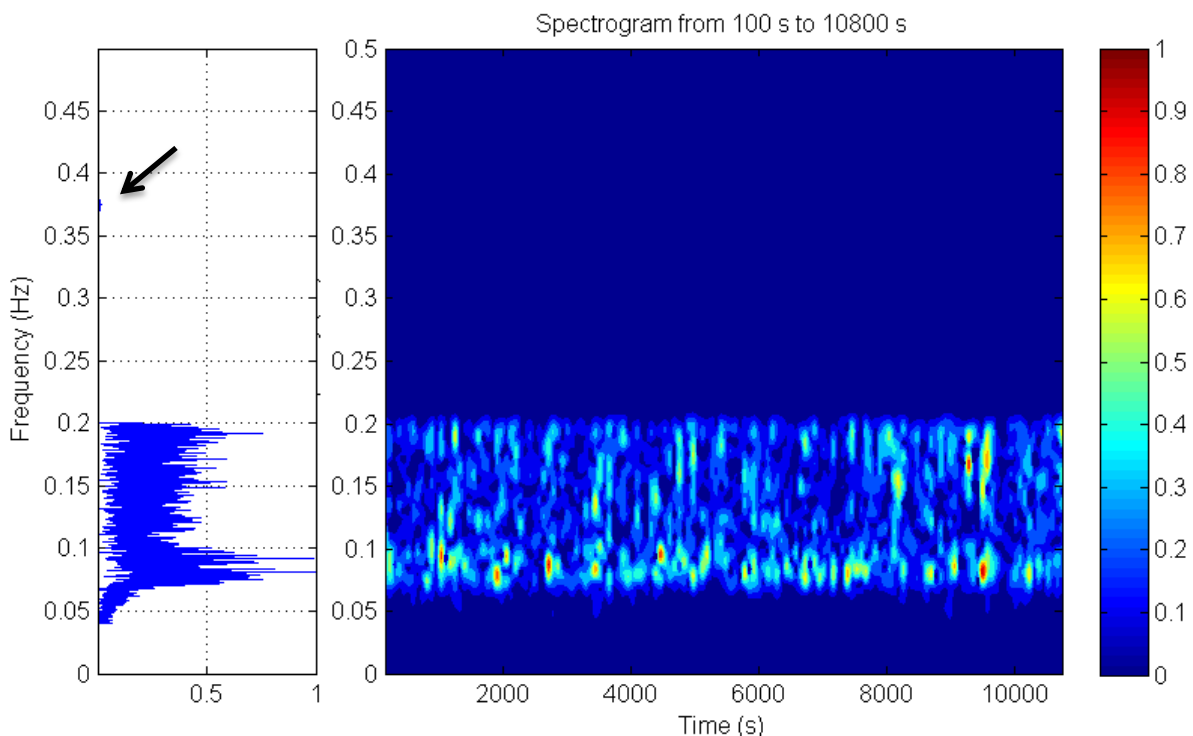


Figure 7.31 The spectrum and spectrogram of the adjusted FL model's predicted force traces. The black arrow indicates the location of the base natural frequency. For this graph the stiffness has been divided by a factor of 35. Note: The frequency plot on the left hand side is normalised.

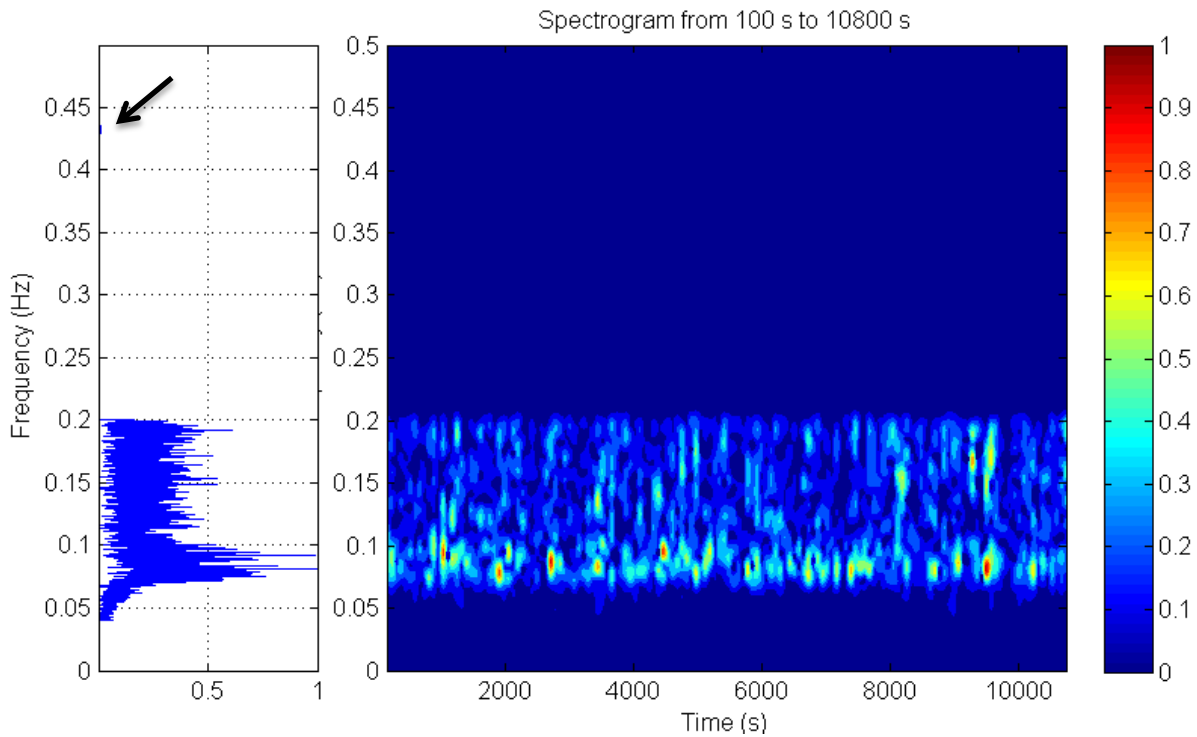


Figure 7.32 The spectrum and spectrogram of the adjusted FL model's predicted force traces. The black arrow indicates the location of the base natural frequency. For this graph the stiffness has been divided by a factor of 15. Note: The frequency plot on the left hand side is normalised.

7.11.2 SIGNIFICANT MOTION ANALYSIS

In section 5.5 the motions in the centre of gravity were analysed through their frequency and time plots. Based on the results, it was found that that the pitch motion was most significant for the cable forces. This section is meant to find whether these findings were correct or not. The results for the centre of gravity motions are:

- A 2% reduction of pitch motion in the centre of gravity results in 0.3% change in cable force standard deviation.
- A 2% reduction of heave motion in the centre of gravity results in 0.08% change in cable force standard deviation.
- A 2% reduction of surge motion in the centre of gravity results in 0.04% change in cable force standard deviation.

The conclusion in Chapter 5 stating that the pitch motion is the most significant motion is therefore correct. It shows to have more influence than both heave and surge.

7.11.3 CONCLUSION OF SENSITIVITY ANALYSIS

The FL model is sensitive to changes in the stiffness values and thus all parameters influencing these stiffness values. In particular the FL model is sensitive to the stiffness value of the second spring (K_2). The dominance of the stiffness values is logical considering that the system is expected to respond quasi-static to the input motions, as stated in section 7.9.2. Furthermore, the analysis in this chapter confirms that the pitch motion is the most dominant of all ship motions and the first mode and its natural frequency has proven that the change in stiffness value has had effect on the noise's response.

7.12 HIGH FREQUENCY DISTURBANCES

Throughout the thesis it is evident that there is high frequency noise present in the data and in the models. There are several factors which can contribute to the presence of this noise and some of them have been mentioned earlier in this thesis. This section will first list all possible causes and then review their effects.

7.12.1 POSSIBLE SOURCES

From reviewing the frequency spectra of the models it can be seen that the RL model and the FL model both show higher frequencies in the system. This can be seen in the examples Figure 7.34 and Figure 7.35. The high frequency noise is already present when differentiating the motion data to obtain their acceleration. Since the noise is found in both the RL model as the FL model the main cause of the noise

must be sought in the input data of both models. However, the noise can be amplified by different calculations, which are performed within the models. Therefore both the data and the models were reviewed.

There is always noise present in data due to some physical effects which cannot be avoided, as stated in section 5.3. Apart from the physical effect there are several effects or calculations which either introduce high frequency noise or which amplify the high frequency noise already present. As stated in section 5.4 differentiation of the data emphasizes the higher frequencies present in the signals. An enumeration is made of possible causes of the high frequency noise introduction and/or enhancement:

1. Spectral leakage.
2. Time step in data traces.
3. Resampling type.
4. Reaction with the first mode.

SPECTRAL LEAKAGE

As explained in section 5.3 and Appendix B, spectral leakage can cause the fast Fourier transform to interpret discontinuities in the data trace as high frequency elements. For spectral leakage to play a role as cause for the high frequency information these distortions must be present and this thesis the distortions can be caused by:

1. The difference in amplitude at the start and end of the time traces.
2. The ensemble averaging which requires the time trace to be divided in sections regardless of start and end amplitude.
3. The filtering window, cutting of some sinusoidal components causing irregularities in the time signal when transformed to time-domain and thus inducing high frequency noise.

As input of the model the complete 3 hour data trace is used. No ensemble averaging took place. There is however an unequal starting and ending amplitude in the 3 hour trace, which causes some discontinuity in how the data is interpreted in the fast Fourier transform. This can be a cause of the high frequency noise but that would mean that this noise should be present in all displacement traces and in the measured cable forces. After testing the influence of spectral leakage, it was found that mitigation of this effect slightly reduces the high frequency information present in the filtered data traces.

Another cause of spectral leakage present in the model input is the filtering window used, which contains no smoothing function. The filter cuts off a range of sinusoids present in the data set which can cause discrepancies when applying the inverse fast Fourier transform to obtain the newly filtered data trace (also called ringing, see Appendix B). When re-applying the fast Fourier transform to the time traces containing this ringing effect, one should be able to see the frequency distortions it causes. After researching this effect, it was found that the filtering of the data does not affect or barely affects the high frequency range of a data trace.

TIME STEP IN THE DATA TRACES

Because the data is kept as close as possible to the actual measured data, as stated in section 5.2, the motion data could be too discontinuous to use as input data. For the displacement trace this poses no problem but the high frequency issue could be caused by differentiating these to accelerations. An example of the effect is given in Figure 7.33.

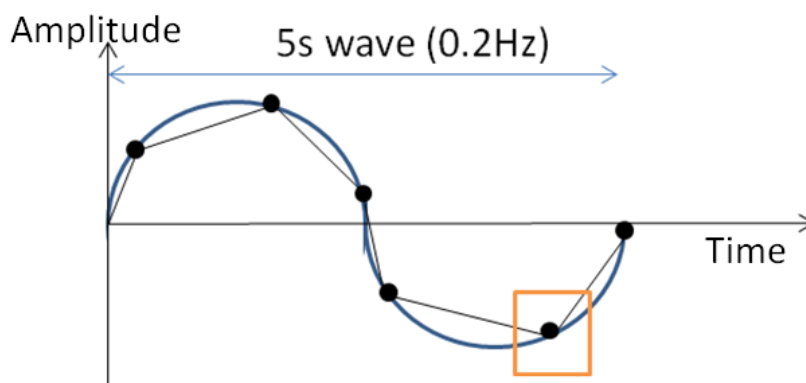


Figure 7.33 Sketch describing sampling complication for the smallest measured natural wave.

In the figure it can be seen that the peaks of the sinusoid can be “missed” while sampling. If these points are not interpolated with a hyperbola, the sudden direction change causes the differentiation of the displacement trace to show instant changes in velocity and thus infinite acceleration peaks (after differentiating again), which means high frequency disturbances can be observed in the frequency plots of the accelerations. The presence of this effect is shown in Figure 7.34 and Figure 7.35.

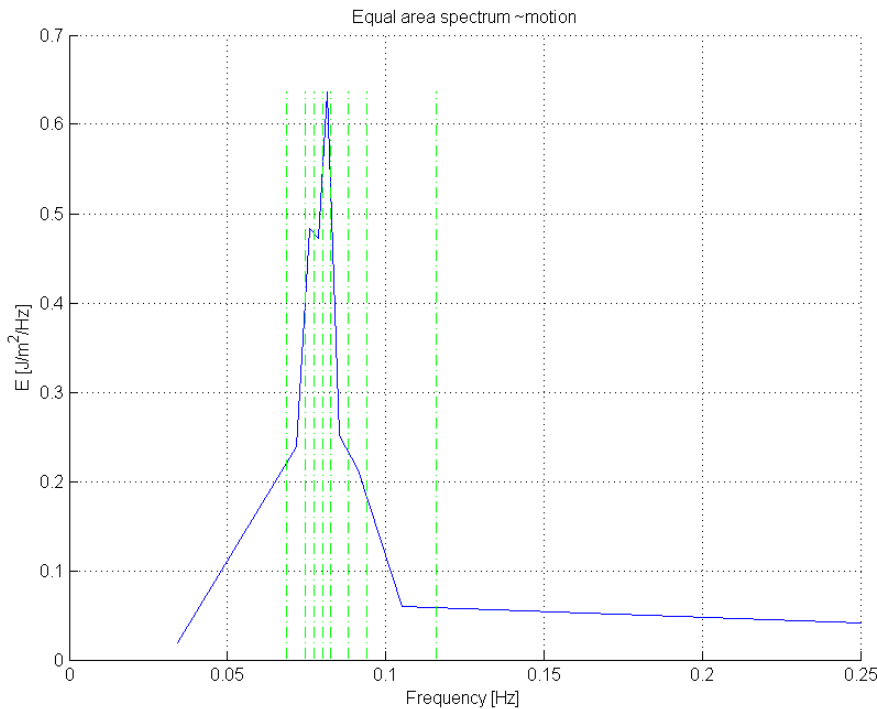


Figure 7.34 Binned frequency spectrum of the pitch displacement. It shows little high frequency information.

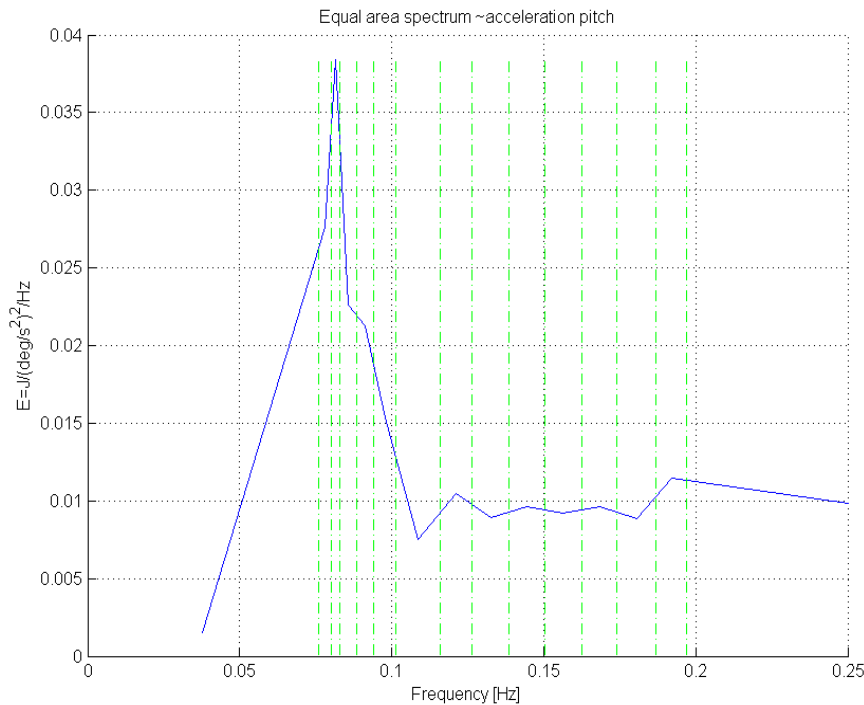


Figure 7.35 Binned frequency spectrum of the pitch acceleration. It shows more high frequency information.

However, since differentiation takes place in the frequency domain the data is interpreted as the sine wave itself by the fast Fourier transform, instead of the separate points. In an ideal situation the effect that the black lines in Figure 7.33 sketch should not have any influence. However, cubic interpolation of the displacement time traces before differentiation does smoothen the data traces and provides more data points for the fast Fourier transform. Slight inaccuracies currently present in transformation of the time domain to the frequency domain could therefore be smaller. After testing this effect, it is apparent that interpolating the displacement time traces using cubic interpolation reduces the high frequency

noise after differentiating twice. The results show slightly less high frequency information in comparison with the original acceleration plots where the data trace was kept at a 1 second, 1 value data trace.

RESAMPLING TYPE

As stated in Chapter 5 the time stamped values are not stamped at exactly 1 Hz but the time stamps are a few milliseconds off target. To resample these specific time stamps the interpolation function "nearest" is used. Since the time shift the value undergoes with this interpolation is just a few milliseconds it is expected that the interpolated value must not be far off the actual value of the measured sinusoidal motion. However, the summed effect of all shifts can influence the shape of the sinusoid the measurements indicate and thus the frequency it represents. This effect would then already be visible in the displacements as higher frequency influence. Again, this noise which is induced by this is emphasised by the differentiation of the displacements.

REACTION WITH THE FIRST MODE

In section 7.8.5 it was found that a possible cause of the high frequency information is the system's response in the first natural mode. In section 7.9.1 and section 7.11 it became clear that the increase in stiffness of the system did indeed reduce a part of the high frequency noise, as the high frequency range (0.13 Hz up to 0.2 Hz) apparently exhibited a resonance response to the first mode. Also, in section 7.9.2 it was found that the choice of damping percentage of the separate modes has influence on the high frequency noise present in the system. Suppressing the high frequency reaction was most effective when damping modes 2 to 5 with an higher percentage of the critical damping.

7.12.2 CONCLUSION

Form the previous section it can be concluded that the filtering window type is not a cause of the high frequency noise present in the models. It is however apparent that spectral leakage by a different start and end amplitude in the time trace has some influence. The time steps used in the motion displacement time traces also affects the high frequency noise visible in the predictions. The effect of the "nearest" type interpolation used might be a cause and will need to be reviewed, which is noted in the recommendations of this thesis. Additionally, when the FL model using modal damping is utilised one can suppress the high frequency noise in the predictions. The increasing of damping of modes 2-5 did show to be successful in reducing the high frequency noise.

In summary the high frequency noise can be caused by:

- Un-avoidable physical effects: Noise introduced by the measurement equipment itself; radio frequency interference; electromechanical interference; moisture and temperature.
- Spectral leakage due to the different amplitude at the beginning and at the end of the displacement or acceleration time trace used before applying the fast Fourier transform.
- The "nearest" resampling type used when resampling the data as described in section 5.2, this is however not proven as of yet.
- Time step used for the displacement traces in combination with the differentiation to acceleration values.

The high frequency noise can be reinforced by:

- Response with the first modes of the FL model.

7.13 EVALUATION OF THE FL MODEL ANALYSIS

In this chapter, the predictions of the FL model are reviewed in terms of comparison with the measured cable forces. It can be said that the FL model is a reasonable model for predicting the cable forces for this data time trace considered and it offers flexibility in future analysis of uplift because expansion is possible for this model. On a total mean value 1.89E4 kN of it can predict the force peaks of the cable forces with an accuracy of 8.1kN on average. The standard deviation, in worst case scenario, can predict the standard deviation of the cable forces with an accuracy of 9.9 kN (order of 3,7%).

The FL model indicates that the most sensitive frequencies in the system are the ones closest to the fundamental mode. The fundamental natural frequency is 1.9 Hz for the current FL model. The stiffness of the system is the main factor which influences the predictions of the FL significantly; particularly the stiffness value of the winded wire ropes connecting the hang-off frame and the stinger. The ship motion which is most significant for the forces in the cables is the pitch motion.

The viscous damping used in the FL model is not a realistic representation of the dissipation in the actual system. Therefore the damping introduced in the system is an estimated or fitted parameter which

accounts for some dissipation in the system. Improving the damping terms and thus removing this limitation is one of the recommendations of this thesis. Furthermore, the model does not account for non-linear effects influencing the cable stiffness of the wires, which is another limitation of this model and is included as one of the recommendations of this thesis.

The noise in the measured data has proven to be reinforced by some calculation methods and more high frequency noise is caused by some of these methods as well. High frequency noise can (possibly) be caused by:

- Un-avoidable physical effects: Noise introduced by the measurement equipment itself; radio frequency interference; electromechanical interference; moisture and temperature.
- Spectral leakage due to the different amplitude at the beginning and at the end of the displacement or acceleration time trace used before applying the fast Fourier transform.
- The "nearest" resampling type used when resampling the data as described in section 5.2, this is however not proven as of yet.
- Time step used for the displacement traces in combination with the differentiation to acceleration values.

The high frequency noise can be reinforced by:

- Response with the first modes of the FL model.

8. COMPARISON OF FL AND RL MODELS

The RL model provides reasonable predictions of the cable forces. The results of the RL model were presented in section 6.2.3. In summary it can be stated:

- The maximum normalised cross-covariance is 0.721.
- The standard deviation: 212 kN, which is 55.7 kN off target.
- The mean peak amplitude difference is -92.2 kN off target.
- The correlation in time and amplitude indicates an average distance of: 140.98 off target.

Therefore, the RL model shows a frequency difference and underestimates the force amplitudes when compared with the measured cable forces. An accurate determination of the amplitudes and standard deviation is however essential for predicting the likelihood of uplift to occur. On a total mean value of 1.89E4 kN it can predict the force peaks of the cable forces occurring with an accuracy of -92.2 kN on average and the standard deviation over the total time trace is 55.7 kN off target (approximately 20.8% off target). This value is too optimistic since it does not account for a worst case scenario input error. Including worst case scenario the input error the standard deviation is 22.2% off target.

The limitation of the RL model is that it is not possible, using this model, to see the interaction between the stinger and the sheaves, while the load cell which measures these cable forces could actually be influenced by these sheaves and their interactions with the equipment. Furthermore, the model does not allow for expansion or the adjustment of model parameters. It is not possible using the RL model to create a more accurate prediction of the amplitudes of the cable forces occurring. A detailed description of the RL model can be found in Chapter 6.

The results of the FL model were presented in section 7.8.3. In summary it can be stated:

- The maximum normalised cross-covariance is 0.732.
- The standard deviation: 270.6 kN, which is 2.9 kN off target. Note that the uncertainty by input errors is larger than this standard deviation value therefore the actual accuracy is 9.9 kN.
- The mean peak amplitude difference is 8.1 kN off target.
- The correlation in time and amplitude indicates an average distance of: 118.4 off target.

Therefore, the FL model slightly overestimates the force amplitudes when compared with the measured cable forces. On a total mean value 1.89E4 kN of it can predict the force peaks of the cable forces with an accuracy of 8.1kN on average. The standard deviation, in worst case scenario, can predict the standard deviation of the cable forces with an accuracy of 9.9 kN (order of 3,7%). It appears that the model is preferable because it accounts for stretching of the cables it allows for relative motion of the stinger and the top sheaves.

However, the viscous damping used in the FL model is not a realistic representation of the dissipation in the actual system. Therefore the damping introduced in the system is an estimated or fitted parameter which accounts for some dissipation in the system. Improving the damping terms and thus removing this limitation is one of the recommendations of this thesis. Furthermore, the model does not account for non-linear effects influencing the cable stiffness of the wires, which is another limitation of this model and is included as one of the recommendations of this thesis.

It can be concluded that the FL model is the better model for the prediction of the cable forces in this thesis. This is determined not only by its better overall performance, but additionally because of the flexibility it provides in the consideration of the case in which the stinger is immersed into the water.

9. CONCLUSION AND RECCOMENDATIONS

This last chapter of this thesis contains the conclusion answering the research questions and problem statement of section 2. The first section contains the conclusions and the successive sections contain the recommendations. There are two recommendation sections which are meant for readers with the purpose of continuing on this research path. The first recommendation section is meant for readers who aim to continue on the uplift analysis and the second section is meant for those readers which would like to improve the predictions of the model.

9.1 CONCLUSIONS

The goal of this thesis is to predict the cable forces in the hang-off system based on ship motions in a 2-D plane. The dynamic model should be able to predict both the mean force value and its dynamic amplitude with sufficient detail using the ship motions as an input. Two models were developed to reach this goal: The Rigid Links model (RL model) and the Flexible Links model (FL model). The main differences of the RL and FL model are that the FL model accounts for: cable flexibility, relative motion of the hang-off system and the stinger, stinger dynamics, sheave dynamics, some descriptive damping, optionally inclusion of sheave friction and static buoyancy.

Based on the research results in this thesis it can be concluded that the most accurate model to predict the cable forces in the hang-off system based on ship motions is the FL model. The FL model is preferable because it accounts for stretching of the cables it allows for relative motion of the stinger and the top sheaves. Consequently, the FL model describes the system response more accurately than the RL model. The FL model can predict the standard deviation of the cable forces with an accuracy of 9.9 kN (order of 3,7%), which is essentially the uncertainty due to input errors including the uncertainty due to errors in the measured cable forces. This accuracy of on a total predicted mean cable force of 1.89E4 kN (with an accuracy of order 0.08%) can be regarded satisfactory for the data time trace considered. The FL model is not only considered the best choice because of its better overall performance, but additionally because of the flexibility it provides in the consideration of the case in which the stinger is immersed into the water.

When studying the FL model's sensitivity, the stiffness values appeared to be governing. This is logical considering that the resonance frequency of the system is well above the excitation frequencies of the wave spectrum (which has its maximum frequency at 0.2 Hz in this thesis) it is exposed to. This means the system response for the FL model is quasi-static and thus the stiffness in the system dominates. The first and closest eigenfrequency, considering the FL model, is 1.9 Hz (or 0.52 seconds period). Logically, the most sensitive excitation frequencies are the frequencies closest to this first eigenfrequency. Additionally it was proven that the pitch motion is the most influential motion when considering the cable forces.

The limitation on the FL model is that damping is introduced as a viscous term which is not a realistic representation of the dissipation in the actual system. Therefore the damping introduced in the system is currently an estimated or fitted parameter which accounts for some amount of dissipation in the system. Furthermore, it does not account for non-linear effects influencing the cable stiffness of the wires.

Throughout the thesis noise was present in the predictions of the models. It has been researched what the possible causes of the presence of this noise are. It is apparent that spectral leakage has some influence on the presence of noise in the predictions. Furthermore, the time steps used in the motion displacement time traces in combination with the differentiation to acceleration time traces affects the high frequency noise visible. The effect of the "nearest" type interpolation used might as well be a cause and will need to be reviewed, which is noted in the recommendations of this thesis. The high frequency noise in the predictions can be amplified by the first mode of the FL model. If the noise is present in frequencies close to the eigenfrequencies of the modelled system the model will exhibit resonance in response to a false excitation. Furthermore it is found that high frequency noise can be suppressed by using the modal damping applied in the FL model and increasing the damping on the second and higher modes.

9.2 RECOMMENDATIONS FOR FURTHER UPLIFT ANALYSIS

The current predictions by the FL model are considered accurate enough for the current data trace considered. When one wishes to continue the uplift analysis it is recommended to first test the model's

results for a similar case. Subsequently, the FL model can be expanded for submerged situations. One should then take into account the following points as defined in Chapter 4:

- Dynamic buoyancy (as static buoyancy is already captured in the model).
- Wave forces.
- Current forces.
- Slamming.

Consequently, these physical effects are implemented in the model, a threshold value should be defined which indicates the minimum tension required in the hang-off cables. The cable tension may never reach values below this threshold to avoid (risk of) uplift. The threshold value contains a safety factor which accounts for the current uncertainties in the stiffness, due to non-linear effects, and the damping, due to it being an estimate.

When finalised, the model can be used in the following manner:

- Before operation, the acquired weather predictions can be translated into expected ship motions during operation.
- The motions are then used as input for the FL model which will generate a force time trace containing a mean force and a standard deviation.
- These statistical characteristics of the predicted cable forces can be used to calculate the chance that the cable forces will reach a value below the specified threshold value.
- Based on this chance the company can decide to continue and perform the operation or not.

When uplift poses a risk for significant periods of time during an project one could review options to mitigate the uplift if uplift would occur. A mitigation measure could for example be the use of hydraulic equipment attached to the flippers on the hang-off frame (see Figure 1.4), to prevent the ropes from becoming slack when the cable tension is too small.

9.3 RECOMMENDATIONS FOR MORE DETAILED ANALYSIS

If one is interested in a better fit of the predicted and measured data, the primary recommendation is to get a physical grasp on the damping applied. This can be performed possibly by changing the current application of the damping in the equations and/or using a different type of damping instead of the viscous damping. Suggestions for a different application of damping are:

- Use a dissipation form originating from internal dissipation in de wires.
- Account for dissipation by micro slip of the wires on the sheaves.
- Insert velocity dependent friction (even though its contribution is expected to be small).
- Use of structural damping.

Note that the enumeration above has the purpose of understanding the system better in physical terms, not to improve the accuracy of the model. To obtain more detailed results in comparison with the measured data trace, one should first consider that the current error by input data is too large to quantify an exact fit. If the accuracy of the FL model is smaller than the error by the input motions, one should consider to improve the accuracy of the measurement equipment before attempting to obtain a better fit to the data.

A third point to consider when continuing this research path is to define the stiffness of the system more accurately by reviewing the (non-linear) effects of:

- Young's modulus dependent on stresses
- Differential diameter due to tension the wire ropes.
- Fatigue and wear & tear.
- The effects of hysteresis
- The effects of the bends around the sheaves on the stiffness locally
- Research the effects of unequal load distribution and in turn the effects of it on the stress and tension related parameters as the Young's modulus and the diameter of the wire rope.

The last recommendation if one continues with this research path is to mitigate the high frequency noise present in the data. There are multiple ways to achieve this:

- Testing the effect of the interpolation type "nearest". Using another interpolation type when effect is significant.
- Mitigating the spectral leakage by usage of a windowing function when filtering.
- Interpolating the motion data to smaller time steps before differentiating them in the frequency domain.

BIBLIOGRAPHY

- [1] P. Demeersseman, *Naval Architect*, Delft, Zuid-Holland: Allseas, 2015.
- [2] D. H. Shreve, "IRD Balancing," IRD Mechanalysis, Inc., November 1995. [Online]. Available: www.irdbalancing.com/downloads/SIGCOND2_2.pdf. [Accessed 2015].
- [3] D. P. Mitchell and A. N. Netravali, "Reconstruction Filters in Computer Graphics," AT&T Bell Laboratories, 1988. [Online]. Available: <http://www.cs.utexas.edu/~fussel/courses/cs384g-fall2013/lectures/mitchell/Mitchell.pdf>. [Accessed 01 10 2015].
- [4] L. H. Holthuijsen, *Waves in oceanic and coastal waters*, Third ed., New York, New York: Cambridge university press, 2009, pp. 57, 324-334.
- [5] C. Vuijk, P. Van Beek, F. Vermolen and J. Van Kan, *Nummerieke methoden voor differentiaalvergelijkingen*, First ed., Delft, Zuid-Holland: VSSD, 2006, pp. 25-37.
- [6] C. Zdzislaw, "Institute of aviation, Warsaw, since 1926," 2001. [Online]. Available: <http://www.ilot.edu.pl/KONES/2001/JOK2001%20NO%201-2/R36.pdf>. [Accessed 05 09 2015].
- [7] J. Massie and W. Journée, *Offshore hydromechanics*, First ed., Delft, Zuid-Holland: TU Delft, 2001, pp. 11-12, 11-16.
- [8] J. Van Aubel, *Graduate*, Delft: Allseas, 2015.
- [9] The MathWorks, Inc., "xcov," [Online]. Available: <http://nl.mathworks.com/help/signal/ref/xcov.html;jsessionid=4bb5fc5d6ddf78fc766fefe982df>. [Accessed 01 05 2015].
- [10] The MathWorks, Inc., "std," [Online]. Available: <http://nl.mathworks.com/help/matlab/ref/std.html>. [Accessed 01 06 2015].
- [11] The MathWorks, Inc., "corrcoef," [Online]. Available: <http://nl.mathworks.com/help/matlab/ref/corrcoef.html>. [Accessed 01 06 2015].
- [12] Schaeffler Technologies AG & Co. KG, "Roller bearings," Schaeffler Group Industrial, 01 November 2014. [Online]. Available: http://medias.ina.com/medias/en!hp.tg.cat/tg_hr*ST4_102160011. [Accessed 01 07 2015].
- [13] A. Slocum, "Fundamentals of design," MIT, 01 01 2008. [Online]. Available: <http://pergatory.mit.edu/resources/FUNdaMENTALS.html>. [Accessed 01 07 2015].
- [14] J. Spijkers, A. Vrouwenvelder and E. Klaver, *Structural Dynamics CT4140, part 1- structural vibrations*, Delft, Zuid-Holland: Delft University of Technology, 2005, pp. 24-59/204.
- [15] K. Feyrer, *Wire ropes; Tension, Endurance, Reliability*, Springer, Ed., Stuttgart: Springer-Verlag Berlin Heidelberg, 2007.
- [16] J. R. Taylor, "Intro Physics labs," Warshington University in St. Louis, [Online]. Available: physics.wustl.edu/introphys/Phys117_118/Lab_Manual/Tutorials/ErrorAnalysisTutorial.pdf. [Accessed 01 10 2015].
- [17] The MathWorks, Inc., "fft, Discrete Fourier transform," [Online]. Available: <http://matlab.izmiran.ru/help/techdoc/ref/fft.html>. [Accessed 11 03 2015].
- [18] T. Stilson, "Anti-aliasing," Princeton University, 17 10 1996. [Online]. Available: <http://soundlab.cs.princeton.edu/learning/tutorials/sensors/node21.html>. [Accessed 01 11 2015].
- [19] D. Hershberger, G. J. Ogonowski and R. A. Orban, "Peak modulation control in digital transmission systems," 2007. [Online]. Available: http://www.orban.com/brochures/white_papers_faqs/Peak%20Modulation%20Control%20in%20Digital%20Transmission%20Systems.pdf. [Accessed 01 11 2015].
- [20] P. H. S. LLC, "Overlap Percentage," Pioneer Hill Software LLC, [Online]. Available: https://www.spectraplus.com/DT_help/overlap_percentage.htm. [Accessed 01 10 2015].
- [21] K. M. M. Prabhu, *Window functions and their applications in signal processing*, 20130809 ed., Boca Raton: CRC Press, Taylor & Francis Group, 2014, p. 295.
- [22] J. O. Smith, *Spectral audio signal processing*, S. U. Center for Computer Research in Music and Acoustics (CCRMA), Ed., W3K Publishing, 2011.
- [23] The MathWorks, Inc., "Choose a Solver," [Online]. Available: <http://nl.mathworks.com/help/simulink/ug/types-of-solvers.html>. [Accessed 05 08 2015].
- [24] The MathWorks, Inc., "ode45," 01 01 2006. [Online]. Available: <http://nl.mathworks.com/help/matlab/ref/ode45.html>. [Accessed 01 07 2015].

LIST OF TABLES

TABLE 1.1 SPECIFICATIONS OF THE AUDACIA.	18
TABLE 5.1 ERRORS OF THE MEASUREMENT EQUIPMENT.	32
TABLE 5.2 EXAMPLE OF DATA RESULTS AFTER DATA FILTERING IN THE FREQUENCY-DOMAIN FOR THE MEASURED CABLE FORCES.	37
TABLE 5.3 THE FREQUENCIES OF INTEREST FROM THE FREQUENCY PLOTS OF THE SHIP ACCELERATIONS AND MEASURED CABLE FORCES. THE TABLE INCLUDES RANGES OF FREQUENCIES OF INTEREST. THE NUMBERING CORRESPONDS TO THE FIGURES BELOW.	38
TABLE 6.1 PROPERTIES OF THE MEASURED CABLE FORCES.	48
TABLE 6.2 TIME-TRACE PROPERTIES OF THE RL MODEL.	49
TABLE 6.3 RESULTS OF THE REVIEWING METHODS FOR THE RL MODEL.	50
TABLE 7.1 SCHEMATISATION PARAMETERS.	57
TABLE 7.2 EFFECTS OF THE ORIGINAL AND THE NEW CALCULATION ON THE CABLE TENSION (T) RELATIVE TO THE SITUATION WITHOUT THE WEIGHT OF THE SHEAVES AND THE LOWER BLOCK STRUCTURE.	72
TABLE 7.3 STATIC TESTS 1 AND 2 WITH THEIR DESCRIPTION AND THEIR EXPECTATIONS.	73
TABLE 7.4 HARMONIC EXCITATION TESTS 1, 2 AND 3: THEIR DESCRIPTION AND THEIR EXPECTATIONS.	75
TABLE 7.5 PROPERTIES OF THE MEASURED CABLE FORCES.	78
TABLE 7.6 TIME-TRACE PROPERTIES OF THE RL MODEL.	79
TABLE 7.7 RESULTS OF THE REVIEWING METHODS FOR THE RL MODEL.	79
TABLE 7.8 TIME-TRACE PROPERTIES OF THE FL MODEL USING DIRECT TIME INTEGRATION.	81
TABLE 7.9 RESULTS OF THE REVIEWING METHODS FOR THE DIRECT TIME-INTEGRATION FL MODEL.	83
TABLE 7.10 TIME-TRACE PROPERTIES OF THE FL MODEL USING THE MODAL ANALYSIS APPROACH.	85
TABLE 7.11 RESULTS OF THE REVIEWING METHODS FOR THE DIRECT TIME-INTEGRATION FL MODEL.	86
TABLE 7.12 ADJUSTED PARAMETER VALUES OF THE ADJUSTED FL MODEL USING DIRECT TIME INTEGRATION.	87
TABLE 7.13 TIME-TRACE PROPERTIES OF THE ADJUSTED FL MODEL USING THE DIRECT TIME-INTEGRATION METHOD WITH ADJUSTED PARAMETERS.	88
TABLE 7.14 RESULTS OF THE REVIEWING METHODS FOR THE DIRECT TIME-INTEGRATION ADJUSTED FL MODEL.	89
TABLE 7.15 ADJUSTED PARAMETER VALUES OF THE ADJUSTED FL MODEL USING MODAL ANALYSIS.	90
TABLE 7.16 TIME-TRACE PROPERTIES OF THE ADJUSTED FL MODEL USING MODAL ANALYSIS.	90
TABLE 7.17 RESULTS OF THE REVIEWING METHODS FOR THE MODAL ANALYSIS METHOD FL MODEL.	91
TABLE 7.18 RESULTS OF UNCERTAINTY ANALYSIS, RL MODEL.	93
TABLE 7.19 RESULTS OF UNCERTAINTY RANGE, ADJUSTED FL MODEL USING DIRECT TIME-INTEGRATION.	93
TABLE 7.20 TOTAL INFLUENCE OF THE ERROR ON THE VALUES OF THE MEASURED CABLE FORCES.	94

LIST OF FIGURES

FIGURE 1.1 THE AUDACIA.	17
FIGURE 1.2 AUDACIA POINTS OF INTEREST.	18
FIGURE 1.3 HANG-OFF WIRES AND SHEAVE BLOCK.	18
FIGURE 1.4 FLIPPERS SUPPORTING THE DEAD ENDS OF HANG-OFF CABLE WITH LOAD CELLS. © HANS@FOTOVLIEGER.NL.	19
FIGURE 1.5 SIDE-VIEW OF THE FLIPPERS ON TOP OF THE STINGER HANDLING FRAME.	19
FIGURE 1.6 SIDE VIEW (LEFT) AND FRONT VIEW (RIGHT) OF THE LOWER BLOCK STRUCTURE AND ITS CONNECTION TO THE STINGER.	20
FIGURE 1.7 AXIS CONVENTIONS USED IN CALCULATIONS.	20
FIGURE 2.1 SKETCH OF CABLE FORCE VARIATION POTENTIALLY CAUSING UPLIFT.	23
FIGURE 4.1 RESULT OF THE GENERAL ANALYSIS.	29
FIGURE 5.1 EXAMPLE SKETCH OF THE "PREVIOUS" AND "NEAREST" INTERPOLATION TYPE.	32
FIGURE 5.2 FLOW CHART OF THE FILTERING PROCESS AND THE DATA ANALYSIS.	33
FIGURE 5.3 UNFILTERED DENSITY SPECTRUM OF STINGER HANG-OFF SYSTEM MEASURED CABLE FORCES.	34
FIGURE 5.4 FILTERED DENSITY SPECTRUM OF STINGER HANG-OFF SYSTEM MEASURED CABLE FORCES. NOTE THAT THE X- AXIS HAS BEEN REDUCED IN SIZE IN COMPARISON WITH THE PREVIOUS FIGURE.	34
FIGURE 5.5 THE ENERGY DENSITY SPECTRUM OF THE MEASURED CABLE FORCES. BIN BOARDERS ARE SHOWN WITH GREEN DOTTED LINES.	36
FIGURE 5.6 THE EFFECT OF DIFFERENTIATION: EMPHASIZING THE HIGHER FREQUENCIES.	37
FIGURE 5.7 BINNED FREQUENCY SPECTRUM OF THE MEASURED CABLE FORCES. NUMBERS CORRESPOND WITH TABLE 5.3.	38
FIGURE 5.8 BINNED FREQUENCY SPECTRUM OF THE PITCH ACCELERATION. NUMBERS CORRESPOND WITH TABLE 5.3. ...	39
FIGURE 5.9 NORMALISED NEGATIVE PITCH ACCELERATION [RAD/S ²] AND NORMALISED MEASURED CABLE FORCES [KN].	40
FIGURE 6.1 SKETCH OF THE MEASUREMENT MOTION LOCATIONS AND THE MEASUREMENT LOCATION OF THE CABLE FORCES.	43
FIGURE 6.2 SKETCH OF THE RIGID BODY MODELLED WITH THE LINEARIZED DYNAMICAL EQUATIONS.	44
FIGURE 6.3 EXAMPLE OF Δt AND ΔA IN A GRAPH. THE BASIS FOR CALCULATION OF THE PEAK CORRELATION IN TIME AND AMPLITUDE.	46
FIGURE 6.4 FREQUENCY PLOT OF THE MEASURED CABLE FORCES. THE SPECTRUM IS NON-BINNED BUT HAS BEEN FILTERED.	47
FIGURE 6.5 SPECTROGRAM OF THE MEASURED CABLE FORCES, USING A HAMMING WINDOWING FUNCTION. NOTE: THE FREQUENCY PLOT ON THE LEFT HAND SIDE IS NORMALISED.	48
FIGURE 6.6 TIME TRACE OF THE RL MODEL AND THE MEASURED CABLE FORCE.	49
FIGURE 6.7 CROSS COVARIANCE OF THE FORCE PREDICTION BY THE RL MODEL AND THE MEASURED CABLE FORCES.	50
FIGURE 6.8 THE FREQUENCY SPECTRUM OF THE RL MODEL. THE SPECTRUM IS NON-BINNED BUT HAS BEEN FILTERED. ...	51
FIGURE 6.9 SPECTROGRAM OF THE RL MODEL, USING A HAMMING WINDOWING FUNCTION. NOTE: THE FREQUENCY PLOT ON THE LEFT HAND SIDE IS NORMALISED.	52
FIGURE 7.1 SCHEMATISATION OF THE MODEL FUNCTIONALITY. NOTE: α IS THE SHEAVE ROTATION ANGLE & ϕ IS THE STINGER ROTATION ANGLE.	55
FIGURE 7.2 OUTPUT PARAMETERS OF THE MODEL AND SOME MODEL CHARACTERISTICS.	55
FIGURE 7.3 HANG-OFF SYSTEM LAYOUT. ADDITIONALLY CABLE AND SHEAVE NUMBERING IS GIVEN.	56
FIGURE 7.4 SCHEMATISATION OF THE HANG-OFF SYSTEM.	58
FIGURE 7.5 ROTATIONAL FRICTION (LEFT) AND ROTATION BY THE SHEAVE (RIGHT).	65
FIGURE 7.6 THE CALCULATION OF NORMAL FORCE BY THE TENSIONS OF CABLES ON BOTH SIDES OF THE SHEAVE.	66
FIGURE 7.7 REPRESENTATIVE RADIUS FOR INERTIA CALCULATIONS.	70
FIGURE 7.8 REMINDER OF THE LOWER BLOCK STRUCTURE LOCATION.	72
FIGURE 7.9 RESULTS OF STATIC TEST 1. SHEAVE 6 ALSO STAYS IN EQUILIBRIUM POSITION, AS EXPECTED.	73
FIGURE 7.10 RESULT OF THE FREE VIBRATION TEST. SHEAVE 6 SHOWS OSCILLATIONS AFTER INITIAL DISPLACEMENT OF 10%, AS EXPECTED.	74
FIGURE 7.11 RESULTS OF DYNAMIC TEST 1. THE STINGER SHOWS LITTLE TO NO DISPLACEMENT BY THE EXCITATION FAR INTO THE MASS-DOMINATED REGIME, THUS THE HIGH FREQUENCY CUSTOM θ EXCITATION. THE RESULTS ARE AS EXPECTED.	75
FIGURE 7.12 RESULTS OF DYNAMIC TEST 2. THE STINGER REACTS QUASI-STATIC TO THE LOW FREQUENCY CUSTOM θ EXCITATION. AS EXPECTED.	76
FIGURE 7.13 THE STINGER'S RESPONSE TO AN EXCITATION IN THE NATURAL FREQUENCY, AS EXPECTED.	76
FIGURE 7.14 FREQUENCY PLOT OF THE MEASURED CABLE FORCES. THE SPECTRUM IS NON-BINNED BUT HAS BEEN FILTERED.	77
FIGURE 7.15 SPECTROGRAM OF THE MEASURED CABLE FORCES, USING A HAMMING WINDOWING FUNCTION. NOTE: THE FREQUENCY PLOT ON THE LEFT HAND SIDE IS NORMALISED.	78

FIGURE 7.16 THE FREQUENCY SPECTRUM OF THE RL MODEL. THE SPECTRUM IS NON-BINNED BUT HAS BEEN FILTERED. .	79
FIGURE 7.17 SPECTROGRAM OF THE RL MODEL, USING A HAMMING WINDOWING FUNCTION. NOTE: THE FREQUENCY PLOT ON THE LEFT HAND SIDE IS NORMALISED.	80
FIGURE 7.18 TIME TRACE OF THE FL MODEL USING THE DIRECT TIME-INTEGRATION METHOD. THE FIGURE ALSO INCLUDES THE TIME TRACE OF THE RL MODEL FOR COMPARISON.	81
FIGURE 7.19 NON-BINNED, FILTERED SPECTRUM OF THE FL MODEL USING THE DIRECT TIME-INTEGRATION METHOD. ...	82
FIGURE 7.20 SKETCH OF THE CROSS-COVARIANCE TIME STEPS AND ITS INFLUENCE ON THE RESULTING CROSS COVARIANCE VALUE.	83
FIGURE 7.21 SPECTROGRAM OF THE FL MODEL USING THE DIRECT TIME-INTEGRATION METHOD. NOTE: THE FREQUENCY PLOT ON THE LEFT HAND SIDE IS NORMALISED.	83
FIGURE 7.22 TIME TRACE OF THE FL MODEL USING THE MODAL ANALYSIS METHOD. THE FIGURE ALSO INCLUDES THE TIME TRACE OF THE RL MODEL FOR COMPARISON.	85
FIGURE 7.23 NON-BINNED, FILTERED SPECTRUM OF THE FL MODEL USING THE MODAL ANALYSIS APPROACH.	85
FIGURE 7.24 SPECTROGRAM OF THE FL MODEL USING THE MODAL ANALYSIS METHOD. NOTE: THE FREQUENCY PLOT ON THE LEFT HAND SIDE IS NORMALISED.	86
FIGURE 7.25 TIME TRACE OF THE FL MODEL USING THE DIRECT TIME-INTEGRATION METHOD WITH ADJUSTED PARAMETERS. THE FIGURE ALSO INCLUDES THE TIME TRACE OF THE RL MODEL FOR COMPARISON.	88
FIGURE 7.26 NON-BINNED, FILTERED SPECTRUM OF THE ADJUSTED FL MODEL USING THE DIRECT TIME-INTEGRATION METHOD.	88
FIGURE 7.27 SPECTROGRAM OF THE ADJUSTED FL MODEL USING THE DIRECT TIME-INTEGRATION METHOD. NOTE: THE FREQUENCY PLOT ON THE LEFT HAND SIDE IS NORMALISED.....	89
FIGURE 7.28 TIME TRACE OF THE FL MODEL USING THE MODAL ANALYSIS METHOD WITH ADJUSTED PARAMETERS. THE FIGURE ALSO INCLUDES THE TIME TRACE OF THE RL MODEL FOR COMPARISON.	90
FIGURE 7.29 NON-BINNED, FILTERED SPECTRUM OF THE FL MODEL USING THE MODAL ANALYSIS METHOD.	91
FIGURE 7.30 SPECTROGRAM OF THE ADJUSTED FL MODEL USING THE MODAL ANALYSIS METHOD. NOTE: THE FREQUENCY PLOT ON THE LEFT HAND SIDE IS NORMALISED.	92
FIGURE 7.31 THE SPECTRUM AND SPECTROGRAM OF THE ADJUSTED FL MODEL'S PREDICTED FORCE TRACES. THE BLACK ARROW INDICATES THE LOCATION OF THE BASE NATURAL FREQUENCY. FOR THIS GRAPH THE STIFFNESS HAS BEEN DIVIDED BY A FACTOR OF 35. NOTE: THE FREQUENCY PLOT ON THE LEFT HAND SIDE IS NORMALISED.	95
FIGURE 7.32 THE SPECTRUM AND SPECTROGRAM OF THE ADJUSTED FL MODEL'S PREDICTED FORCE TRACES. THE BLACK ARROW INDICATES THE LOCATION OF THE BASE NATURAL FREQUENCY. FOR THIS GRAPH THE STIFFNESS HAS BEEN DIVIDED BY A FACTOR OF 15. NOTE: THE FREQUENCY PLOT ON THE LEFT HAND SIDE IS NORMALISED.	96
FIGURE 7.33 SKETCH DESCRIBING SAMPLING COMPLICATION FOR THE SMALLEST MEASURED NATURAL WAVE.	97
FIGURE 7.34 BINNED FREQUENCY SPECTRUM OF THE PITCH DISPLACEMENT. IT SHOWS LITTLE HIGH FREQUENCY INFORMATION.	98
FIGURE 7.35 BINNED FREQUENCY SPECTRUM OF THE PITCH ACCELERATION. IT SHOWS MORE HIGH FREQUENCY INFORMATION.	98

APPENDIX A. MATLAB FOR DATA ANALYSIS

READOUT DATA

The format in which the data is obtained from the data logger is ".csv". This means all data points are given as a string which includes names, values, times and dates. An example is given in Figure A.1 Example of string output of the data logger in the ".csv" file.. Each time stamp is a string of data containing the information shown in the figure.

AU-413L6-SER-001.ROOT.PHOCT.Heave,"2015-01-05 00:00:02.290",-0.074,1

Figure A.1 Example of string output of the data logger in the ".csv" file.

Matlab is able to read out all data in the ".csv" file using the *textscan* function. The Matlab script is coded such that it finds the parameters by their data logger names. It indexes the parameters and it gives each parameter its own name and unit. Then the script searches for each logger name in the ".csv" files and when it finds a string line with the corresponding logger name it reads out the value and timestamp corresponding. So essentially, Matlab reads out the data and sorts the information by:

- Indexing
- Full data logger names
- Short names
- Units
- Values
- Timestamps

FINDING TIME RANGES

As mentioned before in Chapter 5 the data imported in Matlab contains time jumps, has no exact sampling and contains distortions. To find these time gaps created by the time jumps one must search for the time ranges which do contain data and the time ranges which do not. The finding time-ranges script searches for these ranges in the data given by the "Readout data" script. It creates ranges of usable data (ranges with time stamps and values) and with that finds starting and ending times of all time gaps. The script described in section 5.2 will then fill these gaps with interpolated values.

FREQUENCY-DOMAIN

To transform the resampled time traces the fast Fourier transform (FFT) is used. Matlab has a built-in function called *fft* which calculates the discrete Fourier transform (DFT) of the input data with the fast Fourier transform method. More information on this Matlab function, the discrete Fourier transform and the fast Fourier transform is given in Appendix B.

APPENDIX B. FAST FOURIER TRANSFORM

The Fourier transform is based on the Fourier theorem which essentially states that any wave form, such as the ship motion input of this thesis, can be represented as the sum of sinusoids. The fast Fourier transform is a method to translate a wave signal in the time-domain into the frequency-domain. In the frequency-domain the signal is represented as magnitudes as function of frequency. Since each sinusoid, in the total sum of the sinusoids, contains its own frequency and amplitude it is a method of viewing the decomposed signal's build-up of sinusoids. Since the input signals in this thesis are discrete signals the discrete Fourier transform must be applied. For this purpose the fast Fourier transform (hereafter: "fft") is used which is a computationally effective form of the discrete Fourier transform. To translate the signal in frequency-domain back into the time-domain one can use the inverse fast Fourier transform (hereafter: "ifft"). The functions used for a discrete Fourier transform and a discrete inverse Fourier transform are given in equations B.1 and equations B.2 respectively.

$$Y(k) = \sum_{n=0}^{N-1} X(n) e^{-\frac{i2\pi kn}{N}} \quad \text{B.1}$$

$$X(n) = \frac{1}{N} \sum_{k=0}^{N-1} Y(k) e^{-\frac{i2\pi kn}{N}} \quad \text{B.2}$$

In which:

Y(k)	:	Amplitude and phase in a complex number of the frequency k.
X(n)	:	Value at time step index j.
N	:	Number of time samples.
n	:	Time step index.
k	:	Frequency [Hz].
i	:	Imaginary unit or imaginary number.

In Matlab these equation would obtain the form of equation B.3 and B.4, since Matlab cannot use an index of value zero. Matlab uses a fast Fourier transform algorithm to calculate the discrete Fourier transform equations. The algorithm used is the Cooley-Tukey algorithm [17].

$$Y(k) = \sum_{j=1}^n X(n) \left(e^{-\frac{2\pi i}{N}} \right)^{(n-1)(k-1)} \quad \text{B.3}$$

$$X(n) = \frac{1}{N} \sum_{k=1}^n Y(k) \left(e^{-\frac{2\pi i}{N}} \right)^{-(n-1)(k-1)} \quad \text{B.4}$$

SPECTRAL LEAKAGE

The Fourier transform interprets the finite data set as a circular form of constituent parts, both in time-domain as in frequency domain. In time domain this means that the wave forms are considered as if the last sample time connects with the first sampling time, so the signal repeats itself. This is an ideal situation which rarely occurs when using measured data. When the data does not connect in amplitude in the first and last time step, the function "reads" them as shown in Figure B.1. This distortion in the signal creates high frequency noise which can be seen in the frequency-domain of the signal after the application of fft [2]. To minimise effects of spectral leakage a windowing function can be used.

This type of distortion in this thesis can be caused by:

1. The unrelated start and end of the time traces.
2. The ensemble averaging which requires the time trace to be divided in sections regardless of start and end amplitude.
3. The filtering window, cutting of some sinusoidal components causing irregularities in the time signal when transformed to time-domain and thus inducing high frequency noise.

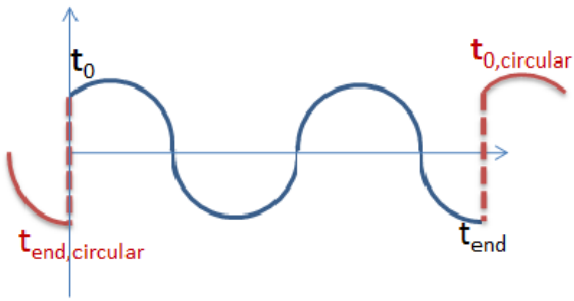


Figure B.1 Spectral leakage due to difference in amplitude of t_0 and t_{end} .

RINGING

The filtering type used to filter the data is a type of “brick wall” filter. The filter removes frequencies from a spectrum and improves in frequency- and in time-domain of a data set. However the filter can also introduce an effect which is called ringing. When cutting off frequencies in the frequency-domain one could see a type of impulse response at the window edges in the time domain, which dies out over time. However, if the band width of the filter is large enough and the energy in the cut-off frequencies is not very high the ringing effect will not have influence on the time-domain signal. [18] [3] [19]

ROUND-OFF ERROR

When translating the data from time-domain to frequency-domain the fft function creates a complex conjugate value array to represent the data. However, when working with measured data there is always a minimum resolution at which the data is measured. This means the measured values can rounded off solely by the resolution of the measurement equipment. Another cause of errors is the numerical errors which are introduced by Matlab when performing calculations. These errors cause the result of the fft to not be exactly conjugate symmetric. If one would apply an ifft to this data set of non-exact conjugate values one would obtain complex values for a parameter as, for example, speed or displacement. To prevent this it is advised to use the symmetric function in the ifft in order to forcibly symmetrise the data array.

APPENDIX C. ADDITIONAL DATA ANALYSIS RESULTS

This appendix contains some additional results of Chapter 5. It contains the time and frequency plots of the roll motions from which it was concluded that they showed no correlation with time and frequency plots of the measured cable forces. Another effect which must be pointed out using the frequency plots of the roll motion is the increase in high frequency content of the data traces when differentiating the displacement data traces.

PITCH

In Chapter 5 it has been noted that the frequency content in the higher frequency regions is amplified due to differentiation of the displacement traces. This effect can be observed in the frequency spectra of the pitch motions when comparing the frequency plot of the pitch displacement and the frequency plot of the pitch acceleration. The pitch displacement is shown in Figure C.1. The pitch acceleration is shown in Figure C.2.

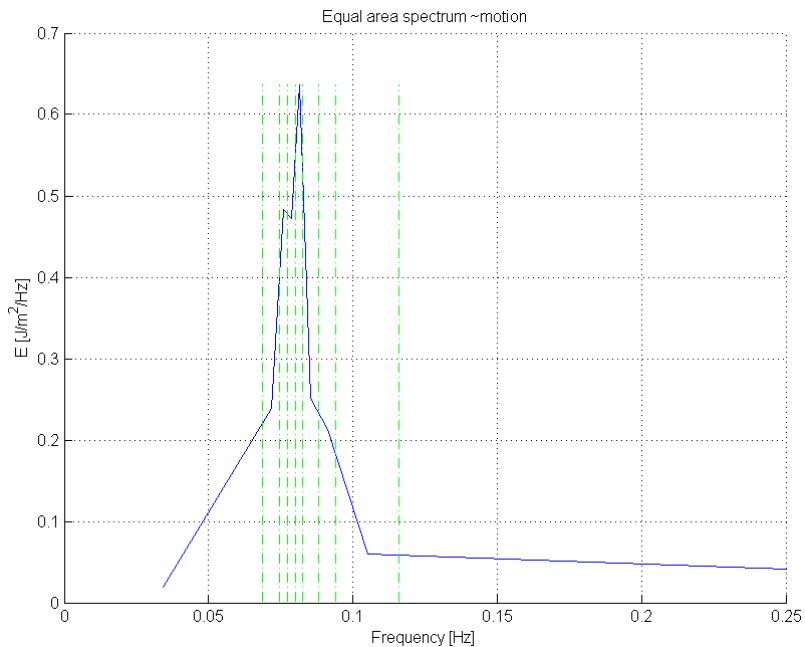


Figure C.1 Frequency spectrum plot of pitch displacement at the centre of gravity of the vessel.

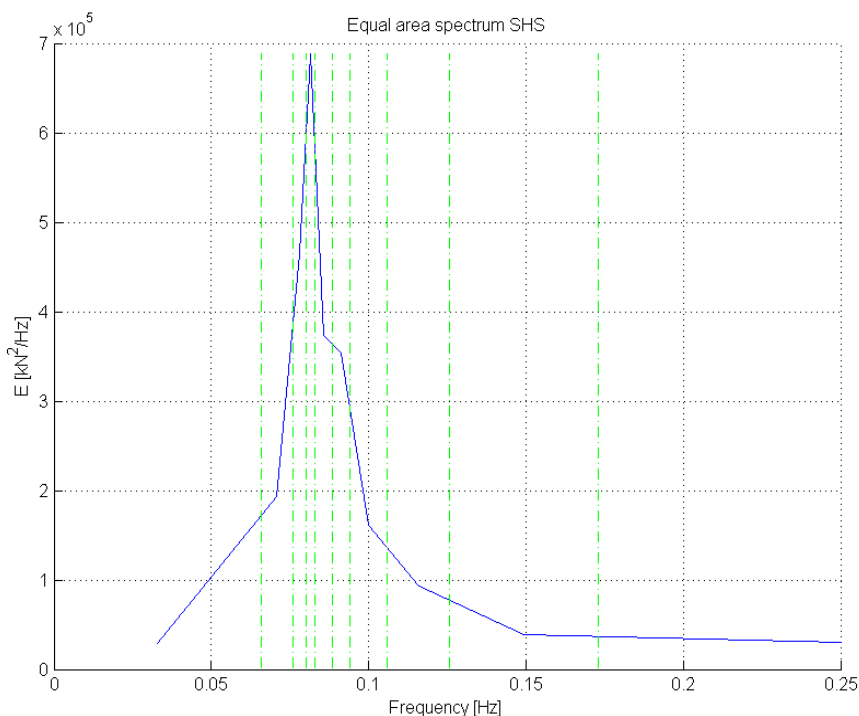


Figure C.2 Frequency spectrum plot of pitch acceleration at the centre of gravity of the vessel

ROLL

This sections presents the time and frequency plots of the roll accelerations. They have been presented here as it was evident by reviewing them that the roll motion shows no correlation with time and frequency plots of the measured cable forces. The frequency plot of the roll acceleration can be found in Figure C.3. The time-domain plot of the roll acceleration can be found in Figure C.4.

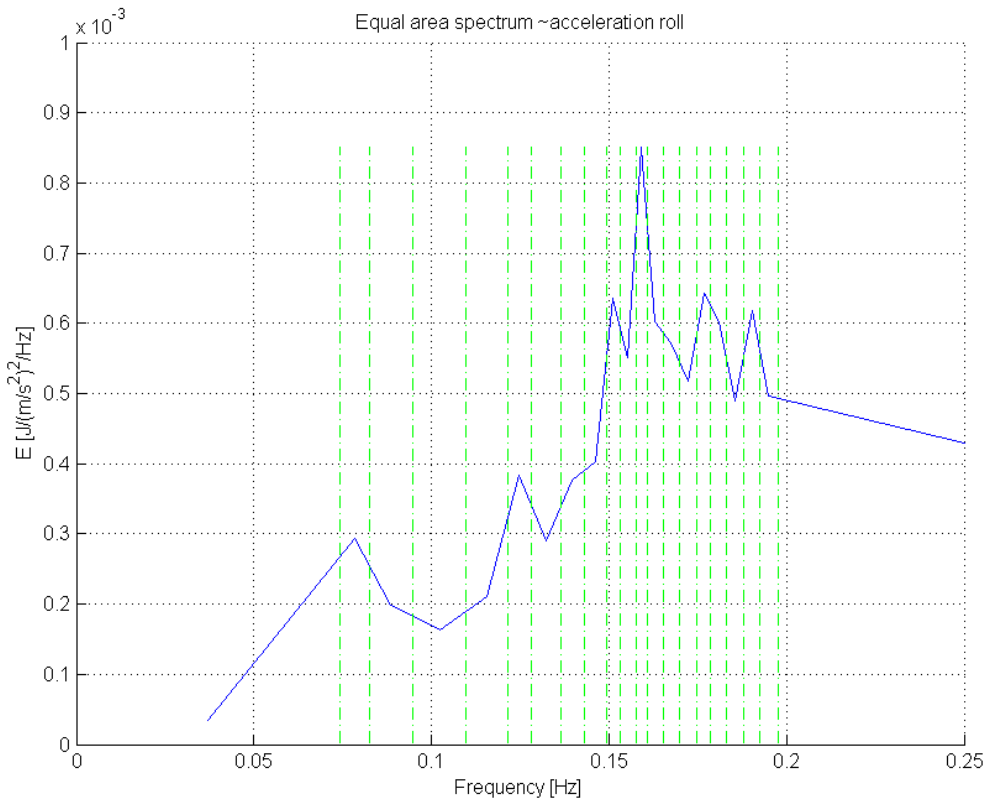


Figure C.3 Frequency spectrum plot of roll acceleration at the centre of gravity of the vessel.

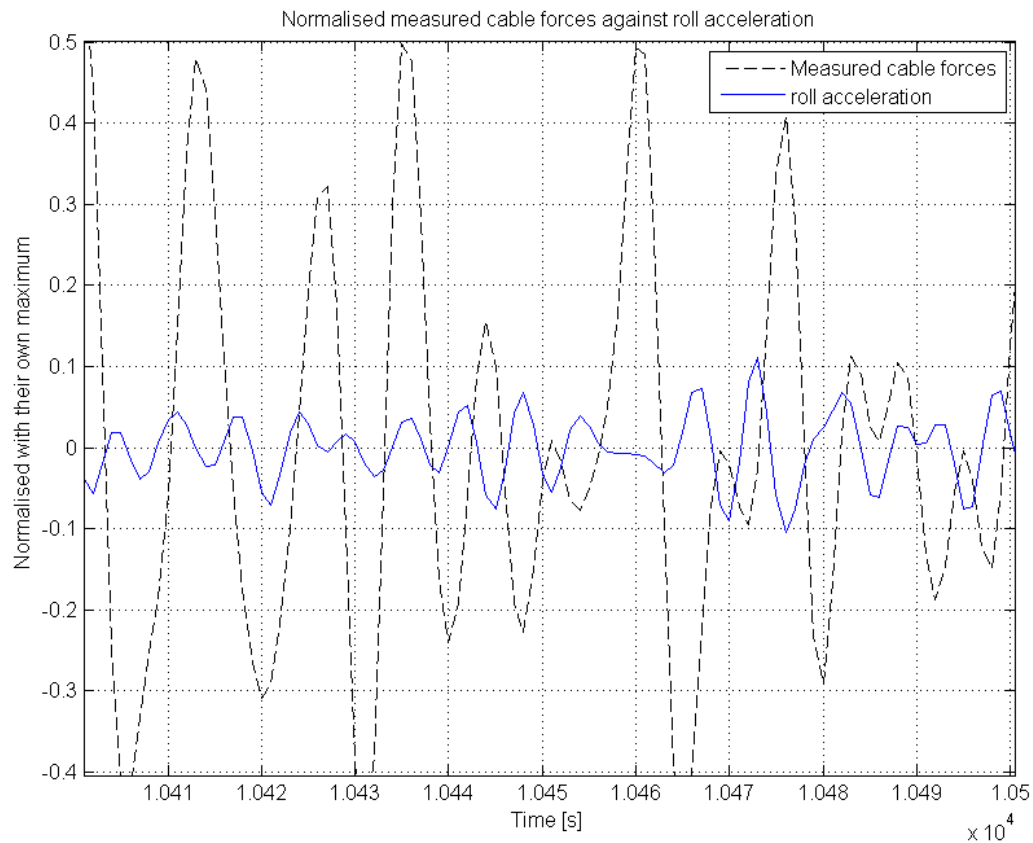


Figure C.4 Normalised time trace of roll acceleration at the centre of gravity of the vessel.

ACCELERATION PLOTS OF HEAVE AND SURGE

This appendix contains the additional results of the acceleration frequency spectra of the heave and surge motion. The frequency spectrum of the surge acceleration can be found in Figure C.5. The frequency spectrum of the heave acceleration is given in Figure C.6. They have been presented complementary to Table 5.3 in Chapter 5.

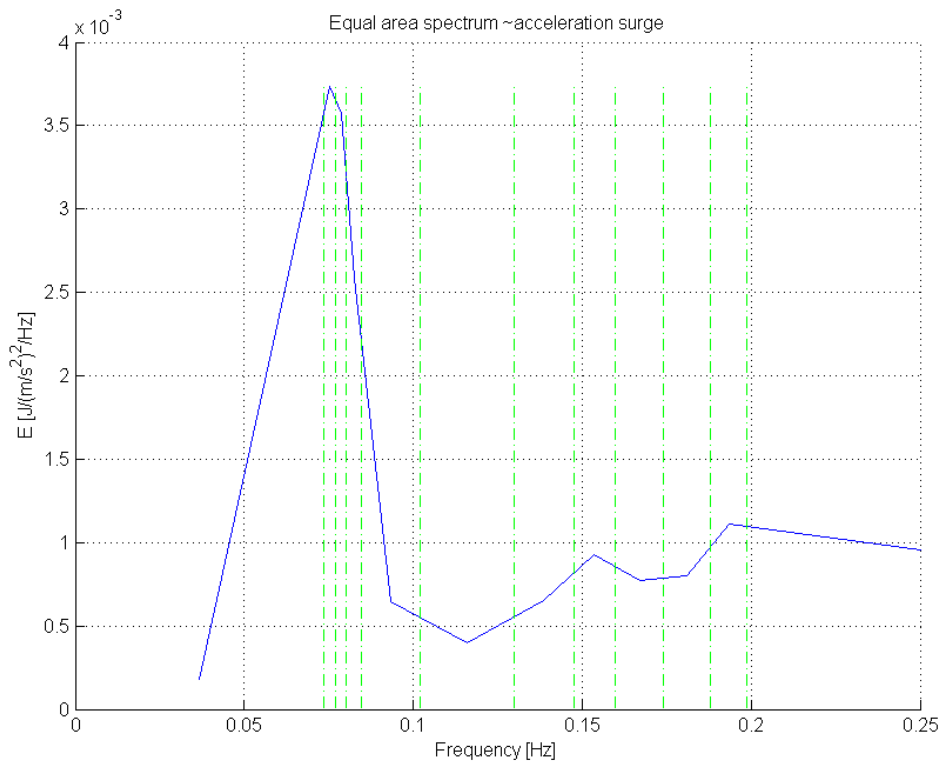


Figure C.5 Frequency spectrum plot of surge acceleration at the centre of gravity of the vessel.

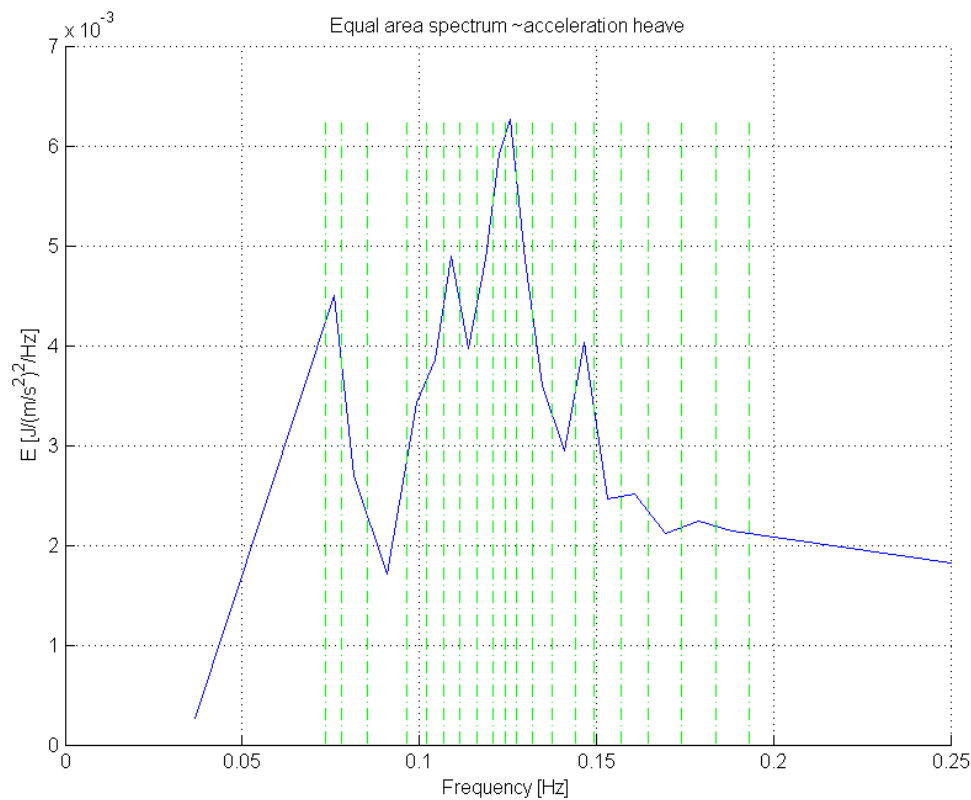


Figure C.6 Frequency spectrum plot of heave acceleration at the centre of gravity of the vessel.

APPENDIX D. EQUATIONS OF MOTION

This appendix continues on the derivation of the equations of motions of section 7.3. In that section all energy terms are given and the small angle approximation is explained. It is not explained how the Lagrangian terms were derived and the equations of motions are not shown in the section for sake of brevity and only a small representation of the equations is given. This appendix gives the details on the derivation of the equations.

As a reminder the equations of the Lagrangian formalism are shown equations D.1 and D.2. The equations respectively are the Lagrange function and Euler-Lagrange equation.

$$L = T - V \quad \text{D.1}$$

$$\frac{d}{dt} \frac{\delta L}{\delta \dot{q}} - \frac{\delta L}{\delta q} = 0 \quad \text{D.2}$$

In which:

L	:	The Lagrangian function.
t	:	Time.
q	:	Generalised coordinate.
T	:	Kinetic energy in the system.
V	:	Potential energy in the system.

These equations will be differentiated to the general coordinates of the system.

DIFFERENTIATION OF THE LAGRANGIAN FORMALISM FOR φ

When differentiating the kinetic terms the derivation of equation D.3 is performed:

$$\frac{\delta}{\delta t} \frac{\delta L}{\delta \dot{\varphi}} = \frac{\delta}{\delta t} \frac{\delta T}{\delta \dot{\varphi}} \quad \text{D.3}$$

Note that some integrals result in a large, complex equation. Therefore they were solved using Matlab. This is why for the z- and x-acceleration numbers were filled in the brackets instead of functions of lengths and angles.

When differentiating the potential terms equation D.4 is used:

$$-\frac{\delta L}{\delta \varphi} = \frac{\delta V}{\delta \varphi} \quad \text{D.4}$$

DIFFERENTIATION OF THE LAGRANGIAN FORMALISM FOR α

When differentiating the kinetic terms the derivation of equation D.5 is performed:

$$\frac{\delta}{\delta t} \frac{\delta L}{\delta \dot{\alpha}} = \frac{\delta}{\delta t} \frac{\delta T}{\delta \dot{\alpha}} \quad \text{D.5}$$

There is only one kinetic term dependent on the velocity of the sheaves. Therefore there was only one differentiation necessary for the kinetic part of the sheave motion. Though, there are 44 separate sheaves for which this needs to happen, as shown in equation D.6. Therefore, the parameter n in the equation D.6 represents sheave numbers 1 up to 44.

$$\frac{\delta}{\delta t} \frac{\delta T_{Sheaves}}{\delta \dot{\alpha}_n} = I_{sh,n} \ddot{\alpha}_n \text{ for } n = 1, \dots, 44 \quad \text{D.6}$$

When differentiating the potential terms equation D.7 is used.

$$-\frac{\delta L}{\delta \alpha_n} = \frac{\delta V}{\delta \alpha_n} \quad \text{D.7}$$

Of all the linear potential terms stated in section 7.3, only the spring terms are dependent on alpha.

THE RESULTING EQUATIONS OF MOTION

If the equations are differentiated and the results are rewritten, one obtains the equations of motion of the system. All resulting equations of motion are given below.

In section 7.3 a general form of the equations of motion are given through example equations. These contain constants which are also used in the Matlab model. After the list of equations of motion these example equations are shown and the definitions of the constants are given.

Eq. O. M. 1	$I_{sh,1} \cdot \ddot{\alpha}_1 + (K_{31} + K_2)R^2\alpha_1 = R^2K_2\alpha_{25} + RK_2L_0 \cos \beta \varphi - RK_2(L_c - L_A) \cos \beta \theta$
Eq. O. M. 2	$I_{sh,2} \cdot \ddot{\alpha}_2 + 2 \cdot K_2R^2\alpha_2 = K_2R^2\alpha_{25} + K_2R^2\alpha_{26}$
Eq. O. M. 3	$I_{sh,3} \cdot \ddot{\alpha}_3 + 2 \cdot K_2R^2\alpha_3 = K_2R^2\alpha_{26} - K_2R^2\alpha_{27}$
Eq. O. M. 4	$I_{sh,4} \cdot \ddot{\alpha}_4 + 2 \cdot K_2R^2\alpha_4 = K_2R^2\alpha_{27} + K_2R^2\alpha_{28}$
Eq. O. M. 5	$I_{sh,5} \cdot \ddot{\alpha}_5 + 2 \cdot K_2R^2\alpha_5 = K_2R^2\alpha_{28} + K_2R^2\alpha_{29}$
Eq. O. M. 6	$I_{sh,6} \cdot \ddot{\alpha}_6 + (K_1 + K_2)R^2\alpha_6 = R^2K_2\alpha_{29} + RK_2L_0 \cos \beta \varphi - RK_2(L_c - L_A) \cos \beta \theta$
Eq. O. M. 7	$I_{sh,7} \cdot \ddot{\alpha}_7 + (K_1 + K_2)R^2\alpha_7 = R^2K_2\alpha_{30} + RK_2L_0 \cos \beta \varphi - RK_2(L_c - L_A) \cos \beta \theta$
Eq. O. M. 8	$I_{sh,8} \cdot \ddot{\alpha}_8 + 2 \cdot K_2R^2\alpha_8 = K_2R^2\alpha_{30} + K_2R^2\alpha_{31}$
Eq. O. M. 9	$I_{sh,9} \cdot \ddot{\alpha}_9 + 2 \cdot K_2R^2\alpha_9 = K_2R^2\alpha_{31} + K_2R^2\alpha_{32}$
Eq. O. M. 10	$I_{sh,10} \cdot \ddot{\alpha}_{10} + 2 \cdot K_2R^2\alpha_{10} = -K_2R^2\alpha_{32} + K_2R^2\alpha_{33}$
Eq. O. M. 11	$I_{sh,11} \cdot \ddot{\alpha}_{11} + 2 \cdot K_2R^2\alpha_{11} = K_2R^2\alpha_{33} + K_2R^2\alpha_{34}$
Eq. O. M. 12	$I_{sh,12} \cdot \ddot{\alpha}_{12} + (K_{32} + K_2)R^2\alpha_{12} = R^2K_2\alpha_{34} + RK_2L_0 \cos \beta \varphi - RK_2(L_c - L_A) \cos \beta \theta$
Eq. O. M. 13	$I_{sh,13} \cdot \ddot{\alpha}_{13} + (K_{33} + K_2)R^2\alpha_{13} = R^2K_2\alpha_{35} + RK_2L_0 \cos \beta \varphi - RK_2(L_c - L_A) \cos \beta \theta$
Eq. O. M. 14	$I_{sh,14} \cdot \ddot{\alpha}_{14} + 2 \cdot K_2R^2\alpha_{14} = K_2R^2\alpha_{35} + K_2R^2\alpha_{36}$
Eq. O. M. 15	$I_{sh,15} \cdot \ddot{\alpha}_{15} + 2 \cdot K_2R^2\alpha_{15} = K_2R^2\alpha_{36} - K_2R^2\alpha_{37}$
Eq. O. M. 16	$I_{sh,16} \cdot \ddot{\alpha}_{16} + 2 \cdot K_2R^2\alpha_{16} = K_2R^2\alpha_{37} + K_2R^2\alpha_{38}$
Eq. O. M. 17	$I_{sh,17} \cdot \ddot{\alpha}_{17} + 2 \cdot K_2R^2\alpha_{17} = K_2R^2\alpha_{38} + K_2R^2\alpha_{39}$
Eq. O. M. 18	$I_{sh,18} \cdot \ddot{\alpha}_{18} + (K_1 + K_2)R^2\alpha_{18} = R^2K_2\alpha_{39} + RK_2L_0 \cos \beta \varphi - RK_2(L_c - L_A) \cos \beta \theta$
Eq. O. M. 19	$I_{sh,19} \cdot \ddot{\alpha}_{19} + (K_1 + K_2)R^2\alpha_{19} = R^2K_2\alpha_{40} + RK_2L_0 \cos \beta \varphi - RK_2(L_c - L_A) \cos \beta \theta$
Eq. O. M. 20	$I_{sh,20} \cdot \ddot{\alpha}_{20} + 2 \cdot K_2R^2\alpha_{20} = K_2R^2\alpha_{40} + K_2R^2\alpha_{41}$
Eq. O. M. 21	$I_{sh,21} \cdot \ddot{\alpha}_{21} + 2 \cdot K_2R^2\alpha_{21} = K_2R^2\alpha_{41} + K_2R^2\alpha_{42}$
Eq. O. M. 22	$I_{sh,22} \cdot \ddot{\alpha}_{22} + 2 \cdot K_2R^2\alpha_{22} = -K_2R^2\alpha_{42} + K_2R^2\alpha_{43}$
Eq. O. M. 23	$I_{sh,23} \cdot \ddot{\alpha}_{23} + 2 \cdot K_2R^2\alpha_{23} = K_2R^2\alpha_{43} + K_2R^2\alpha_{44}$
Eq. O. M. 24	$I_{sh,24} \cdot \ddot{\alpha}_{24} + (K_{34} + K_2)R^2\alpha_{24} = R^2K_2\alpha_{44} + RK_2L_0 \cos \beta \varphi - RK_2(L_c - L_A) \cos \beta \theta$
Eq. O. M. 25	$I_{sh,25} \cdot \ddot{\alpha}_{25} + 2 \cdot K_2R^2\alpha_{25} = K_2R^2\alpha_1 + K_2R^2\alpha_2$
Eq. O. M. 26	$I_{sh,26} \cdot \ddot{\alpha}_{26} + 2 \cdot K_2R^2\alpha_{26} = K_2R^2\alpha_2 + K_2R^2\alpha_3$
Eq. O. M. 27	$I_{sh,27} \cdot \ddot{\alpha}_{27} + 2 \cdot K_2R^2\alpha_{27} = -K_2R^2\alpha_3 + K_2R^2\alpha_4$
Eq. O. M. 28	$I_{sh,28} \cdot \ddot{\alpha}_{28} + 2 \cdot K_2R^2\alpha_{28} = K_2R^2\alpha_4 + K_2R^2\alpha_5$
Eq. O. M. 29	$I_{sh,29} \cdot \ddot{\alpha}_{29} + 2 \cdot K_2R^2\alpha_{29} = K_2R^2\alpha_5 + K_2R^2\alpha_6$
Eq. O. M. 30	$I_{sh,30} \cdot \ddot{\alpha}_{30} + 2 \cdot K_2R^2\alpha_{30} = K_2R^2\alpha_7 + K_2R^2\alpha_8$

Eq. O. M. 31 $I_{sh,31} \cdot \ddot{\alpha}_{31} + 2 \cdot K_2 R^2 \alpha_{31} = K_2 R^2 \alpha_8 + K_2 R^2 \alpha_9$

Eq. O. M. 32 $I_{sh,32} \cdot \ddot{\alpha}_{32} + 2 \cdot K_2 R^2 \alpha_{32} = K_2 R^2 \alpha_9 - K_2 R^2 \alpha_{10}$

Eq. O. M. 33 $I_{sh,33} \cdot \ddot{\alpha}_{33} + 2 \cdot K_2 R^2 \alpha_{33} = K_2 R^2 \alpha_{10} + K_2 R^2 \alpha_{11}$

Eq. O. M. 34 $I_{sh,34} \cdot \ddot{\alpha}_{34} + 2 \cdot K_2 R^2 \alpha_{34} = K_2 R^2 \alpha_{11} + K_2 R^2 \alpha_{12}$

Eq. O. M. 35 $I_{sh,35} \cdot \ddot{\alpha}_{35} + 2 \cdot K_2 R^2 \alpha_{35} = K_2 R^2 \alpha_{13} + K_2 R^2 \alpha_{14}$

Eq. O. M. 36 $I_{sh,36} \cdot \ddot{\alpha}_{36} + 2 \cdot K_2 R^2 \alpha_{36} = K_2 R^2 \alpha_{14} + K_2 R^2 \alpha_{15}$

Eq. O. M. 37 $I_{sh,37} \cdot \ddot{\alpha}_{37} + 2 \cdot K_2 R^2 \alpha_{37} = -K_2 R^2 \alpha_{15} + K_2 R^2 \alpha_{16}$

Eq. O. M. 38 $I_{sh,38} \cdot \ddot{\alpha}_{38} + 2 \cdot K_2 R^2 \alpha_{38} = K_2 R^2 \alpha_{16} + K_2 R^2 \alpha_{17}$

Eq. O. M. 39 $I_{sh,39} \cdot \ddot{\alpha}_{39} + 2 \cdot K_2 R^2 \alpha_{39} = K_2 R^2 \alpha_{17} + K_2 R^2 \alpha_{18}$

Eq. O. M. 40 $I_{sh,40} \cdot \ddot{\alpha}_{40} + 2 \cdot K_2 R^2 \alpha_{40} = K_2 R^2 \alpha_{19} + K_2 R^2 \alpha_{20}$

Eq. O. M. 41 $I_{sh,41} \cdot \ddot{\alpha}_{41} + 2 \cdot K_2 R^2 \alpha_{41} = K_2 R^2 \alpha_{20} + K_2 R^2 \alpha_{21}$

Eq. O. M. 42 $I_{sh,42} \cdot \ddot{\alpha}_{42} + 2 \cdot K_2 R^2 \alpha_{42} = K_2 R^2 \alpha_{21} - K_2 R^2 \alpha_{22}$

Eq. O. M. 43 $I_{sh,43} \cdot \ddot{\alpha}_{43} + 2 \cdot K_2 R^2 \alpha_2 = K_2 R^2 \alpha_{22} + K_2 R^2 \alpha_{23}$

Eq. O. M. 44 $I_{sh,44} \cdot \ddot{\alpha}_{44} + 2 \cdot K_2 R^2 \alpha_2 = K_2 R^2 \alpha_{23} + K_2 R^2 \alpha_{24}$

Eq. O. M. 45

$$\begin{aligned} & \ddot{\varphi} \left(M_1 \frac{L_1^2}{3} + M_2 \left(L_1^2 + L_1 L_2 \cos(\eta) + \frac{L_2^2}{3} \right) \right. \\ & \quad + M_3 \left(L_1^2 + L_2^2 + 2 L_1 L_2 \cos(\eta) + L_3 L_1 \cos(\eta - \delta) + L_3 L_2 \cos(\delta) \right. \\ & \quad \left. \left. + \frac{L_3^2}{3} \right) + m_{LBS} L_0^2 + 20 * m_{sh} L_0^2 \right) + K_2 L_0^2 \cos^2(\beta) \cdot 40 \varphi \\ & = K_2 L_0 \cos^2(\beta) \cdot 40 (L_C - L_A) \theta \\ & \quad + (g + \ddot{z}_A) \left(M_1 \cos(\gamma) \frac{L_1}{2} + \frac{M_2}{L_2} \cos(\gamma) (1.7335E03) \right. \\ & \quad \left. + \frac{M_3}{L_3} \cos(\gamma) (2.9576E03) + m_{LBS} L_0 \cos(\gamma) - 20 * m_{sh} L_0 \cos(\gamma) \right) \\ & \quad - \ddot{x}_A \left(M_1 \sin(\gamma) \frac{L_1}{2} + \frac{M_2}{L_2} \sin(\gamma) (1.7335E3) \right. \\ & \quad \left. + \frac{M_3}{L_3} \sin(\gamma) (2.9576E3) + m_{LBS} L_0 \sin(\gamma) + 20 * m_{sh} L_0 \sin(\gamma) \right) \\ & \quad + K_2 L_0 \cos(\beta) R (\alpha_1 + \alpha_6 + \alpha_7 + \alpha_{12} + \alpha_{13} + \alpha_{18} + \alpha_{19} + \alpha_{24}) \end{aligned}$$

The example equations are given below in equation D.8 up to D.11. After the example equations the constants used in the FL model are given. The next few paragraphs contain information on how to use the indices.

Equation D.8 is given in a general form. As stated in the parameter descriptions the parameter "s" can take on multiple values, depending on the sheave you want to consider. As an example, equation of sheave 19 one should use the value 19 for the parameter "s" and the corresponding "s2" value of 40. Hence, the equation of motion for sheave 19 is obtained.

Equation D.9 works in the same way as described in the paragraph above. The parameter "m" can take on multiple values as indicated in the parameter descriptions below. The example equation of sheave 1 can thus be obtained through using the value 1 for "m" and using the corresponding "p" value of 1.

Equation D.10 the parameter "x" in this equation can be utilized in the same way as described in the previous two paragraphs. This equation can be used for all other sheaves than those of Equation D.8 and D.9. Corresponding to each sheave number value of "x" the right hand side of the equation requires the sheave previous and sequential to the considered sheave in the wire rope system. The right hand side can thus describe a wide variety of sheave numbers corresponding to the parameter value of "x". In addition to that, the terms on the right hand side of the equation can be either positive or negative, depending on the sheave considered.

$$\ddot{\alpha}_s \cdot C_6 + \alpha_s \cdot C_7 = C_5 \cdot \varphi - C_8 \cdot \theta + C_9 \cdot \alpha_{s2} \quad \mathbf{D.8}$$

Applies on example sheave 19 for s=19

$$\ddot{\alpha}_m \cdot C_6 + \alpha_m \cdot C_{1p} = C_5 \cdot \varphi - C_8 \cdot \theta + C_9 \cdot \alpha_{m2} \quad \mathbf{D.9}$$

Applies on example sheave 1 for m=1

$$\ddot{\alpha}_x \cdot C_6 + \alpha_x \cdot 2 \cdot C_9 = \pm C_9 \cdot \alpha_{prev,x} \pm C_9 \cdot \alpha_{seq,x} \quad \mathbf{D.10}$$

Applies on example sheave 14 for x=14

$$\ddot{\varphi} \cdot C_1 + \varphi \cdot C_2 = \theta \cdot C_4 + (\ddot{z}_A + g) \cdot C_3 - \ddot{x}_A C_{10} + C_5 \cdot (\alpha_1 + \alpha_6 + \alpha_7 + \alpha_{12} + \alpha_{13} + \alpha_{18} + \alpha_{19} + \alpha_{24}) \quad \mathbf{D.11}$$

In which:

- s : Index which can take the values of 6, 7, 18 and 19
s2 : Index which can take the values of 29 for s=6, 30 for s=7, 39 for s=18, and 40 for s=19
m : Index which can take the values of 1, 12, 13, and 24
m2 : Index which can take the values of 25 for m=1, 34 for m=12, 35 for m=13, and 44 for m=24
p : Index which can take the values of 1 for m=1, 2 for m=12, 3 for m=13, and 4 for m=24
x : Index which can take the value of 1 up to 44 with the exception of 1, 6, 7, 12, 13, 18, 19 and 24
 $\alpha_{prev,x}$: Index which indicates the previous sheave connected to the cable in the system. Corresponding to the parameter "x" with an value of 14, the sheave number of the previous sheave is 35. For this value of "x" the term should be positive
 $\alpha_{seq,x}$: Index which indicates the sequential sheave connected to the cable in the system. Corresponding to the parameter "x" with an value of 14, the sheave number of the sequential sheave is 36. For this value of "x" the term should be positive
 θ : Pitch at the COG in [rad]
 \ddot{z}_A : z-acceleration in point A (main hinge) in [m/s²]
 \ddot{x}_A : x-acceleration in point A (main hinge) in [m/s²]
g : Gravitational acceleration in [m/s²]
 $C_{1...14}$: Constants containing mass terms, arms, angles and other factors

$$C_1 = M_1 \frac{L_1^2}{3} + M_2 \left(L_1^2 + L_1 L_2 \cos(\eta) + \frac{L_2^2}{3} \right) + M_3 \left(L_1^2 + L_2^2 + 2L_1 L_2 \cos(\eta) + L_3 L_1 \cos(\eta - \delta) + L_3 L_2 \cos(\delta) + \frac{L_3^2}{3} \right) + m_{LBS} L_0^2 + 20 * m_{sh} L_0^2$$

$$C_2 = K_2 L_0^2 \cos^2(\beta) \cdot 40$$

$$C_3 = M_1 \cos(\gamma) \frac{L_1}{2} + \frac{M_2}{L_2} \cos(\gamma) (1.7335E03) + \frac{M_3}{L_3} \cos(\gamma) (2.9576E03) + m_{LBS} L_0 \cos(\gamma) - 20 * m_{sh} L_0 \cos(\gamma)$$

$$C_4 = K_2 L_0 \cos^2(\beta) \cdot 40 (L_c - L_A)$$

$$C_5 = K_2 L_0 \cos(\beta) R$$

$$C_6 = I_{sh,x}$$

$$C_7 = (K_1 + K_2) R^2$$

$$C_8 = R K_2 (L_c - L_A) \cos \beta$$

$$C_9 = K_2 R^2$$

$$C_{10} = M_1 \sin(\gamma) \frac{L_1}{2} + \frac{M_2}{L_2} \sin(\gamma) (1.7335E3) + \frac{M_3}{L_3} \sin(\gamma) (2.9576E3) + m_{LBS} L_0 \sin(\gamma) + 20 * m_{sh} L_0 \sin(\gamma)$$

$$C_{11} = (K_{31} + K_2) R^2$$

$$C_{12} = (K_{32} + K_2) R^2$$

$$C_{13} = (K_{33} + K_2) R^2$$

$$C_{14} = (K_{34} + K_2) R^2$$

APPENDIX F. MODAL ANALYSIS

GENERAL

Before beginning with the actual modal analysis some preparatory calculations need to be performed. The eigenvectors and eigenvalues need to be obtained in order to continue the analysis. Since the system is a 45 degree of freedom system these vectors are obtained through numerical calculation in Matlab, using the *eig* function. This function yields a vector of eigenfrequencies (of size M) and a matrix of corresponding eigenvectors (of size MxM). The eigenvectors represent principal modes of vibration. It should be pointed out that when one solves the eigenvalue problem one assumes that all the degrees of freedom have their maximum values at the same time. An M degree of freedom system has M eigenmodes.

For the modal analysis it is also assumed that the forced motion can be described by a summation of synchronised motions, just as when solving for the eigenvectors. Only now the eigenvectors are multiplied with an unknown time function. The assumption in equation form is shown in equation F.1.

$$\underline{x}(t) = \sum_{i=1}^N \hat{\underline{x}}_i u_i(t) = \underline{E} \underline{u}(t) \quad \text{F.1}$$

In which:

- \underline{x} : Generalized displacements of all degrees of freedom.
- $\hat{\underline{x}}_i$: i^{th} Normal mode of the system.
- $u_i(t)$: Modal time function.
- \underline{E} : Eigen matrix containing all eigenvectors or normal modes.

Using this assumption, the system of equations of motion is uncoupled which means they are made independent of each other. The modal analysis thus allows the equations of motion of the physical degrees of freedom, where they are coupled, to be translated in the mathematical domain, where they are uncoupled. In the mathematical domain the system of decoupled differential equations can be solved for its decoupled degrees of freedom or also called the generalized degrees of freedom. The equations with which the physical system is translated to mathematical domain and decoupled are given in the next section. Firstly, some more preparatory calculations and characteristics the modal analysis uses are described.

The modal analysis is largely based on the orthogonality conditions of eigenvectors. The orthogonality condition of the eigenvectors essentially is based on the fact that if two different orthogonal vectors are multiplied their result is zero. This orthogonality condition can be used to diagonalise the matrices during the modal analysis. Thus when diagonalising the mass and stiffness matrixes the orthogonality property of the eigenvectors is used as shown in equations F.2 and F.3. For detailed analysis please refer to [14].

$$\hat{\underline{x}}_s^T \underline{M} \hat{\underline{x}}_r = 0, \text{ for } s \neq r \quad \text{F.2}$$

$$\hat{\underline{x}}_s^T \underline{K} \hat{\underline{x}}_r = 0, \text{ for } s \neq r \quad \text{F.3}$$

Before using the eigenvectors to decouple the system of equations of motion they must be normalised to make them unique. In this thesis mass normalisation was applied using equation F.4.

$$\underline{E}_{Norm} = \frac{\underline{E}}{\sqrt{\underline{E}^T \underline{M} \underline{E}}} \quad \text{F.4}$$

In which:

- \underline{M} : Mass matrix.
- \underline{E}^T : Transposed eigenvector matrix.
- \underline{E}_{Norm} : The normalised eigenvector matrix.

EQUATIONS OF MOTION & INITIAL CONDITIONS

The transformation of the equations of motion from the physical domain to the mathematical domain is performed using equation F.1. As example the transformation is applied in equations F.5 up to F.7. equation F.1 is filled in the physical system of degrees of freedom of equation F.5.

$$\underline{M}\ddot{\underline{x}} + \underline{C}\dot{\underline{x}} + \underline{K}\underline{x} = \underline{F}(t) \quad \text{F.5}$$

$$\underline{M}\underline{E}\ddot{\underline{u}} + \underline{C}\underline{E}\dot{\underline{u}} + \underline{K}\underline{E}\underline{u} = \underline{F}(t) \quad \text{F.6}$$

$$\underline{E}^T \underline{M}\underline{E}\ddot{\underline{u}} + \underline{E}^T \underline{C}\underline{E}\dot{\underline{u}} + \underline{E}^T \underline{K}\underline{E}\underline{u} = \underline{E}^T \underline{F}(t) \quad \text{F.7}$$

$$\underline{M}^*\ddot{\underline{u}} + \underline{C}^*\dot{\underline{u}} + \underline{K}^*\underline{u} = \underline{E}^T \underline{F}(t) \quad \text{F.8}$$

In which:

- \underline{M}^* : The diagonal modal mass matrix. If the eigenvectors are mass normalised then the modal mass matrix will become an identity matrix by these operations.
 \underline{C}^* : The modal damping matrix. It often does not diagonalise unlike the modal mass and stiffness matrices.
 \underline{K}^* : The diagonal modal stiffness matrix.
 \underline{F} : Force vector.

As stated in the definitions above the modal damping matrix does not diagonalise unlike the modal the mass and stiffness matrices. There are multiple solutions for this problem. In this thesis, since it is desired to signify the damping as a percentage of the critical damping it is chosen to calculate the critical damping using the modal analysis approach. Then, for each mode the damping was applied by using a certain percentage of that mode's critical damping. The modal critical damping was calculated using equation F.9.

$$d_{ii}^{critical} = 2\sqrt{k_{ii}^* m_{ii}^*} \quad \text{F.9}$$

In which:

- $d_{ii}^{critical}$: Critical modal damping of mode i.
 k_{ii}^* : Modal stiffness of mode i.
 m_{ii}^* : Modal mass of mode i.

The damping matrix was then obtained by applying a, for example, 5% factor of this critical damping. This is shown in equation F.10.

$$d_{ii}^* = 0.05 \cdot d_{ii}^{critical} \quad \text{F.10}$$

In which:

- d_{ii}^* : Modal damping of mode i.

When the equations of motions are rewritten the system will be solved for the unknown time function $u(t)$. The solving for the modal analysis differential equations is no different than solving the ordinary differential equations of Appendix D. The difference lies in the fact that the unknown time function which is solved still needs to be multiplied by the eigenmatrix, as in equation F.1, to obtain the solutions to the equations of motion.

When solving the equations one must not forget to also translate the initial conditions to the modal space. The equations for this are given in F.11 and F.12.

$$\underline{u}_0 = \underline{E}^{-1} \underline{x}_0 \quad \text{F.11}$$

$$\dot{\underline{u}}_0 = \underline{E}^{-1} \dot{\underline{x}}_0 \quad \text{F.12}$$

In which:

- \underline{u}_0 : Modal displacement initial conditions.
 $\dot{\underline{u}}_0$: Modal velocity initial conditions.
 \underline{x}_0 : Displacement initial conditions.
 $\dot{\underline{x}}_0$: Velocity initial conditions.

MATLAB

When calculating the modal mass and modal stiffness matrices it should be pointed out that due to numerical errors the diagonal matrices are in reality completely filled. However, the non-diagonal

elements are less than 5% of the diagonal elements and are supposed to be zero. During calculations therefore only the diagonal values were used.

APPENDIX G. SPECTROGRAM

In a signal composed of multiple sinusoids it is possible that at some points in time certain frequencies are dominant while in other points in time they are not. To gain insight in the frequency behaviour over time spectrograms can be used. A spectrogram is a plot which visualises both the frequency content and the time content of a signal. This way it is visible at what points in time which frequencies are dominant. To create the spectrogram the Matlab function *spectrogram* is used.

SEGMENTING THE SIGNAL & OVERLAP

The spectrogram function divides the signal into multiple segments. The choice of segment size influences the resolution on both time and frequency domain. The shorter the segment, the better the time resolution is. The longer the segment, the better the frequency resolution is.

The segments are by default overlapped with 50% of its segment length. This is because the windowing function reduces the data at the ends of the function. The windowing function thus creates a better frequency resolution due to the mitigation of leakage, but it loses time information. By using overlapping windows the time information is preserved in the spectrogram. Thus both the frequency and time resolution is preserved [20].

WINDOWING FUNCTION

The windowing function is used because the total data trace in time domain is divided into sections and these sections are then translated to frequency domain using the fast Fourier transform. The windowing function reduces the spectral leakage caused by dividing the data trace in time domain. More information on spectral leakage can be found in Appendix B.

In this thesis the windowing function is the hamming window. The hamming window has a good frequency resolution and limited spectral leakage [21]. It also has decent time resolution, however it does show some effect of the Gibbs phenomenon which essentially is the effect of the window transition causing discontinuity in the time-domain [22]. The Gibbs phenomenon is a type of overshoot or ringing, which is explained in Appendix B.

APPENDIX H. MATLAB FOR FL MODEL

This appendix elaborates on the Matlab functions used and the translation of the equations of motion into a form that is usable for Matlab. There is also information on the global build-up of the script to clarify the steps taken within the script.

MODEL BUILD-UP

In this section the Matlab build-up is described. In Figure H.1 an overview is given on the steps taken as preparatory work, for solving the equations, what the results are and what was done with these results. Explanation of the different steps is given in the sections below the figure.

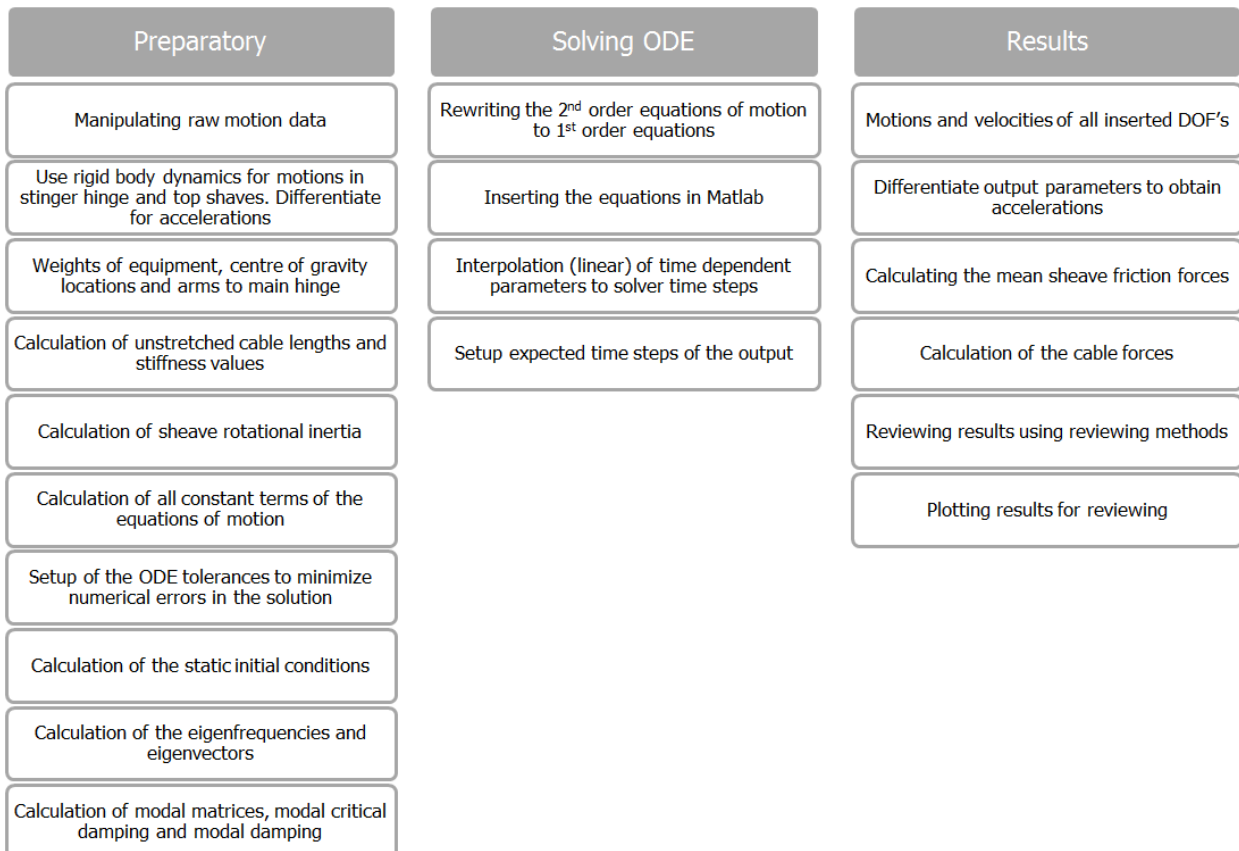


Figure H.1 Schematisation of the model build-up.

Most of the steps should be clear after reading this thesis. A short summation of content is given nonetheless. With "processing of raw motion data" the proceedings in the data analysis chapter, Chapter 5, are meant. Rigid body dynamics is applied to translate the displacements of the centre of gravity to the displacements at the location of the main hinge (point A of Figure 7.4) and the location of the tops heaves (point C of Figure 7.4). Then these displacement traces were differentiated in frequency domain to obtain the accelerations of these locations. Differentiation has already been elaborated on in section 5.4.

The rotational inertia of the sheaves, the sheave friction forces, the calculation of cable forces, the calculation of stiffness values, the calculation of unstretched cable lengths and the static initial conditions have already been elaborated on in section 7.5. The modal analysis calculations have been given and explained in section 7.4 and Appendix D. The reviewing methods and their calculations have been discussed in section 7.8.1.

Of all equipment parts on the stinger and of the cables the weight was found and their centre of gravities locations and thus their force arms to the main hinge are determined. Calculation of the constants in the equations of motion is filling in the values of the variables of the terms derived in Appendix D. The constants contain the mass related terms and the corrected arms of the centres of gravity. They also contain the spring related terms. The constants are calculated in such a way that any change of parameter in the derived terms will automatically recalculate the constants.

There are some topics which will be discussed with more detail. These are the definition of the solver tolerances, the workings of the solver itself, the solver's 1st order input, the internal interpolation steps for the solver and the results the solver give.

DEFINITION OF TOLERANCES

The solver of the ordinary differential equations needs an indication on allowable errors. This is meant to reduce numerical errors in the solution. The smaller the tolerances, the larger the computation time. Therefore, a proper value is chosen by reviewing smoothness of the plots after changing these tolerances while keeping the calculation time of half an hour up to an hour. There are two types of error tolerances which can be defined in Matlab: absolute tolerance and relative tolerance. The tolerances are a type of local error checking procedure. Essentially the solver estimates the error at the end of each time step it makes. The tolerance inputs combined indicate what the acceptable error is. When the estimation of the error results in an error smaller than the accepted error, then the solver continues to the next time step. When the estimated error is too large the solver reduces its step size and recalculates. The relative tolerance measures the error as a percentage of each value. The absolute tolerance is, as the name states, a threshold value which represents the acceptable error for values where the solver results reaches outputs near zero [23]. To clarify both error types and the working of the tolerance Figure H.2 is presented. Eventually the values for the tolerances were:

- Absolute tolerance: $1E10^{-5}$
- Relative tolerance: $1E10^{-5}$

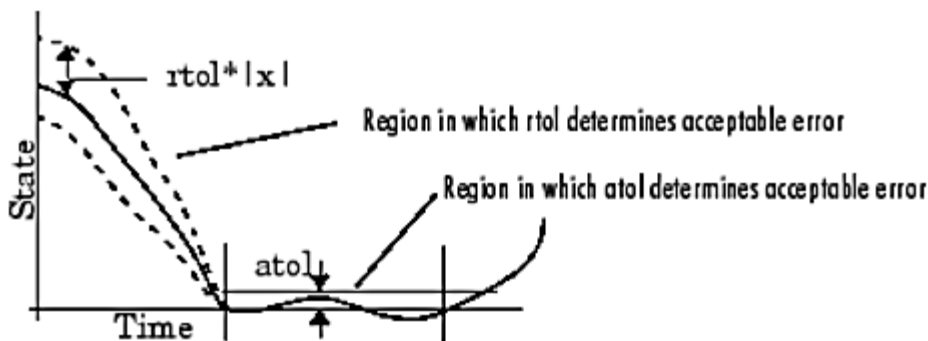


Figure H.2 Relative tolerance (rtol) and absolute tolerance (atol) both illustrated in a sketch for a random graph.

THE SOLVER

The original solver used was the *ode45* solver. This solver however showed to be inefficient when solving the large system of differential equations. Therefore the *ode15s* solver was used instead as advised in [24]. The *ode15s* is a variable-step continuous implicit solver which uses an algorithm based on Numerical Differentiation Formulas to solve the differential equations. The Numerical Differentiation Formulas are based on backward differentiation methods but are more efficient. This solving method belongs to the family of numerical integration methods of ordinary differential equations. This type of solver uses variable internal time steps, depending on the accuracy of the value prediction. It is an effective solver for stiff problems. When a problem is stiff the solutions shows rapid changes in small time steps but main solution is only visible on a longer time scale. Solvers of stiff problems are designed to vary the time steps based on the longer time scale than the time step of the fastest possible change. The *ode15s* solver uses a numerically generated Jacobian matrix to solve the differential equations. The syntax is given in the equation H.1 [24].

$$[T, Y] = \text{ode15s}(\text{odefun}, \text{tspan}, \text{y0}, \text{options}) \quad \text{H.1}$$

In which:

- odefun : Function which calculates the right hand side of the inserted 1st order ordinary differential equations to be solved.
- tspan : Vector which specifies the integration interval. The solver will impose its initial conditions at the first term of tspan.
- y0 : Vector with initial conditions specified by the user. These initial conditions will be applied at tspan(1), as stated before.
- options : Optional function. This parameter can be added optionally. It can be used to change the default integration properties of the *ode15s* solver. In this model it has been used to define the absolute and relative errors allowed when solving.

The *ode15s* solver then integrates the system of differential equations given in the *odefun* function over the indicated timespan *tspan*.

THE SOLVER'S 1ST ORDER INPUT

The derived 2nd order differential equations of Appendix D need to be rewritten in 1st order equations in order to be able to use the *ode15s* solver in Matlab. This is because the only form of equations Matlab accepts is the form in equation H.2.

$$\frac{dq}{dt} = f(t, q) + F_{ex}(t) \quad \text{H.2}$$

In which:

- q : Generalised coordinate.
- t : Time.
- F_{ex} : External force(s) dependent on time.
- f(t,q) : Some function.

The solver used for solving the ordinary differential equations is the *ode15s* function of Matlab. It should be noted that the ship motions which are part of the force terms in the equations of motions are time dependent. This motion data has a resolution of 1 value each second. However, the time steps the solver internally makes while solving the differential equation are of variable size and much smaller than 1 second. Therefore, during each time step the solver makes, internally the ship motion values will need to be interpolated to that specific (internally defined) time point. The interpolation, for the sake of calculation speed, has been chosen as an linear interpolation type. Note that the internal solver steps cannot be defined by the user of the solver, only the output time steps the solver should give results of can be defined by the solver. The output time step and time range in this thesis is chosen equal to the time step and range of the measured data.

SOLVER RESULTS

The solver outputs are motion and velocity values of the DOF for each second of the chosen output time range. The output is thus a matrix with each column representing a degree of freedom's motion or velocity and each row representing a time step. The matrix has a complementary vector indicating the time steps at which these output values are valid. For clarity a general form of the output is given in equations H.3 and H.4.

$$Y_{num} = \begin{bmatrix} dof1(mot), t(1) & dof1(vel), t(1) & \dots & dof45(mot), t(1) & dof45(vel), t(1) \\ \vdots & \vdots & \ddots & \vdots & \vdots \\ dof1(mot), t(end) & dof1(vel), t(end) & \dots & dof45(mot), t(end) & dof45(vel), t(end) \end{bmatrix} \quad \text{H.3}$$

$$T_{num} = \begin{bmatrix} t_1 \\ \vdots \\ t_{end} \end{bmatrix} \quad \text{H.4}$$

In which:

- Ynum : Solver output matrix containing all motion (mot) and velocity (vel) values of the DOF's.
- Tnum : Solver output vector containing the time steps corresponding to the row values of Y.
- dof : Degree of freedom

PEAK MATCHING FOR REVIEWING

For some of the reviewing methods stated in section 7.8.1 it is necessary to know the peak values of the predicted and measured data traces. Also, these peak values must be "matched". Because the peaks of the predicted time traces and the measured time trace do not always occur at the same time instant (as can be seen throughout the thesis) the peaks which should correspond with each other need to be matched. This is necessary for peak amplitude and time comparison as performed in several reviewing methods.

The function build to perform this defines a threshold value. The main function of the threshold value is to leave out the low amplitude irregularities present in the data traces for the peak matching. This means only the peaks with maximum values above the threshold value will be considered important enough for peak matching.

All maxima of the peaks with values larger than the threshold value are saved. For all peak values of the measured data trace (or reference peak) a corresponding peak value of the predicted time traces needs to be found. The threshold time difference between peaks is 4 seconds. This means that a corresponding peak will be sought for in the time range of 4 seconds before the reference peak and 4 seconds after the reference peak. If a corresponding peak is found, the peaks are paired and used in the peak comparison. In the event that no corresponding peak can be found, the reference peak is removed from the saved set of peaks.

APPENDIX I. CALCULATION OF BLOCK MASS CONTRIBUTION

In Figure I.1 the sketch is shown with which the calculations were performed. Note the Δang -angles are deliberately shown as very large angles, while in reality these angles are small angles. Furthermore, no friction is accounted for in this sub analysis, thus the force T_1 is assumed equal to T_2 .

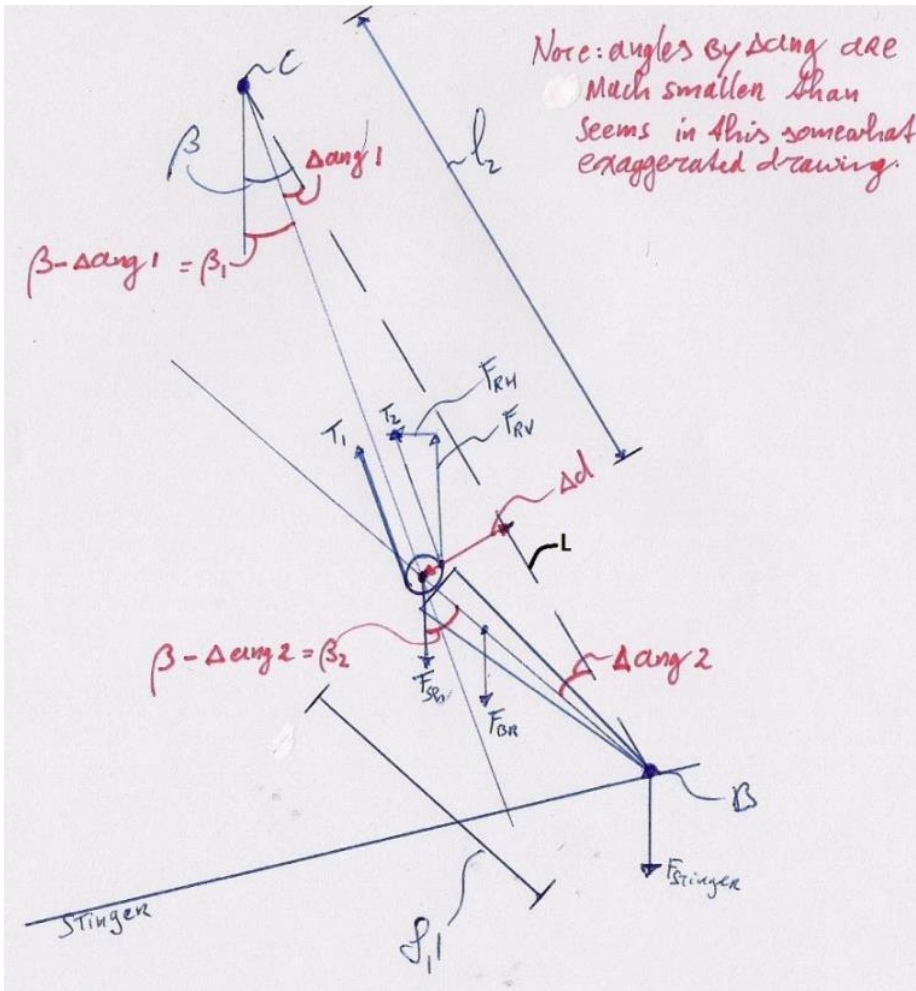


Figure I.1 Lower block structure sketch for validation of assumption considering the contribution of the lower block structure.

The units of the above parameters are given in Table I.1.

Symbol	Name	Unit
β_1	Hang-off angle of cables	rad
β_2	Hang-off angle of lower block structure	rad
$\Delta\text{ang}1$	Angular difference of cables with linear line connection point B and C	rad
$\Delta\text{ang}2$	Angular difference of LBS with linear line connection point B and C	rad
Δd	Distance of linear line between point C and B to the lower sheave block	m
F_{BR}	Force lower block structure	N
F_{RH}	Horizontal component of tension T	N
F_{RV}	Vertical component of tension T	N
F_{sh}	Force by the lower sheave block	N
$F_{stinger}$	Force by the stinger	N
F_z	Force in z-direction	N
L_{lbsp}	Length lower block structure projected on the linear line between point C and B.	m
l_2	Cable length projected on the linear line between point C and B.	m
$M_{/B}$	Moment about point B	Nm
T_c	Cable tension	N

Table I.1 List of symbols for calculation of block mass contribution.

Considering the geometry of the system, equations I.1 up to I.3 apply.

$$\Delta d = l_2 \cdot \tan(\Delta \text{ang}1) \quad \text{I.1}$$

$$L_{lbsp} = 8.1 \cdot \cos(\Delta \text{ang}2) \quad \text{I.2}$$

$$\Delta d = L_{lbsp} \cdot \tan(\Delta \text{ang}2) \quad \text{I.3}$$

Since the Δang -angles are small angles, the above equations can be rewritten as in equations I.4 and I.5. Therefore both angles can be expressed in one another, as in equation I.6.

$$\Delta d = l_2 \cdot \Delta \text{ang}1 \quad \text{I.4}$$

$$\Delta d = 8.1 \cdot \Delta \text{ang}2 \quad \text{I.5}$$

$$\Delta \text{ang}1 = \frac{8.1 \cdot \Delta \text{ang}2}{l_2} = 0.5148 \cdot \Delta \text{ang}2 \quad \text{I.6}$$

The tension parameters T_1 and T_2 are equal in magnitude. From now on they will both be noted as T and are vectorised in a vertical and horizontal component to make the calculations easier. This is performed in equation I.7.

$$T_c = \frac{F_{RV}}{\cos(\beta_1)} = \frac{F_{RH}}{\sin(\beta_1)} \quad \text{I.7}$$

Now, two equations are set-up which are equation I.8 and I.9. The sum of vertical forces and the sum of moments around point B. Note that the calculations are performed for a single sheave, which is why the external forcing, which represents the totals of each equipment type, are divided over 20.

$$\sum F_z = 2 \cdot F_{RV} - F_{sh} - F_{BR} - F_{stinger} = 0 \quad \text{I.8}$$

$$\sum M_{/B} = 0 = F_{BR} \sin(\beta_2) \cdot \frac{(8.1 - R) \cdot 2}{3} + F_{sh} \sin(\beta_2) \cdot 8.1 + 2 \cdot F_{RH} \cos(\beta_2) \cdot 8.1 - 2 \cdot F_{RV} \sin(\beta_2) \cdot 8.1 \quad \text{I.9}$$

The sum of vertical forces can be rewritten in equation I.10.

$$F_{RV} = \frac{F_{sh} + F_{BR} + F_{stinger}}{2} \quad \text{I.10}$$

Equation I.7 was used to insert in the sum of moments, after which the sum of moments was rewritten. This resulted in equations I.11 up to I.13.

$$0 = F_{BR} \sin(\beta_2) \cdot \frac{(8.1 - R) \cdot 2}{3} + F_{sh} \sin(\beta_2) \cdot 8.1 + 16.2 \cdot T_c (\sin(\beta_1) \cos(\beta_2) - \cos(\beta_1) \sin(\beta_2)) \quad \text{I.11}$$

$$0 = F_{BR} \sin(\beta_2) \cdot \frac{(8.1 - R) \cdot 2}{3} + F_{sh} \sin(\beta_2) \cdot 8.1 + 16.2 \cdot T_c \sin(\beta_1 - \beta_2) \quad \text{I.12}$$

$$0 = F_{BR} \sin(\beta - \Delta \text{ang}2) \cdot 4.9667 + F_{sh} \sin(\beta - \Delta \text{ang}2) \cdot 8.1 - 16.2 \cdot T_c \sin(\Delta \text{ang}1 + \Delta \text{ang}2) \quad \text{I.13}$$

Inserting equation I.6 in equation I.13 yields the following derivations: equations I.14 up to I.17.

$$T_c = \frac{F_{RV}}{\cos(\beta - \Delta ang2 \cdot 0.5148)} = \frac{F_{BR} \sin(\beta - \Delta ang2) \cdot 4.9667}{16.2 \cdot \sin(1.5148 \cdot \Delta ang2)} + \frac{F_{sh} \sin(\beta - \Delta ang2) \cdot 8.1}{16.2 \cdot \sin(1.5148 \cdot \Delta ang2)} \quad \mathbf{I.14}$$

$$F_{RV} = \frac{\sin(\beta - \Delta ang2)}{\sin(1.5148 \cdot \Delta ang2)} \left(\frac{F_{BR} \cdot 4.9667}{16.2} + \frac{F_{sh} \cdot 8.1}{16.2} \right) \cos(\beta - \Delta ang2 \cdot 0.5148) \quad \mathbf{I.15}$$

Note: $\Delta ang2$ is a small angle!

$$F_{RV} = \frac{\sin(\beta) - \cos(\beta) \Delta ang2}{1.5148 \cdot \Delta ang2} \left(\frac{F_{BR} \cdot 4.9667}{16.2} + \frac{F_{sh} \cdot 8.1}{16.2} \right) (\cos(\beta) + \sin(\beta) \Delta ang2 \cdot 0.5148) \quad \mathbf{I.16}$$

$$0 = \left(\frac{\sin(\beta) \cos(\beta)}{1.5148} + \Delta ang2 \left(-F_{RV} - \frac{\cos(\beta)^2}{1.5148} + \sin(\beta)^2 \cdot 0.3398 \right) - \cos(\beta) \sin(\beta) (\Delta ang2)^2 \cdot 0.3398 \right) \left(\frac{F_{BR} \cdot 4.9667}{16.2} + \frac{F_{sh} \cdot 8.1}{16.2} \right) \quad \mathbf{I.17}$$

Since the force terms F_{BR} & F_{sh} cannot be zero the following must apply:

$$0 = \frac{\sin(\beta) \cos(\beta)}{1.5148} + \Delta ang2 \left(-F_{RV} - \frac{\cos(\beta)^2}{1.5148} + \sin(\beta)^2 \cdot 0.3398 \right) - \cos(\beta) \sin(\beta) (\Delta ang2)^2 \cdot 0.3398 \quad \mathbf{I.18}$$

This second degree equation of equation I.18 can be solved for $\Delta ang2$, which can be inserted into equation I.7. When not using the vertical stinger force in the calculation of sum of vertical forces, one can apply F_{RV} calculated without $F_{STINGER}$ to obtain the tension purely due to the block moment.